EXPERIMENTAL BIOMEDICAL RESEARCH

ISSN 2618-6454

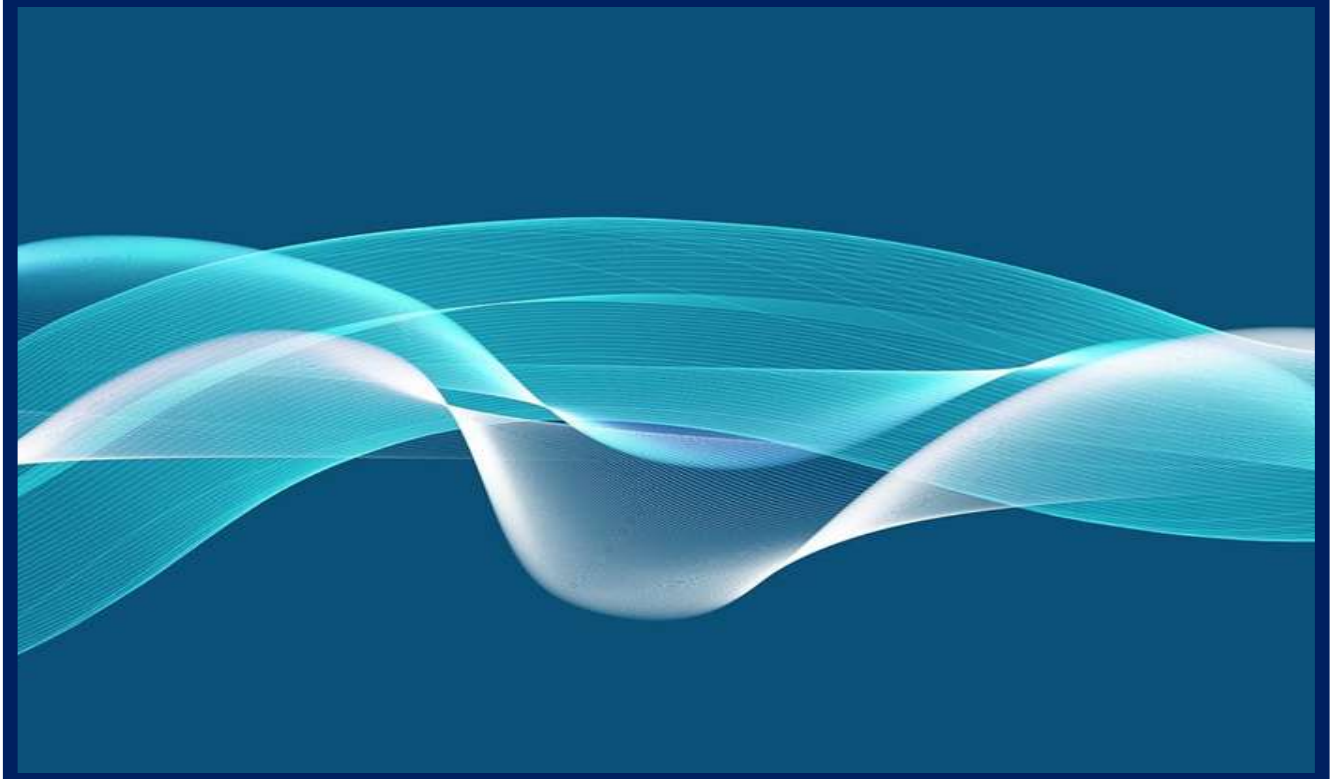

2023 / Vol. 6 / No. 1 Jan-Mar

ISSN 2618-6454
9 772618 645003

http:// www.experimentalbiomedicalresearch.com

EXPERIMENTAL BIOMEDICAL RESEARCH
VOLUME 6/ ISSUE 1 / JAN – MAR / 2023

ISSN 2618-6454

AUTHOR GUIDELINES

INSTRUCTIONS FOR AUTHORS

Experimental Biomedical Research publishes articles in English. Since the journal does not offer translation services, if the language of the manuscripts is not enough, the editors may refuse the manuscript or ask the author to seek language editorial services to bring the manuscript to minimum standards for the review process. If your manuscript is accepted it will be checked by our copyeditors for spelling and formal style before publication.

If you would like to submit a Review, please contact Editor-in Chief at info@experimentalbiomedicalresearch.com.

Online Submission

The articles must be submitted by the corresponding author via the Online Submissions System. If authors encounter technical problems with online submission, they may contact with support team at info@experimentalbiomedicalresearch.com.

Corresponding author

The corresponding author's must do: complete submission of manuscript files; storage of the article and all related documents and giving original data when necessary; contributions of the authors and explanations of conflict of interest disclosures; approval for submission; and the final proof control.

ORCID ID

ORCiD IDs of the corresponding author and other authors must be submitted during the registration process. This section is mandatory.

As part of our commitment to ensuring an ethical, transparent and fair peer review process, Experimental Biomedical Research is a publisher who signed ORCID open letter. ORCID provides a unique and persistent digital identifier that distinguishes researchers from every other researcher, even those who share the same name, and, through integration in key research workflows such as manuscript and grant submission, supports automated linkages between researchers and their professional activities, ensuring that their work is recognized.

The collection of ORCID iDs from corresponding authors is now part of the submission process of this journal. If you already have an ORCID iD you will be asked to associate that to your submission during the online submission process. We also strongly encourage all co-authors to link their ORCID ID to their accounts in our online peer review platforms. It takes seconds to do: click the link when prompted, sign into your ORCID account and our systems are automatically updated. Your ORCID iD will become part of your accepted publication's metadata, making your work attributable to you and only you. Your ORCID iD is published with your article so that fellow researchers reading your work can link to your ORCID profile and from there link to your other publications.

If you do not already have an ORCID iD please follow this link to create one.

Author Declaration, Funding and Financial Conflicts of Interest

Authors should provide a cover letter declares: that the article submitted has not been published elsewhere and is not under review; that the submission has been approved by all co-authors and, if necessary, by the responsible authorities and the institute. The publisher will not be responsible in cases of any claims for compensation.

All authors should disclose commercial ties or consulting, stock or share interests or patent license arrangements that can be viewed as a conflict of interest in relation to the manuscript presented (**Author Declaration Form & Conflict Of Interest Statement**).

Permissions

Obtaining permission form the copyright owner/ owners is obligatory for figures, tables or texts that previously published elsewhere if the authors want to add them to their manuscripts. Without this evidence, any material used in the article will be deemed to be an original product of the authors.

Units of measurement

The *International System of Units* (SI) is the modern form of the metric system, and is the most widely used system of measurement. Therefore, units of measurement should be presented using the International System of Units in Experimental Biomedical Research.

Abbreviations

Abbreviations are defined at the first mention and are then used continuously. The authors should always be used standard abbreviations and generic names of the drugs. Additionally, the abbreviations presented in the Tables and Figures must

be compatible with SI. If registered trademarks are used, the name and country of the manufacturer must be given in parentheses following the generic name on the first use.

Preparation of Manuscript

Title Page

The title page should include: manuscript title, the name(s), the affiliation(s) and address (es) of the author(s).

The corresponding author information should include the e-mail address, the 16-digit ORCID ID, telephone number(s) and full mailing address.

Disclosure of conflict of interest, funding organizations and acknowledgments of people, grants, funds, etc. should be placed in the last section on the title page.

Abstract

Abstracts must not exceed 250 words. The abstract should describe with subheadings; *Aim, Method, Results, and Conclusions*. Abstracts should not be contain any unexplained abbreviations or references. It is crucial that the abstract be an accurate summary of the contents of the paper.

Keywords

4 to 6 keywords are sufficient which can be recommended by the **"Index Medicus Subject Headings": MeSH (http://www.nlm.nih.gov/mesh/meshhome.html)**.

Main Text

The main text should describe with subheadings; *Introduction, Methods and Materials, Results, Discussion and Conclusions*. Manuscripts should be submitted in Microsoft Office Word formats and arranged as 12-point Times New Roman for text. References to literature, figures and tables should be placed in the order of their citation in the text. The Author(s) should not use italics, bold or underlined words in the texts. Please use only generic names of drugs.

Introduction: Introduction to a research report should provide a context for the study and specify the particular aims of the reported study. In this section, the emphasis should be on brevity, for the introduction is not meant to be a detailed review but merely a capsule summary that provides a rationale for the second and most important part which is a clear statement as to why the study was undertaken.

Metods and Materials : In this section, the researcher should clearly write the methods used. The materials section should contain the information requested when the reported results need to be expanded and elaborated. It is also important to carry out appropriate statistical tests and to state the sources of the drugs and chemicals used.

Results: In this section, the authors should clearly written information collected using the methods described to achieve the objectives of the study.

Discussion: The discussion section is critical, the information collected is evaluated in relation to the objectives of the study and the context in which the study begins, and any inconsistency between the results is explained and elaborated.

References: It is important that the authors cite appropriate and up-to-date articles for information and comments in the text.

Conflicts of Interest

Authors must declare all relevant interests that could be perceived as conflicting. Authors should explain why each interest may represent a conflict. If no conflicts exist, the authors should state this. Submitting authors are responsible for coauthors declaring their interests.

References

Number references in the order they are mentioned in the text; do not alphabetize. Reference citations in the text should be identified by numbers in square brackets. In listing references (Format AMA), follow NLM Style Guide , abbreviating names of journals according to Index Medicus. Indicate each author's family name followed by a space and initials closed up without periods. Author names should be separated with a comma, never using the conjunction "and" between entries. All authors must be listed for papers with 1 to 3 authors. For papers with more than 3 authors, only the first 3 authors must be listed, followed by et al.

For online journals or articles published online ahead of print, provide the DOI number, if possible, rather than the URL. URLs used in references will not be made hyperlinks.

Journal article

List the first three authors;

Dilek G, Calik Y, Ozkuk K. Effect of vitamin D level and polypharmacy on the risk of falls in the elderly. Exp Biomed Res. 20214 ;(2): 81-88.

More than three authors followed by et al.

Yenigun V, Azzawri A, Acar M, et al. Alcoholic extract of Tarantula cubensis (Theranekron®) induce autophagy on gastric cancer cells. Exp Biomed Res. 2021;4(2): 89-98.

Chapter in a book

Luck H. Catalase. In: Bergmeyer HU, edİtor. Methods of Enzymatic Analysis. New York: Academic Press; 1971. p. 885-93.

Online document

Doe J. Title of subordinate document. In: The dictionary of substances and their effects. Royal Society of Chemistry. [cited 2016 Dec 27]. Available from:http://www.rsc.org/dose/title of subordinate document.

The authors are responsible for the accurate and in full presentation in accordance with the journal's style of references.

Preparation of Figures and Tables

The figures and tables should be uploaded electronically by a separate file and should be stated consecutively in the text. Each table should have an explanatory heading, and if numerical measurements are made, the units should be added to the column header. Figures should be presented in vector image formats (Illustrator, EPS, WMF, FreeHand, CorelDraw, PowerPoint, Excel etc.) or in bitmap formats (Photoshop, TIFF, GIF, JPEG, etc.). Bitmap images should be at least 300 dpi resolution.

Supplementary Materials

Authors can submit one file of supplementary material such as audio files, video clips, or datasets. A section titled "Supplementary Material" should be included before the references list with a concise description for each supplementary material file. Authors are responsible for providing the final supplementary materials files that will be published along with the article.

English Language Editing

Editors and reviewers should ensure the clarity of English language of the article in assessment of the manuscript. Therefore, articles without clear language will not be forwarded for review process.

If any help needed in writing in English one can consider the following:

- Ask for help from a co-worker who is a native English speaker in sake of clarity of the text.
- Applying to a professional english language editing service to improve the quality of the language and grammar of the text.

Authors should aware that the use of a language editing service does not warrant an article to be accepted for publication in this journal.

ETHICAL STANDARDS

Ethical Responsibilities of Authors

Experimental Biomedical Research journal will follow the **Committee on Publication Ethics (COPE)** guidelines on how to deal with potential acts of misconduct. For this reason, authors should protected the journal trust, the professionalism of the scientific authorship, and must refrain from misrepresenting the consequences of research that could destroy all scientific effort.

Plagiarism checking

Articles sent to Experimental Biomedical Research journal are checked for possible plagiarism by using an appropriate software (**iThenticate**). However, corresponding and co-authors are responsible for any fraud, intentional or unintentional malpractice.

Research involving human participants and/or animals

Experimental Biomedical Research adopt ICMJE Recommendations on Protection of Research Participants. For more information, **click here!**

In addition to ICMJE recommendations, we also support 3Rs principals **(Replacement, Reduction and Refinement)** for humans and animals usage in research. Briefly 3Rs are mentioned below, and more information can be **accessed here!**

Replacement: approaches which avoid or replace the use of animals

Reduction: approaches which minimise the number of animals used per experiment

Refinement: approaches which minimise animal suffering and improve welfare

All work should be done with the permission of local human subjects or animal care committees (institutional and national) and clinical trials should be registered to legislation. The official numbers from these committees must be found in the Materials and Methods section (or text describing the experimental procedures).

1) Statement of human rights

The studies involving human participants should state that the research has been endorsed by the institutional and / or national research ethics committee and that it is conducted in accordance with the ethical standards set out in the **Helsinki Declaration** , and that subsequent changes are also met.

2) Statement on the welfare of animals

If you have done experimental research on animals, authors should indicate whether the international, national and / or institutional guidelines for the care and use of the animals are followed, and whether the work has been approved by an institutional research ethics committee.

Informed consent

If manuscripts report the results of an experimental research of human subjects, all authors must fulfill the **International Committee of Medical Journal Editors (ICMJE)** requirements on confidentiality and informed consent from patients and study participants. Therefore;

1- Informed consent is obtained from all participants before they are included in the work.

2- Distinguishing details of the participants examined (name, date of birth, identification numbers and other information) should not be published in print, photographs and genetic profiles.

3-Where someone is deceased, please make sure that you have written permission from the family or estate.

4-If the identification features are changed to protect anonymity as in genetic profiling, the authors should assure that the changes do not distort scientific meaning.

Authors may use this **Patient Consent Form**, which sent to the journal if requested.

The journal reserve the right to reject manuscripts that do not comply with the above-mentioned guidelines.

Publication charges

There are no submission fees, publication fees, or page fees for the journal Experimental Biomedical Research.

Copyright and License Policy

Copyright (c): *Author(s)*

License*-This journal is licensed under a* ***Creative Commons Attribution 4.0 International License.***

Journal articles are published under the CC BY license (https://creativecommons.org/licenses/by/4.0/). Authors retain the copyright and full publishing rights without restrictions and agree to make their original works completely available and free to use, copy and/or redistribute in all formats without permission, as long as the authors and the original source are properly cited.

Proofs

Accepted articles are sent as portable document format (PDF) files, along with proof by e-mail to the relevant author for approval. Corrections to PDF evidence should be limited to posting errors only, and no significant additions / deletions should be made. Authors are responsible for all statements made in their work, including changes made by the copy editor and authorized by the author concerned. Authors are strongly advised to thoroughly examine the PDF evidence and return the proofs within 3 days.

Post-publication correction/retraction process

A published version of an article may need to be modified. This can be in the form of a Correction notice or a Retraction. In this case, necessary changes will be made after careful consideration by the Chief Editor, who is also supported by the Experimental Biomedical Research Editorial Team, to ensure that they are made in accordance with the guidelines of Committee on Publication Ethics (COPE).

Any necessary changes will be permanently linked to the original article and accompanied by a post-publication notice to ensure the integrity of the scientific record and to keep readers fully informed of any necessary changes. All correction and retraction notices are free to access at the point of publication.

Correction notice

An error or omission that may affect the interpretation of the article will be published as a "Correction notice", which does not impair its scientific integrity.

All major errors are accompanied by a correction notice that provides clear details of the errors and changes made in the published version.

Any minor errors will not be accompanied by a separate correction notice. Instead a footnote will be added to the article detailing to the reader that the article has been corrected.

Retractions

A Retraction notice will be issued in the following cases:

- A major error in the analysis or methods that invalidate the results in the article.
- Research misconduct or publication misconduct due to research without required ethical approvals, fabricated data, manipulated images, plagiarism, duplicate publication.

The decision to withdraw an article will be made in accordance with COPE guidelines and will include research conducted in collaboration with the Experimental Biomedical Research Chief Editor and Editorial Team.

In cases where a decision to withdraw an article is made:

- A "retracted" watermark is added to the published version of the article.
- A separate retraction notice titled "Withdrawal: [article title]" will be posted in connection with the retracted article.
- The withdrawal statement is paginated and published in the online issue of the journal.

Archiving

This journal utilizes the LOCKSS and CLOCKSS systems to create a distributed archiving system among participating libraries and permits those libraries to create permanent archives of the journal for purposes of preservation and restoration.

Repository policy

Published version: OA publishing, no embargo, Licence-CC BY, For all licenses, authors retain copyright and full publication rights without restriction.

Experimental Biomedical Research

E-mail: info@experimentalbiomedicalresearch.com

Completed authorship forms may be mailed to this address.

Peer Review Policy-Process

Experimental Biomedical Research is an online-only, international, peer-reviewed, open access journal and is committed to maintaining the high quality of the peer-review process. Experimental Biomedical Research reviews new submissions according to journal guidelines. When they meet all criteria, they are sent to two referees (double blind) and all manuscripts are read by reviewers, and revisions to the manuscript may be required. If the decision conflicts between two reviewers, it will be send to third peer reviewer. The typical review will take in 2-4 weeks. As a result of the evaluations, one of the following decisions is made by the Editor-in-Chief in line with the opinions and suggestions of the referees:: 1) accepted manuscript without revisions, 2) invite authors to resubmit the manuscript after minor or major changes while the final decision is kept pending, 3) or reject the manuscript. When the manuscript is returned for revision prior to acceptance, the revised manuscript must be submitted within 30 days after the author's receipt of the referee's reports. Revised article: Accept/Reject/Re-revise. The final decision is sent to the authors.

Double blinded peer review process

Manuscript Submission

- New submission via online system
- Cover letter, author and co-author details, manuscript and separate files

Pre- Quality Assessment

- Plagiarism check
- Qualification in the English language editing
- Ensuring that the manuscript adheres to the stylistic and bibliographic requirements outlined in the Author Guidelines (Experimental Biomedical Research- Submission and Publication Checklist)
- Sent back to author for approval of edits

Peer Review

- Double-blind peer review undertaken by experts in the field
- As a result of the evaluations, one of the following decisions is made by the Editor-in-Chief in line with the opinions and suggestions of the referees: 1) accepted manuscript without revisions, 2) invite authors to resubmit the manuscript after minor or major changes while the final decision is kept pending, 3) or reject the manuscript.

- Revision made by authors on the basis of reviewer recommendations (revisions must be highlighted and accompanied by a letter in response to each comment by the reviewers)
- Revised article: Accept/Reject/Re-revise

Copy Editing

- Professional checking for the composition and organization (formatting) of the paper against the journal guidelines
- Reference styling and proof corrections
- Author's confirmation of the final edited manuscript before publication
- In this version, corrections to PDF evidence should be limited to posting errors only, and no significant additions / deletions should be made

Publishing

- Accepted article is sent for generating the galley proof
- Online publication of the manuscript

ISSN 2618-6454

Exp Biomed Res 2023; 6(1): 1-5 **DOI: 10.30714/j-ebr.2022.164**

Experimental Biomedical Research *Original article*

Viability effects on cell cycle synchronization of different prostate cancer cell lines: A brief report

Bodil Hernroth, Helena Tassidis*

Department of Bioanalyze, Kristianstad University, SE-291 88 Kristianstad, Sweden

ABSTRACT

Aim: Serum deprivation is often used to synchronize cells in G0/G1 phase for comparative *in vitro* studies. Here we aimed to investigate the effect on viability of the three commonly used prostate cancer-cell lines PC3, LNCaP and DU145 after serum deprivation.

Methods: The cell lines were cultured in standard culture medium (controls) and under serum deprivation for 48 and 72 h. Then the proportion of cells in G0/G1 phase was analysed by flow cytometry and cell morphology was microscopically investigated. The cells were allowed to recover for three days in standard culture condition before cell viability (using MTT assay) was analysed.

Results: In comparison to control cells, significant effects on cell cycle arrest in G0/G1 phase were noted for DU145 and PC3 cells and the cell morphology was negatively affected in a time-dependent manner. These parameters were unaffected in LNCaP cells. After three days of recovery, the viability of DU145 and PC3 cells was significantly reduced compared to LNCaP.

Conclusions: Serum deprivation showed different effects on the prostate cancer cells, probably due to differences in growth rate. Such effects on viability should be considered as an obstacle for comparative studies.

Key words: Serum deprivation, synchronization, cell cycle, viability.

**Helena Tassidis,*
Department of Bioanalyze, Kristianstad University, SE-291 88 Kristianstad, Sweden
E-mail: helena.tassidis@hkr.se
Received: 2022-11-06 / Revisisons: 2022-11-12
Accepted: 2022-11-16 / Published: 2023-01-01

Introduction

The stage of aggressive, metastatic prostate cancer is incurable and the major challenge is therapeutic resistance to androgen-deprivation therapy (ADT) and chemotherapy [1-3]. Thus, there is a great demand for development and much research is underway to overcome the resistance through e.g. improvements of cytotoxic drugs, inconsistent cell cycle signals, or development of death signals [4]. For this kind of studies human prostate cancer (PCa) cell lines are commercially available and it is crucial to include different biological characteristics, represented by e.g. the commonly used PC3, DU145, LNCaP cell lines.

The PC3 cell line is of epithelial origin and was isolated from bone metastases with low degree of differentiation [5]. The DU145 cell line is of primary prostate adenocarcinoma origin and isolated from a central nervous system metastasis [6]. Androgen receptors are expressed [7] but the cell line is not androgen sensitive and has a lower metastatic potential than PC3 cells [8]. The LNCaP cell line was established from metastasis

in lymph node [9] and represents early androgen dependent PCa.

For comparative or kinetic studies of cell cycle progression, or to distinguish cell cycle stage sensitivity it is highly desirable to synchronize the cells. Serum deprivation has long been known to arrest cells in G0/G1 phase by withdrawing growth factors and other related components from cultured cells [10]. However, as reviewed by Davis et al. [11] consequences on the overall physiology of the cell should be better explored since tumour cells may have different requirements of serum content. Here, we intended to compare the response to synchronization in G0/G1 phase in the PCa-cell lines PC3, DU145 and LNCaP and possible consequences on their viability.

Materials and Metods

Prior to the serum deprivation experiment, the cell lines were cultured in standard cell culture conditions. PC3 and DU145 were maintained in Dulbecco's modified Eagle's medium (DMEM; Life Technologies) and LNCaP in Roswell Park Memorial Institute 1640 (RPMI 1640; Life Technologies) supplemented with 10% fetal calf serum (FCS; Life Technologies) and 1% penicillin-streptomycin (PenStrep; 100 U/ml; Sigma–Aldrich) [12]. For the experiment they were subcultured into 35- or 60-mm culture dishes without antibiotics (Polystyren, Sarstedt) until reaching 90% confluence. Then, the culture medium was replaced with specified serum concentrations during different culture times (as indicated in the Figure 1) and control cells were maintained in standard culture conditions (10% serum).

Cell morphology was documented with light-microscopy and cell cycle phases were analysed with flow cytometry. Briefly, cells were fixed with 70% ice-cold ethanol and treated with 50 mg/ml RNase A (Roche) and 50 mg/ml PI (Sigma-Aldrich) for 30 min. The cells were then subjected to flow cytometry (Novocyte™; ACEA Bioscience, San Diego, CA, USA). Data acquisition and cell-cycle distribution (Watson model) were carried out using NovoExpress (Novocyte™; ACEA) [12]. After recovery in standard culture conditions for three days, cell viability was analysed using 3-(4,5-dimethyl-thiazol-2-yl)-2,5-diphenyl-tetrazolium bromide (MTT; Cell Proliferation Kit I, Roche) according to the manufacturer´s instructions. In brief, cells were seeded into 96-well plates (Sarstedt) at a cell density of 2 000 cells/well with standard culture conditions. After three days of recovery 0.5 mg/ml MTT was added and the optical density was measured in a microplate reader after solubilization (Victor™ X4, # 2030 Multilabel Reader; Perkin Elmer Inc., Akron, OH, USA) at wavelength of 595 nm. Data analysis as described in the Figure 1.

Results

LNCaP cells showed no obvious morphological changes and no significant changes of the proportion of cells in G1/G0 phase (Figure 1a). This proportion was high (~75%) even in those not exposed to deprivation. After 48 h deprivation of the DU145 and PC3 cell lines morphological differences were noted and after 72 h a lot of rounded, detached cells were shown (Figure 1b and c). The proportion of cells in G0/G1 phase increased significantly in a time dependent manner (Figure 1b and c).

After three days of recovery, the viability of LNCaP was not affected for those starved for 48 h but slightly reduced after 72 h treatment (Figure 1d). The viability of DU145 and PC3 cells was significantly reduced after serum deprivation for 48 and 72 h respectively, particularly for PC3 cells.

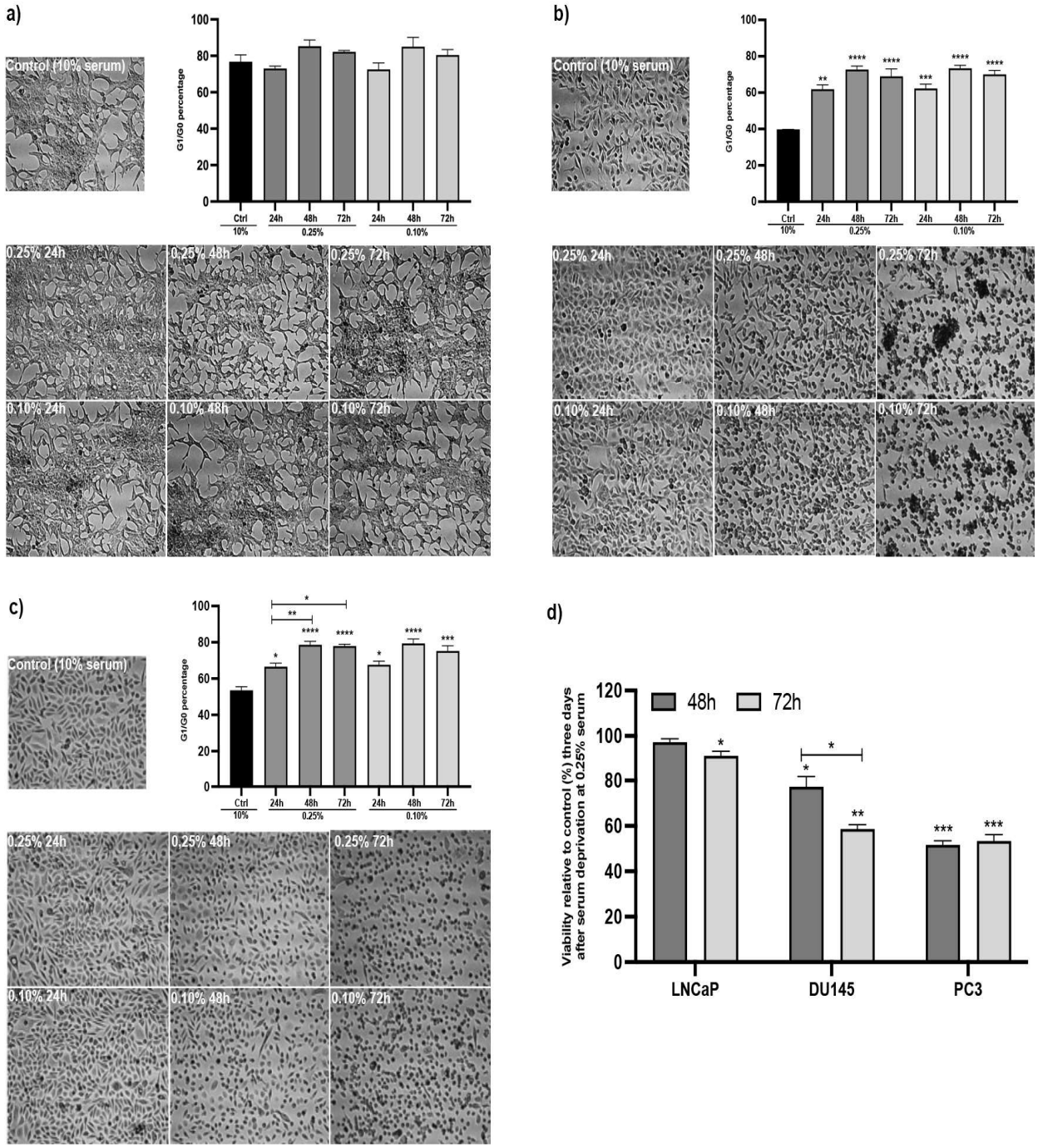

Figure 1. Morphology and flow cytometric analysis of cell cycle after serum deprivation for either 48 or 72 h a) LNCaP, b) DU145 and c) PC3. Cell viability (MTT-assay) was analysed after three days of recovery d). Data are expressed as mean ± SEM of at least three independent experiments for cell cycle analysis and two independent experiments performed in triplicates for viability after recovery. Shapiro-Wilk test was used to analyse normal distribution and ordinary one-way ANOVA with Tukey's test for multiple comparison was used to analyse statistical significance using Prism 9.00. Statistically significantly differences compared to controls are indicated as: *$p<0.05$, **$p<0.01$, ***$p<0.001$, and ****$p<0.0001$.

Discussion

The results showed different response upon serum deprivation between the three classical cell lines commonly used for *in vitro* experiments in PCa research. LNCaP is a slow-growing PCa cell line with a doubling time of 60-72 h depending on serum concentration [13] which could explain the insignificant effect after 72 h of deprivation. The faster doubling time (33-34 h) [13] of PC3 cells is more energy demanding and a likely reason for the lower viability compared to that for LNCaP. It has been reported that PC3 and DU145 after serum deprivation and G1 arrest were more sensitive to anandamide compared to that of LNCaP [14]. However, according to the results of the present study it is difficult to determine whether the difference is due to LNCaP not being affected by the deprivation and thus coping better with the toxic treatment [14]. Thus, time of serum deprivation should be adapted to the doubling time of each cell line to obtain comparable, viable cells after cell cycle synchronization.

Conclusion

Impaired condition in response to serum deprivation is important to take into account in experimental studies where e.g. treatments using different PCa cell lines are compared. Effects of cell cycle synchronization on cell viability should thus always be considered prior to the experiments.

Acknowledgement: *The authors thank Ms. Sofie Isaksson for laboratory assistance.*

Funding: *The authors received no financial support for the research, authorship, and/or publication of this article.*

Conflict of Interest: *The authors declare that they have no conflict of interest.*

Ethical statement*: Ethics committee decision was not taken as it was a cell culture study.*

References

[1]Crawford ED, Petrylak D, Sartor O. Navigating the evolving therapeutic landscape in advanced prostate cancer. Urol Oncol. 2017;35S:S1-S13.

[2]Siegel RL, Miller KD, Jemal A. Cancer Statistics, 2017. CA Cancer J Clin. 2017;67(1):7-30.

[3]Wade CA, Kyprianou N. Profiling Prostate Cancer Therapeutic Resistance. Int J Mol Sci. 2018;19(3).

[4]Vaux DL, Strasser A. The molecular biology of apoptosis. Proc Natl Acad Sci U S A. 1996;93(6):2239-44.

[5]Tai S, Sun Y, Squires JM, et al. PC3 is a cell line characteristic of prostatic small cell carcinoma. Prostate. 2011;71(15):1668-79.

[6]Stone KR, Mickey DD, Wunderli H, et al. Isolation of a human prostate carcinoma cell line (DU 145). Int J Cancer. 1978;21(3):274-81.

[7]Alimirah F, Chen J, Basrawala Z, et al. DU-145 and PC-3 human prostate cancer cell lines express androgen receptor: implications for the androgen receptor functions and regulation. FEBS Lett. 2006;580(9):2294-300.

[8] Pulukuri SM, Rao JS. Matrix metalloproteinase-1 promotes prostate tumor growth and metastasis. Int J Oncol. 2008;32(4):757-65.

[9] Horoszewicz JS, Leong SS, Chu TM, et al. The LNCaP cell line--a new model for studies on human prostatic carcinoma. Prog Clin Biol Res. 1980;37:115-32.

[10] Brooks RF. Regulation of fibroblast cell cycle by serum. Nature. 1976;260(5548):248-50.

[11] Davis PK, Ho A, Dowdy SF. Biological methods for cell-cycle synchronization of mammalian cells. Biotechniques. 2001;30(6):1322-6, 8, 30-1.

[12] Hernroth B, Holm I, Gondikas A, et al. Manganese Inhibits Viability of Prostate Cancer Cells. Anticancer Res. 2018;38(1):137-45.

[13] Cunningham D, You Z. In vitro and in vivo model systems used in prostate cancer research. J Biol Methods. 2015;2(1).

[14] Mimeault M, Pommery N, Wattez N, et al. Anti-proliferative and apoptotic effects of anandamide in human prostatic cancer cell lines: implication of epidermal growth factor receptor down-regulation and ceramide production. Prostate. 2003;56(1):1-12.

Exp Biomed Res 2023; 6(1): 6-13 **DOI: 10.30714/j-ebr.2022.165**

Experimental Biomedical Research *Original article*

Anti-proliferative effects of salmon calcitonin on SH-SY5Y neuroblastoma *in vitro*

Muhammed Ismail Varol[1*], Seyda Karabork[2], Ayhan Cetinkaya[3]

[1]*Department of Medical Biology, Bolu Abant İzzet Baysal University, Faculty of Medicine, Bolu, Türkiye*

[2]*Department of Medical Microbiology, Bolu Abant İzzet Baysal University, Faculty of Medicine, Bolu, Türkiye*

[3]*Department of Physiology, Bolu Abant İzzet Baysal University, Faculty of Medicine, Bolu, Türkiye*

ABSTRACT

Aim: We aimed to examine the potential cytotoxic effect of salmon calcitonin, which is one of the components that regulates mineral metabolism and prevents the increase in the amount of calcium, on SH-SY5Y cells, a neuroblastoma cell line.

Methods: SH-SY5Y cells were cultured in DMEM medium in the presence of 37°C and 5% CO_2 in conventional culture flasks. MTT assay was applied to investigate the effect of calcitonin individually on SH-SY5Y cells by treatment different concentrations for 24 h and performed.

Results: In cells cultured with salmon calcitonin applied at different concentrations (0.1, 1, 3.125, 6,25, 12.5, 25, 50 and 100 nM/ml), anti-proliferation was statistically significant at concentrations of 50 and 100 nM/ml compared to the control group. It showed that 50 nM/ml and 100 nM/ml had the highest cytotoxic effect on SH-SY5Y for 24 h

Conclusions: Considering the proliferation curve of SH-SY5Y, the results show that salmon calcitonin treatment potentiated the proliferative activities by inhibiting cell viability in SH-SY5Y cells at concentrations of 50 and 100 nM/ml. Further studies exploring salmon calcitonin's protective effects may prove successful and maybe it is a promising agent for cancer treatment.

Key words: Salmon calcitonin, SH-SY5Y, anti-proliferative effect, neuroblastoma.

✉ * *Dr. Muhammed Ismail Varol,*

Department of Medical Biology, Bolu Abant İzzet Baysal University, Faculty of Medicine, Bolu, Türkiye

E-mail: muhammedismail.varol@ibu.edu.tr

Received: 2022-06-15 / Revisisons: 2022-08-13

Accepted: 2022-11-24 / Published: 2023-01-01

Introduction

It is known that cancer is the most important cause of death worldwide. There are extensive studies on the development of less toxic anti-cancer drugs that continue intensively to find potential targets and promising anti-cancer approaches [1, 2]. Neuroblastoma is one of the extra cranial solid tumors seen in one in 7000 live births among childhood cancers [3]. It is a biologically diverse tumor with varying clinical course and prognosis depending on age at diagnosis, histology, and molecular pathway characteristics [4]. In its treatment, alkylating agents with serious side effects such as cisplatin are used [5]. In addition, despite aggressive treatments, treatment success is very low due to high drug resistance [6].

Since SH-SY5Y can be transformed into various types of functional neurons by the addition of specific compounds, it is preferred as a suitable model for studies on

neurodegenerative disorders and modeling neurodegenerative diseases.

Salmon calcitonin (sCT) is a single-chain peptide hormone containing 32 amino acids with a molecular weight of approximately 3500 Da. There are four types of sCT used in the clinic: human, pig, eel, and sCT derived [7]. The main role of calcitonin is to regulate mineral metabolism and help to eliminate the increase in calcium level called 'calcium stress' [8]. Evidence has been suggested that sCT is closely related to the glutamatergic system such as NMDA and AMPA receptors and causes glutamate release [9, 10, 11].

In the literature, antiproliferative effects on the different one of sCT were not found. However, there are studies on calcitonin (CT). One of these demonstrated expression (calcitonin-induced) of transforming growth factor (TGF-21) as an antiproliferative on Lactotrophs in rats [12]. In another study, it was stated that CT was associated with the breasts [13]. They determined that calcitonin inhibited it at a rate of 1/4 in primary tumors (expression of uPA mRNA).

In a different study, it was shown that CT and its receptor (CTR) significantly reduced tumor growth with its autocrine supplement, and they also stated that it is a potential option in invasive cancers. In the details of the study, they emphasized that the urokinase type plasminogen activator and survivin were at a low rate, thus activating the uPA-uPAR axis and the PI-3-kinase-Akt-survivin pathway [14]. However, the effects of sCT on the CNS still remain unclear. There are many studies on the neuroblastoma cell line in the literature [15, 16]. No specific data were found on the effect of sCT on SH-SY5Y. In this study, we aimed to investigate the anti-proliferative effect of sCT in SH-SY5Y neuroblastoma cells, which are frequently preferred in neurotoxicity and neurodegenerative processes.

Materials and metods

We confirm that no permission from an ethical committee is necessary for the cell cultures utilized in the study. The study was carried out *in vitro* and was carried out using Bolu Abant İzzet Baysal University, Faculty of Medicine, and Physiology Department research laboratory and cell culture laboratory facilities.

Drugs and reagents

sCT used in the study was obtained from CT (natural, 98%, Santa Cruz Biotechnology, Inc. CAS 47931-85-1 Dallas, TX, USA). Fetal bovine for cell culture experiment (Sigma-Aldrich, Schnelldorf, Germany), penicillin-streptomycin as antibiotic (Capricorn Scientific Ebsdorfergrund, Germany), trypsin, EDTA solution (Hyclone, Logan, UT, USA), dimethyl sulfoxide (DMSO), phosphate buffered water (PBS) and Dulbecco's Modified Eagle Medium/F-12 (DMEM/F-12) medium (Pan-Biotech, Aidenbach, Germany). In the *in vitro* assay step, sCT was diluted to different concentrations by dissolving in high-grade water to obtain final concentrations.

Cell culture

The SH-SY5Y human neuroblastoma cell line purchased from ATCC (ATCC CRL-2266, Manassas, VA, USA) was used in this study. The cell culture protocol was performed as described in previously published studies [17]. Briefly, cells were rapidly thawed in a 37°C water bath and then centrifuged at 3000 rpm for 4 minutes. After centrifugation, all cells were cultured in 75 cm flasks containing supplemented DMEM/F12 mixture/full medium supplemented with 10% heat-inactivated FBS and 1% penicillin-streptomycin at 37°C in a humidified incubator with 5% CO_2. The next day, the growth medium

was changed to remove any DMSO that may be present in the freezing medium. Cells were maintained at log phase and medium was replaced with fresh medium every 3-4 days. Cell morphologies and growth rates of the cell line were monitored daily under an inverted microscope (Olympus CKX41, Tokyo, Japan) and passaged by separation with 0.25% Trypsin-EDTA when cells reached 70-80% confluence.

Drug administration - Salmon calcitonin treatment:

After reaching the appropriate confluence, the cells were passaged and 100 µl equal volumes of sCT concentrations prepared to be 0.1, 1, 3.125, 6,25, 12.5, 25, 50 and 100 nM/ml were given to the cells and used defined times incubated. For each dose, 2 wells were inoculated and cells were incubated in a humid environment at 37ºC in a 5% CO_2 air mixture.

Cell viability assay

Trypan blue was used to determine cell viability and cell numbers. BioRad TC20 Automated Cell Counter (California, USA) was used to measure cell viability and cell numbers. Cytotoxicity experiments were performed in duplicate and GraphPad Prism 5.0 software (GraphPad Software, San Diego, USA) was used for data analysis. All cells were counted and approximately $1.5x10^4$ cells were seeded into wells in a total volume of 200 µL in 96-well plates. Plates were then incubated at 37 °C for 24 hours for cell attachment.

First, the dose was determined, for this the cells in the wells were harvested with 0.5% trypsin and centrifuged. After discarding the supernatant portions, they were suspended with 1 ml of medium and counted with an Automated Cell Counter. The ID50 (Inhibition dose 50%) dose for sCT was determined by recording the total cell counts. Eight different doses were administered to see the effects of sCT on SH-SY5Y.

When the cell line was ready for 70-80% confluence in flasks, they were seeded into 96-well plates and after 24 h of holding, different dilutions of sCT (0.1, 1, 3.125, 6,25, 12.5, 25, 50 and 100 nM/ml) were added) was incubated for 48 hours. Cells incubated in 10% FBS were used as positive control and the viability of the cells was evaluated by MTT (3-[4,5-dimethylthiazol-2-yl]-2,5-diphenyl- tetrazolium bromide) (Serva, Germany) method. Briefly, 10 µl of MTT reagent was added to each well and the 96-well plate was incubated at 37°C for 4 hours, then DMSO was added to the cells. Absorbance values were read with a colorimetric reader (spectrophotometer) (Epoch BioTek Instru-ments, Inc., Highland Park, USA) at 570 nm. The most appropriate proliferative and inhibitory doses of sCT for cells were determined. Thus, the effect of sCT on the viability of cultured cells and the duration of the effective dose were determined. Negative control (Medium control) = salmon calcitonin concentration + DMEM/F12 medium and Positive control (DMSO control) = %10 DMSO was applied. Data from each sCT dose were compared with the mean of the negative control. Control group means and data taken at each dose are given as the mean ± SD of each in two parallels. We used our control group for the test of MTT, in which we evaluated the viability of cells. Untreated cells exposed to maximum solvent concentrations with DMSO were used to determine the metabolic activities of this control group.

Statistical analysis

Statistical analyzes were done with SPSS 26.0 package statistics program (New York, USA). Multi-dimensional statistical evaluations were made on the obtained data. Since the measurement values did not show homogeneous distribution, non-parametric tests were used. The Kruskal-Wallis analysis of variance test was used to evaluate the significance of the difference

between the groups. The difference between two independent groups consisting of continuous variable values was determined with the Mann-Whitney U Test. A probability value of < 0.05 was accepted significant.

Results

In this study, we investigated the anti-proliferative effect of human neuroblastoma cell line SH-SY5Y using sCT as the active ingredient. Neuroblastoma is an extra cranial solid tumor. SH-SY5Y is also widely used in experimental neurological studies, neurodegenerative processes, neurotoxicity and neuroprotection [18]. Eight different doses (0.1, 1, 3.125, 6.25, 12.5, 25, 50 and 100 nM/ml) of sCT were used in the study to demonstrate anti-proliferative effects on SH-SY5Y cell. In culture medium (5% CO_2, 37 °C), SH-SY5Y cells showed normal polygonal morphology (Figure 1).

The anti-proliferative effect of especially 50 and 100 (nM/ml) sCT from eight different doses is clearly noticeable ($p<0.05$). When these two doses are compared with the control group, 100 nM/ml seems to be 1.16 times more effective than 50 nM/ml. Negative control value 0.27; 0.289; 0.208 (mean=0.25) and Positive control value 0.124; 0.148; 0.168 (mean=0.14). Applications of sCT below these two doses did not show an anti-proliferative or proliferative effect (Figure 2).

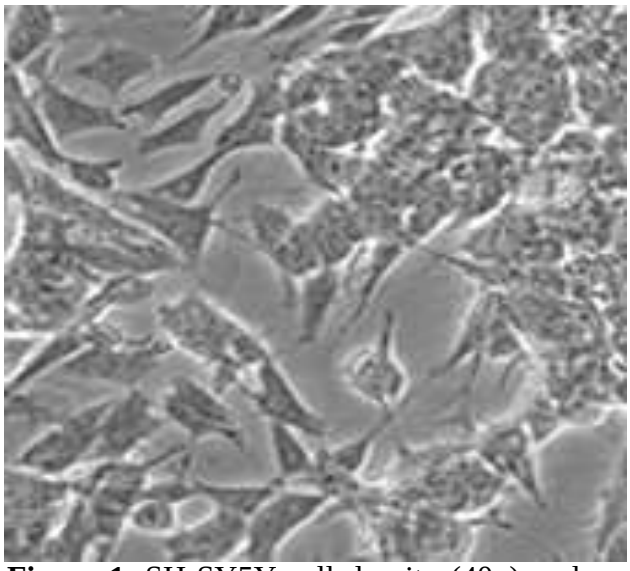

Figure 1. SH-SY5Y cell density (40x) under a light-inverted microscope.

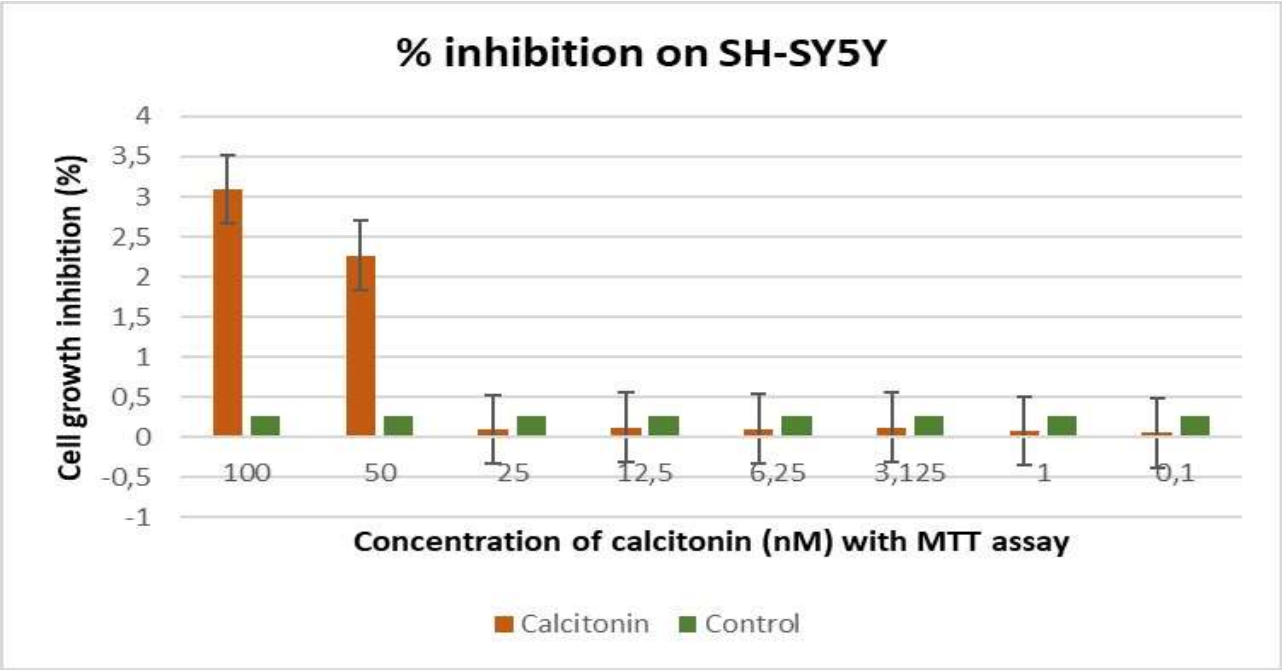

Figure 2. The anti-growth effect using MTT assay after treatment with the salmon calcitonin for 24 h.

sCT administrations below these two doses did not show an anti-proliferative or proliferative effect (Figure 2). According to the results, it is clearly noticed that sCT has an anti-proliferative effect on SH-SY5Y cells at doses of 50 and 100 nM/ml. At other doses and control, the effect is below zero. As shown in Figure 2, treatment of the SH-SY5Y cell line with the sCT displays concentration dependence decline in cell viability. Our results showed that the particularly suppressive effect begins in the first 24 h ($p<0.01$ vs. the control group). The high dose of sCT has a significantly suppressive effect ($p=0.003$ versus control group). The lower dose of sCT, there appears some effect on the SH-SY5Y proliferation but it is not that significantly effect ($p=0.874$). These findings showed that a dose-dependent inhibition of SH-SY5Y proliferation by sCT.

Discussion

Despite the advances in cancer research, one of the problems encountered is that chemotherapy methods can cause serious side effects by damaging cancer cells as well as healthy ones [19]. For this reason, anti-cancer drug researches with low toxicity continue to maintain their importance. Neuroblastoma is becoming more widely known, but there are still no reliable therapies for it. As a result, researchers are looking for new, efficient medications to treat neuroblastoma [20]. The drug sCT is a therapeutic option for many years, which is used in the treatment of postmenopausal (5 years) osteoporosis in women, bone diseases and Paget's disease. Although it has been found to have some antiproliferative, apoptotic effects on some cancers are known, it has not been clarified yet sCT has a friendly or foe effect on cancer [8].

In the current study we investigated the anti-proliferative effects of sCT in SH-SY5Y cell lines. Although the benefits of sCT on some cancer treatments are known [8, 13, 14], there are limited data on neuroblastoma cell line (SH-SY5Y) at different doses is available in the literature. According to the findings of Sabbisetti et al., who report that the effects of sCT are accelerated at concentrations higher than 50 nM, the results presented here showed that sCT could inhibit the growth of SH-SY5Y at higher doses (50-100 nM/ml) for 24 h [21]. Furthermore, according to our research, SH-SY5Y cells treated with sCT at different concentrations for 24 h had a cell number inhibition. It is believed that the reason of the high dose depence is due to the sCT's some properties such as genetic, physiological, and pharmacokinetic variation among different cancer and/or different cell lines.

These findings suggested that sCT might be a medication with some promise for the treatment of neuroblastoma *in vitro*. Additionally, contrasting studies with some calcitonin subtypes have suggested that advantageous effects on nervous system. Researchers showed that sCT is closely related to the glutamatergic system and glutamate releasing [10, 11]. Also one year later, Taşkıran et al. investigated the effect of sCT on glutamate-induced cytotoxicity in C6 glial cells involved in the inflammatory and nitric oxide pathways, due to the main mechanisms and impact on glutamate-induced cytotoxicity are still unknown. As a results of their research, sCT inhibits nitric oxide and inflammatory pathways to protect against glutamate-induced cytotoxicity in C6 glial cells. For those with neurodegenerative symptoms, sCT may be a helpful supportive medication [22]. Therefore, our findings confirm the evidence of inhibition effect of sCT on SH-SY5Y cells. Studies conducted both *in vivo* and *in vitro* have shown that sCT has beneficial effects on the different system especially nervous system and some cancer types such as breast, prostate [23].

One study highlights that CT is a stimulant for angiogenesis [24].

Although it has been mentioned that he possibility of sCT causing cancer has been studied and CT can provide invasion of some tumor by metastases *in vivo*. However, these results contradict other published studies on CT biology [25, 26, 27], so we advise conducting more research on this topic to verify us believe further. Wells et al., Ng et al. and Thomas et al. report significant effect of sCT on different cancer types in their studies [27, 28, 29]. Likewise, it is clear from the information we provided in the current study, sCT shows antiproliferative effects on SH-SY5Y cell line *in vitro* and this research paralles the previous studies. Therefore, sCT may be a tropic agent in cancers especially neuroblastoma. The treatment of the SH-SY5Y cell line with sCT reduced cell viability depending on the dosage for 24 h. The results shown here make it abundantly evident that the presence of sCT had a favorable impact on SH-SY5Y proliferation.

Conclusion

To our knowledge, this is the first study which sCT has been evaluated for its antiproliferative effect on SH-SY5Y for different doses *in vitro*. Thus, the findings provided here sCT is a possible therapeutic candidate for *in vitro* treatment of human neuroblastoma cells. Finally, we advise further future research is needed to understand the mechanism of action of sCT in comparison to SH-SY5Y and other neuroblastoma cell lines.

Acknowledgement: *The cell culture experiments in this article were carried out in the Cell Culture Laboratory of Bolu Abant İzzet Baysal University, Faculty of Medicine, Department of Physiology. Also, who provided us the SH-SY5Y neuroblastoma cell line (CRL-2266) used in our study. We would like to thank Dr. Erkan KILINÇ.*

Funding: *The authors received no financial support for the research, authorship, and/or publication of this article.*

Conflict of Interest: *The authors declare that they have no conflict of interest.*

Ethical statement*: Ethics committee decision was not taken as it was a cell culture study.*

References

[1]Sung H, Ferlay J, Siegel RL, et al. Global cancer statistics 2020: Globocan estimates of incidence and mortality worldwide for 36 cancers in 185 countries. CA Cancer J Clin. 2021;71(3):209-49.

[2]Fimognari C, Lenzi M, Hrelia P. Chemoprevention of cancer by isothiocyanates and anthocyanins: mechanisms of action and structure-activity relationship. Curr Med Chem. 2008;15(5):440-447.

[3]London W, Castleberry R, Matthay K, et al. Evidence for an age cutoff greater than 365 days for neuroblastoma risk group stratification in the Children's Oncology Group. J Clin Oncol. 2005;23(27):6459-6465.

[4] Tucker ER, Danielson LS, Innocenti P, et al. Tackling crizotinib resistance: the pathway from drug discovery to the pediatric clinic. Cancer Res. 2015;75(14):2770-2774.

[5] Applebaum MA, Vaksman Z, Lee SM, et al. Neuroblastoma survivors are at increased risk for second malignancies: a report from the International Neuroblastoma Risk Group Project. Eur J Cancer. 2017;72:177-185.

[6] Marengo B, Monti P, Miele M, et al. Etoposide-resistance in a neuroblastoma model cell line is associated with 13q14. 3 mono-allelic deletion and miRNA-15a/16-1 down-regulation. Sci Rep. 2018;8(1):1-15.

[7] Ostrovskaya, A., Findlay, D., Sexton, et al. Calcitonin. In Reference Module in Neuroscience and Biobehavioral Psychology. Elsevier. 2016;1-12.

[8] Chesnut C, Azria M, Silverman S, et al. Salmon calcitonin: a review of current and future therapeutic indications. Osteoporos Int. 2008;19(4):479-491.

[9] Masi L, Mljccim, B. Metabolism B. Calcitonin and calcitonin receptors. Clin Cases Miner Bone Metab. 2007;4(2):117.

[10] Kilinc E, Dagistan Y, Kukner A, et al. Salmon calcitonin ameliorates migraine pain through modulation of CGRP release and dural mast cell degranulation in rats. Clin Exp Pharmacol Physiol. 2018;45(6):536-546.

[11] Taşkıran AS, Ozdemir E, Gumus E, et al. The effects of salmon calcitonin on epileptic seizures, epileptogenesis, and postseizure hippocampal neuronal damage in pentylenetetrazole-induced epilepsy model in rats. Epilepsy Behav. 2020;113:107501.

[12] Wang YQ, Yuan R, Sun YP, et al. Antiproliferative Action of Calcitonin on Lactotrophs of the Rat Anterior Pituitary Gland: Evidence for the Involvement of Transforming Growth Factor β1 in Calcitonin Action. *Endocrinology*. 2003;144(5):2164-2171.

[13] Han B, Nakamura M, Zhou G, et al. Calcitonin inhibits invasion of breast cancer cells: Involvement of urokinase-type plasminogen activator (uPA) and uPA receptor. International journal of Oncology. 2006;28(4):807-814.

[14] Thomas S, Muralidharan A, Shah, GV. Knock-down of calcitonin receptor expression induces apoptosis and growth arrest of prostate cancer cells. International Journal of Oncology. 2007;31(6):1425-1437.

[15] Sullivan R, Abraham A, Simpson C, et al. Three-month randomized clinical trial of nasal calcitonin in adults with X-linked hypophosphatemia. Calcif Tissue Int. 2018;102(6):666-670.

[16] Cuttler K, Bignoux MJ, Otgaar TC. LRP: FLAG Reduces Phosphorylated Tau Levels in Alzheimer's Disease Cell Culture Models. Journal of Alzheimer's disease: JAD. 2020;76(2):753-768.

[17] Shipley MM, Mangold CA, Mljjovej S. Differentiation of the SH-SY5Y human neuroblastoma cell line. J Vis Exp. 2016;108: e53193.

[18] Xicoy H, Wieringa B, Martens GJ. The SH-SY5Y cell line in Parkinson's disease research: a systematic review. Mol Neurodegener. 2017;12(1):1-11.

[19] Miller KD, Nogueira L, Devasia T, et al. Cancer treatment and survivorship statistics, 2022. CA Cancer J Clin. 2022;72(5):409-436.

[20] Qiu B, Matthay KK. Advancing therapy for neuroblastoma. Nat Rev Clin Oncol. 2022;19(8):515-533.

[21] Sabbisetti VS, Chirugupati S, Thomas S, et al. Calcitonin increases invasiveness of prostate cancer cells: role for cyclic AMP-dependent protein kinase A in calcitonin action. Int J Cancer. 2005;117(4):551-60.

[22] Taskiran AS, Ergul M. The effect of salmon calcitonin against glutamate-induced cytotoxicity in the C6 cell line and the roles the inflammatory and nitric oxide pathways play. Metab Brain Dis. 2021;36(7):1985-1993.

[23] Shah GV, Walter R, Noble MJ et al. Calcitonin stimulates growth of human prostate cancer cells through receptor-mediated increase in cyclic adenosine 3', 5'-monophosphates and cytoplasmic Ca2+ transients. Endocrinology.1994;134(2):596-602.

[24] Chigurupati S, Kulkarni T, Thomas S, et al. Calcitonin stimulates multiple stages of angiogenesis by directly acting on endothelial cells. Cancer Res. 2005;65:8519-29.

[25] Iczkowski KA, Omara-Opyene AL, Kulkarni TR, et al. Paracrine calcitonin in prostate cancer is linked to CD44 variant expression and invasion. Anticancer Res. 2005;25:2075-2083.

[26] Shah GV, Thomas S, Muralidharan A, et al. Calcitonin promotes *in vivo* metastasis of prostate cancer cells by altering cell signaling, adhesion, and inflammatory pathways. Endocr Relat Cancer. 2008;15(4):953-64.

[27] Wells G, Chernoff J, Gilligan JP. et al. Does salmon calcitonin cause cancer? A review and meta-analysis. Osteoporos Int. 2016;27:13-19.

[28] Ng KW, Livesey SA, Larkins RG, et al. Calcitonin effects on growth and on selective activation of type II isoenzyme of cyclic adenosine 3′: 5′-monophosphate-dependent protein kinase in T 47D human breast cancer cells. Cancer Research. 1983;43(2):794-800.

[29] Davis NS, Disant'Agnese A, Ewing JF, et al. The neuroendocrine prostate: characterization and quantitation of calcitonin in the human gland. J Urology.1989;142:884-888.

Exp Biomed Res 2023; 6(1): 14-23 **DOI: 10.30714/j-ebr.2022.166**

Experimental Biomedical Research *Original article*

Evaluation of life quality and sleep problems in children presenting with headache to the pediatric neurology outpatient clinic

Fatih Mehmet Akif Ozdemir[1]*, Halil Celik[2]

[1]*Department of Pediatric Neurology, Dr. Ali Kemal Belviranlı Maternity and Children's Hospital, Konya.*

[2]*Department of Pediatric Neurology, Konya City Hospital, Konya.*

ABSTRACT

Aim: We aimed to investigate the quality of life (QL) and sleep habits (SH) of children presenting to the pediatric neurology outpatient clinic with headache.

Methods: This prospective, cross-sectional and observational survey study included children aged 2-18 who presented to the pediatric neurology outpatient clinics of Dr. Ali Kemal Belviranlı Maternity and Children's Hospital or Konya City Hospital between April and August 2022. QL was assessed using the Pediatric Quality of Life Inventory (PedsQL) and sleep characteristics were evaluated using the Children's Sleep Habits Questionnaire.

Results: The study included 137 patients (56.2% girls) with a mean age of 153.54±34.5 months at presentation. All patients were diagnosed with primary headache; 51.8% had migraine and 48.2% had tension-type headache. Quality of life scores were 69.07±14.96 according to child self-assessment and 66.39±15.37 according to parental assessment. The mean score on the sleep habits questionnaire was 48.01±7.68, and 9.5% of the patients had good sleep quality. Subscale scores showed that the greatest adverse effects on QL were in the areas of emotional functioning and school functioning.

Conclusions: Clinical assessment of patients' QL and SH is important for individualizing treatment and approach in pediatric primary headache.

Key words: Pediatric primary headache, pediatric neurology outpatient, quality of life, sleep.

✉ * *Dr. Fatih Mehmet Akif Ozdemir,*
Department of Pediatric Neurology, Dr. Ali Kemal Belviranlı Maternity and Children's Hospital, Konya.
E-mail: fatihmehmetakif@hotmail.com
Received: 2022-06-15 / Revisisons: 2022-08-13
Accepted: 2022-11-24 / Published: 2023-01-01

Introduction

Headache is an extensive complaint in the children, is among the leading causes of admission to pediatric neurology outpatient clinics [1-3]. The prevalence of headache has been reported as 37-82% in children [1]. Despite its frequency, it is often ignored because it is episodic and not life-threatening. However, chronic and recurrent headaches can seriously impair quality of life (QL) and adversely affect the person's education, family, and professional life. It has been suggested that chronic and recurrent headaches may be an indicator of stressors in a person's life and strain on their social, emotional, and cognitive skills [4].

Primary headaches are those that are not associated with a cause such as toxic or infectious pathologies, malignancy, hydrocephalus, or pseudotumor cerebri [1, 5]. The relationship between headache and sleep is an important issue for primary headache,

especially in childhood. The pathophysiology of headache and its relationship with sleep is complex. Alterations in hypothalamic activation and networks are involved in headache pathophysiology and impaired sleep cycle mechanisms. Orexin and melatonin are also important mediators in the relationship and pathophysiology of sleep and headache [6]. In a study of 622 children with pain, 60% of whom had headache, the most common complaints were sleep problems (53.6%) [7]. We purposed to investigate QL and sleep habits (SH) in children presenting with headache, which is an extensive problem in pediatric neurology outpatient clinics and identify their support needs in this study.

Materials and metods

This observational, prospective, cross-sectional survey aimed to determine to what degree and in which domains (physical, emotional, psychosocial, school) QL is affected in children with headache. We also aimed to identify these patients' SH (e.g., daytime sleepiness, sleep-disordered breathing, parasomnia, frequent night awakenings, sleep anxiety, sleep duration, delayed sleep onset, bedtime resistance) and determine the areas in which these patients need support from healthcare services (physical, emotional, psychosocial, school- and/or sleep-related). QL was evaluated using the Pediatric Quality of Life Inventory (PedsQL) and SH with the Children's Sleep Habits Questionnaire (CSHQ) [8-13].

The study included boys and girls who presented at age 2-18 years with complaints of headache to the pediatric neurology outpatient clinics of Dr. Ali Kemal Belviranlı Maternity and Children's Hospital or Konya City Hospital between April and August 2022. The patients' current age, complaint duration (since first onset), age at first presentation, sex, headache features (frequency and duration of episodes, triggers [e.g., light, sound], time of onset, type, location), daily media use, and physical examination findings were obtained from patient records and recorded in the patient follow-up form.

Patients, who with a complaint of headache Dr. Ali Kemal Belviranlı Obstetrics and Pediatrics Hospital or Konya City Hospital pediatric neurology outpatient clinic between the ages of 2-18, with normal mental and motor functions, without autism and psychotic disorder diagnoses, without additional chronic systemic disease other than headache, given informed consent from their guardian and/or self, and whose hospital records could be accessed to complete file information, were included in the study.

Patients, who did not meet the criteria for inclusion in the study, who and/or their parents/guardians did not want to participate in the study, who were diagnosed with another systemic chronic disease at least 1 year ago, and whose hospital records could not access sufficient file information were excluded from the study.

Data collection

The patient follow-up form prepared by the researchers was completed by the researchers for all children participating in the study, while the PedsQL child form was administered to all literate children over 5 years of age, and the parents completed the PedsQL parent form and the CSHQ.

Statistical analysis

Data were analyzed using IBM SPSS Statistics version 23. The Kolmogorov-Smirnov test was used to assess the normality of data distributions. Differences in the distribution of headache types according to categorical variables were analyzed using Pearson's chi-square test

Table 1. Clinical and demographic properties of the patients**.**

Parameters	**Number (n)**	**Percentage (%)**
Age Group		
5-7 years	11	8
8-12 years	35	25.5
13-18 years	91	66.4
Sex		
Female	77	56.2
Male	60	43.8
Daily Media Use		
<1 hour	50	36.5
>1 hour	87	63.5
Need for Painkillers		
Yes	100	73
No	37	27
Headache-Related School Absence		
Yes	44	32.1
No	93	67.9
Headache Type		
Migraine	71	51.8
Tension-type	66	48.2
Complaint Duration		
≤ 1 month	10	7.3
1-6 months	35	25.5
≥ 6 months	92	67.2
Headache Frequency		
≤ 1/day	49	35.8
1/day - 1/week	65	47.4
> 1/week	23	16.8
Light Triggering		
Yes	85	62
No	52	38
Sound Triggering		
Yes	89	65
No	48	35
Headache Onset Time		
Morning	12	8.8
Afternoon	119	86.9
Evening	6	4.4
Brain MRI		
Normal	112	81.8
Nonspecific abnormality (Arachnoid cyst, nonspecific white matter changes, cerebellar tonsillar herniation)	11	8
Not obtained	14	10.2

with Bonferroni correction for multiple comparisons. Results were presented as frequency (percentage) for categorical variables and as mean ± standard deviation and median (range) for quantitative variables. Level of significance was accepted as p<0.050.

Ethical approval

All study procedures were performed in accordance with the ethical standards of the 1964 Declaration of Helsinki and its later amendments. Ethics committee approval was received for the study [date: 01.04.2022, meeting number: 151, decision number: 2022/3732: (9405)]. Informed consent was obtained from the parents of the children participating in the study and, when appropriate, assent as obtained from the children themselves.

Results

This study included a total of 137 children and adolescents (77 girls, 56.2%). The mean complaint duration was 15.63±18.37 months. All patients were diagnosed as having primary headache, 71 (51.8%) with migraine and 66 (48.2%) with tension-type headaches. The mean age at presentation was 153.54±34.5 months, with 8% of patients in the 5-7 years age group, 25.5% in the 8-12 years age group, and 66.4% in the 13-18 years age group. The mean duration of headache episodes was 9.35±8.71 hours. The exhaustive clinical and demographic properties of the patients are presented in Table 1.

Total PedsQL scores were 69.07±14.96 according to the children's self-assessment and 66.39±15.37 according to parental assessment. The mean CSHQ score was 48.01±7.68, and 90.5% of the children had poor sleep quality (total score > 41). The patients' QL and SH scores are presented in Table 2.

There was a statistically significant difference in the distribution of headache type according to age group (*p*=0.008). This difference was found to be between the 5-7 years and 13-18 years age group. The prevalence rates of migraine and tension-type headaches in children aged 5-7 years were 9.1% and 90.9%, respectively, while in adolescents aged 13-18 these rates were 58.2% and 41.8% (Table 3).

There was no statistically significant difference in the distribution of headache types according to sex (*p*=0.178). The prevalence of migraine was 46.8% in girls and 58.3% in boys. The prevalence of tension-type headache was 53.2% in girls and 41.7% in boys (Table 4).

Table 2. The patients' QL and SH scores.

QL	Scores (mean ± SD)
I) Child Self-Assessment	
Total Scale Score	69.07 ± 14.96
Physical Health	61.68 ± 21.04
Psychosocial Health	69.3 ± 14.64
School Functioning	53.14 ± 24.9
Social	66.82 ± 32.28
Emotional	54.42 ± 21.69
II) Parental Assessment	
Total Scale Score	66.39 ± 15.37
Physical Health	65.72 ± 18.34
Psychosocial Health	66.22 ± 18.08
School Functioning	62.74 ± 18.45
Social	74.96 ± 20.77
Emotional	61.46 ± 19.96
Sleep Habits	
Duration of Night Awakenings (min)	11.17 ± 14
Total Sleep Time (hours)	8.14 ± 1.17
Total Sleep Score	48.01 ± 7.68
Daytime Sleepiness	12.62 ± 2.72
Sleep-Disordered Breathing	3.78 ± 1.33
Parasomnias	9.04 ± 0
Night Awakenings	4.28 ± 1.39
Sleep Anxiety	5.13 ± 1.8
Sleep Duration	4.69 ± 1.76
Delayed Sleep Onset	1.52 ± 0.72
Bedtime Resistance	7.96 ± 2.39
Sleep quality status	
Good quality (≤41), n (%)	13 (9.5)
Poor quality (>41), n (%)	124 (90.5)

Table 3. Distribution of headache type by patient age group.

Parameters	Patient age group			Total	Test Stat.	*p**
	5-7 years**	8-12 years	13-18 years**			
Headache Type						
Migraine	1 (9.1)	17 (48.6)	53 (58.2)	71 (51.8)	9.695	**0.008**
Tension-type	10 (90.9)	18 (51.4)	38 (41.8)	66 (48.2)		

**Pearson's chi-square test; frequency (percentage); **Significant difference between the groups.*

Table 4. Distribution of headache type by patient sex.

Parameters	Sex		Total	Test Stat.	*p**
	Female	Male			
Headache Type					
Migraine	36 (46.8)	35 (58.3)	71 (51.8)	1.811	0.178
Tension-type	41 (53.2)	25 (41.7)	66 (48.2)		

**Pearson's chi-square test; frequency (percent).*

Discussion

This investigation was conducted in two different hospitals in Konya including a total of 137 children with primary headache who had a mean age of 153.54±34.5 months (66.4% aged 13-18 years), showed a slight female preponderance (56.2%) consistent with the literature, and were found to have migraine and tension-type headaches at rates of 51.8% and 48.2%, respectively [14]. In the cited review, some studies reported a higher prevalence of migraine while other reported a higher prevalence of tension headache. The similar rates of migraine and tension headache (with migraine being more common) seen in the study are compatible with the literature [14].

The mean duration of patients' headache episodes was 9.35±8.71 hours, which is longer than reported in the literature [15]. According to self-report, the rate of school absenteeism due to headache was 32.1%. A previous study reported that 1% of all missed school days were caused by headaches, 3.7% of children in school were absent one or more times because of headaches [16]. In their study of adolescents, Linet et al. [17] found that within the 4 weeks prior to being interviewed, 2% of adolescents had missed an entire school day and 9% had missed a part of a day. We believe the higher rate of headache-related absenteeism and longer duration of headache episodes in our study compared to the literature are associated with the greater headache severity in our patients [15-17].

It has been reported in the literature that headache and negative psychological outcomes are higher in adolescents with problematic internet use, and that more than 2 hours of electronic screen exposure in particular is associated with complaints of headache [18-20]. We also found that a most of our patients (63.5%) used digital media for more than 1 hour per day. This finding suggests that 1 hour can be considered a cut-off point and it may be beneficial to limit media use to 1 hour, especially in patients with headache.

Of the children in the study, 73% needed painkillers for headache, 83.2% said they had

headaches more than once a week, and headaches were reported to be triggered by sound in 65% and by light in 62% of the patients. In the literature, sound/noise has been reported as the most common headache trigger (42%) [21]. More severe headache episodes in our patients may also explain the higher need for painkillers in our study compared to the literature, which reported the need for painkillers in approximately half of patients with headache [15, 22].

When examined according to time of day, headaches started most frequently in the afternoon (86.9%), and this rate was 85.9% for migraines and 87.8% for tension-type headaches. In a review of 15 studies on migraine chronobiology, migraines were found to start most frequently in the morning hours (06.00-12.00) in 11 studies and in the afternoon hours (12.00-18.00) in 2 studies [23]. Considering the possible measures that can be taken in terms of modifications to work, school, and sleep patterns according to these findings, we believe that further studies are needed to shed light on this issue.

According to current guidelines, cranial MRI is not routinely recommended with neurological examination for recurrent headache [24-26]. However, in clinical practice, brain imaging studies are often performed because of parental anxiety and physicians' concern about overlooking an important underlying disease (for example, malignancy). There are studies in the literature reporting that 80% of patients with headache undergo neuroimaging [27]. In our study, no abnormality associated with headache was detected in the 123 patients (89.8%) who underwent cranial MRI. However, changes considered nonspecific were detected in 8.9% (n=11) of the patients who underwent MRI (nonspecific white matter changes in 6 patients (55%), arachnoid cyst in 4 (36%), and minimal cerebellar tonsillar herniation in 1 patient (9%). MRI findings were less common in our study compared to a previous study in which 28.9% of patients with recent headache had brain MRI abnormalities (nonspecific gliotic focus in 2.6%, arachnoid cyst in 2.3%, Chiari type 1 in 0.3%) [21].

The patient's mean total score on the PedsQL was 69.07±14.96 according to the children's self-assessment and 66.39±15.37 according to the parents' assessment. Their mean score on the CSHQ was 48.01±7.68. The proportion of patients with good sleep quality was only 9.5% (total sleep score of 41 or lower).

There are a limited number of studies assessing QL in pediatric primary headache with the PedsQL. In children with migraine aged 8-17 years in Austria, the median total PedsQL score was found to be 70.00 (range: 55.00-80.00) according to self-assessment. The QL among patients with primary headache in our study, a large proportion of whom had migraine, is consistent with the literature. Our study is limited cause of no control group. However, the median QL score in the healthy population was reported as 80.00 (range: 60.00-85.00) in another study [28]. Therefore, the total QL scores of the patients with primary headache evaluated in our study were approximately 10 points (12.5%) lower than those reported in the literature for healthy children. This supports the view that primary headaches significantly impair QL.

In our study, the mean total PedsQL score was 3 points lower when assessed by the parents than the child self-assessment. Although the difference was not statistically significant, we believe this might be related either to the parents' more realistic observations or to parental anxiety.

When the QL subscales were examined, it was seen that children with headache had the lowest QL scores in the school functioning and emotional domains, both in the children's self-

assessment and in the parental assessment (Table 2). Similarly, another study evaluating the PedsQL subscales in children with migraine reported significantly lower QL in terms of school functioning (p-adjust=0.04) and significantly less frequent "good" grades than children without migraine (p-adjust=0.048) [28]. In this respect, our study is compatible with the literature and points to the importance of providing school functioning and emotional support to patients with primary headache.

As far as we know, this study is the first to assess SH using the CSHQ in children with primary headache. Since we did not have a control group, we used literature data on SH of healthy children evaluated with the CSHQ for comparison. Based on another Turkish study that reported a mean total sleep score of 46.4±6.6 in healthy children and a German study reporting scores of 42.5±5.66 among healthy children and 26.8±4.62 among healthy adolescents, the mean score in our study (48.01±7.68) indicates poorer SH in children with headache [29-30].

In a study conducted in Germany, 22.6% of healthy child participants and 20% of healthy adolescent participants reported problematic amounts of sleep-related difficulties [30]. A total score lower than 41 on the CSHQ indicates good SH, which was demonstrated by only 9.5% in the patients in our study. This supports the connection between poor SH and primary headaches.

Compared to studies reporting total sleep durations of 8.8±1 hours and 10.2±1 hours in healthy children, our patients had a shorter total sleep duration (8.14±1.17) [29-30]. This suggests that there may be a relationship between primary headache and short sleep time, and that these patients can be recommended to increase their sleep duration to 9-10 hours.

Analysis of SH subscale scores showed that the children with primary headache in our study had higher bedtime resistance, night awakenings, sleep duration, delay of sleep onset, parasomnia, sleep-disordered breathing scores compared to healthy children in the literature [29]. In addition, according to a study in which the mean duration of night awakenings was reported to be 3.1±3.6 min in healthy children, the duration of night awakenings was substantially longer in our patients (11.17±14 min), also supporting the relationship between primary headache and poor sleep quality [29].

When we evaluated the distribution of headache types according to age groups, we determined that tension-type headache was more common between the ages of 5-7 years while migraine headaches were more common among adolescents (13-18 years) (90.9% vs. 58.2%. This is consistent with the literature in which pediatric migraine was reported to be most frequent between the ages of 11 and 15 [31-32]. In a recent study examining the relationship of age and sex with primary headaches, girls were found to be significantly older than boys (11.5±2.7 vs. 10.7±2.6 years). In the same investigation, the mean age was 12.5±2.07 for migraine patients and 10.7±2.03 for patients with tension-type headache. The prevalence of primary headache was also higher in girls than boys. Girls accounted for 119 (66.5%) of the patients diagnosed with migraine and 68 (60.2%) of those with tension-type headache [21]. In our study, although there was no statistically significant difference in the distribution of headache types according to sex, we observed that migraine was more common among boys (58.3%) and tension-type headache was more common in girls (53.2%).

The strength of this study is that we used pediatric-specific tools with demonstrated reliability and validity to assess the SH and QL of pediatric patients with primary headache. Limitations of the investigation are the little

sample size and no control group. Therefore, however objectively the survey-based results were evaluated, caution is warranted when generalizing the study findings to all children with primary headache. We believe that longer follow-up studies including more pediatric patients and healthy control groups should be conducted to further examine the SH and QL of children.

Conclusion

This study underlines the need to evaluate and manage SH and QL in children with primary headache. Clinical evaluation of patients' quality of life and sleep characteristics is critical for reducing drug use in pediatric patients with primary headache, determining recommendations to enhance daily quality of life, and individualizing interventions.

Funding: *The authors received no financial support for the research, authorship, and/or publication of this article.*

Conflict of Interest: *The authors declare that they have no conflict of interest.*

Ethical statement*: Ethics committee approval was received for the study [(date: 01.04.2022, meeting number: 151, decision number: 2022/3732: (9405)].*

References

[1]Kabbouche MA, Kacperski J, O'Brien HL, et al. Headache in Children and Adolescents. In: Swaıman KF, Ashwal S, Ferriero DM et al. Swaıman's Pedıatrıc Neurology. Prıncıples and Practıce. Sıxth Edıtıon. UK/USA; Elsevıer Saunders; 2018. P.647-656.

[2]Rho YI, Chung HJ, Lee KH, et al. Prevalance and clinical characteristics of primary headaches among school children in South Korea: a nationwide survey. Headache. 2012;52(4): 592-599.

[3]Poyrazoğlu HG, Kumandaş S, Canpolat M, et al. The prevalance of migraine and tension-type headache among school-children in Kayseri, Turkey: an evaluation of sensitivity and specificity using multivariate analysis. J Child Neurol. 2015;30(7): 889-895.

[4]Torelli P, Abrignani G, Castellini P, et al. Human psyche and headache: tension-type headache. Neurol Sci. 2008;29 Suppl 1: 93-95

[5]Headache Classification Committee of the International Headache Socıety (IHS). The Internatıonal Classıfıcatıon of Headache Disorders, 3rd edition (beta version). Cephalalgia. 2013;33(9): 629-808.

[6]Holland PR. Headache and sleep: shared pathophysiological mechanisms. Cephalalgia. 2014;34(10):725-744.

[7]Dosi C, Riccioni A, Della Corte M, et al. Comorbidities of sleep disorders in childhood and adolescence: focus on migraine. Nat Sci Sleep. 2013;11;5: 77-85.

[8]Varni JW, Seid M, Rode CA. The PedsQL: measurement model for the pediatric quality of life inventory. Med Care. 1999;37(2): 126-139.

[9]Uneri OS, Agaoglu B, Coskun A, et al. Validity and reliability of Pediatric Quality of

Life Inventory for 2-to 4-year-old and 5-to 7-year-old Turkish children. Qual Lif Res. 2008;17: 307-315.

[10] Cakin Memik N, Agaoglu B, Coşkun A, et al. Çocuklar için yaşam kalitesi ölçeğinin 8-12 yaş çocuk formunun geçerlilik ve güvenilirliği. Çocuk ve Gençlik Ruh Sağlığı Dergisi. 2008;15(2): 87-98.

[11] Cakin Memik N, Agaoglu B, Coskun A, et al. The Validity and Reliability of the Turkish Pediatric Quality of Life Inventory for Children 13- 18 Years Old. Turk Psikiyatri Derg. 2007;18(4): 353-363.

[12] Owens JA, Spirito A, McGuinn M. The Children's Sleep Habits Questionnaire (CSHQ): psychometric properties of a survey instrument for school-aged children. Sleep. 2000;23(8): 1043–1051.

[13] Perdahlı Fis N, Arman A, Ay P, et al. The validity and the reliability of Turkish Version of Children's Sleep Habits Questionnaire. Anatolian J Psychiatry. 2010;11: 151–160.

[14] Albers L, von Kries R, Heinen F, et al. Headache in school children: is the prevalence increasing? Curr Pain Headache Rep. 2015;19(3): 4.

[15] King NJ, Sharpley CF. Headache activity in children and adolescents. J Paediatr Child Health. 1990;26(1): 50-54.

[16] Collin C, Hockaday JM, Waters WE. Headache and school absence. Arch Dis Child. 1985;60(3): 245-247

[17] Linet MS, Stewart WF, Celentano DD, et al. An epidemiologic study of headache among adolescents and young adults. JAMA. 1989;21;261(15): 2211-2216.

[18] Marino C, Lenzi M, Canale N, et al. The 2018 HBSC-Italia Group Problematic Social Media Use: Associations with Health Complaints among Adolescents. Ann. Ist. Super. Sanita. 2020;56(4): 514–521.

[19] Solecki S. The Smart Use of Smartphones in Pediatrics. J Pediatr. Nurs. 2020;55: 6–9.

[20] Çaksen H. Electronic Screen Exposure and Headache in Children. Ann. Indian Acad Neurol. 2021;24(1): 8–10.

[21] Kilic B. Evaluation of the Etiology, Clinical Presentation, Findings and Prophylaxis of Children with Headache. Sisli Etfal Hastan Tip Bul. 2021;17;55(1): 128-133.

[22] Scheller JM. The history, epidemiology, and classification of headaches in childhood. Semin Pediatr Neurol. 1995;2(2): 102-108.

[23] Poulsen AH, Younis S, Thuraiaiyah J, et al. The chronobiology of migraine: a systematic review. J Headache Pain. 2021;19;22(1): 76.

[24] Lewis DW, Ashwal S, Dahl G, et al. Quality Standards Subcommittee of the American Academy of Neurology; Practice Committee of the Child Neurology Society. Practice parameter: evaluation of children and adolescents with recurrent headaches: report of the Quality Standards Subcommittee of the American Academy of Neurology and the Practice Committee of the Child Neurology Society. Neurology. 2002;59(4): 490–498.

[25] Hershey AD. Current approaches to the diagnosis and management of paediatric migraine. Lancet Neurol. 2010;9(2): 190–204.

[26] Shah UH, Kalra V. Pediatric migraine. Int J Pediatr. 2009;2009: 424192.

[27] Alehan FK. Value of neuroimaging in the evaluation of neurologically normal children with recurrent headache. J Child Neurol. 2002;17(11): 807–809.

[28] Koller LS, Diesner SC, Voitl P. Quality of life in children and adolescents with migraine: an Austrian monocentric, cross-sectional questionnaire study. BMC Pediatr. 2019;24;19(1): 164.

[29] Makay B, Kiliçaslan SK, Anik A, et al. Assessment of sleep problems in children with

familial Mediterranean fever. Int J Rheum Dis. 2017;20(12): 2106-2112.

[30] Lewien C, Genuneit J, Meigen C, et al. Sleep-related difficulties in healthy children and adolescents. BMC Pediatr. 2021;16;21(1): 82

[31] Bille B. Migraine and tension-type headache in children and adolescents. Cephalalgia 1996;16: 78.

[32] Stewart WF, Lipton RB, Celentano DD, et al. Prevalence of migraine headache in the United States. Relation to age, income, race, and other sociodemographic factors. JAMA. 1992;267(1): 64–69.

Exp Biomed Res 2023; 6(1): 24-37 **DOI: 10.30714/j-ebr.2022.167**

Experimental Biomedical Research *Original article*

Joint modeling of survival and longitudinal data: Carrico index data example

Ebru Turgal [1*], Beyza Doganay Erdogan [1], Fatma Arslan[2]

[1]*Department of Biostatistics, Ankara University, Faculty of Medicine, Ankara, Türkiye*

[2]*Department of Chest Diseases, Ankara University, Faculty of Medicine, Ankara, Türkiye*

ABSTRACT

Aim: When the respiratory system is unable to adequately absorb oxygen or excrete carbon dioxide, acute respiratory failure (ARF) develops. A current area of study is the survival analysis of patients with acute hypercapnic respiratory failure (AHRF) in the field of pulmonary diseases. In the follow-up period, several biochemical markers are repeatedly measured, such as respiration rate and Carrico Index; however, baseline or averaged values are mostly related to treatment failure. Although this approach is not inaccurate, it causes information loss, which leads to biased estimates. This prospective cohort study primarily looked at the relationship between changes in Carrico Index and failure of treatment in AHRF patients.

Methods: We included 86 patients from Ankara University School of Medicine Pulmonary Diseases Department. The association between the trajectory of the Carrico Index and failure in AHRF patients was examined using a joint modeling approach for longitudinal and survival data.

Results: Results showed that averaged Carrico Index change was inversely and significantly associated with failure (HR: 0.97, 95% CI: -0.05 to 1.97). With hazard ratios of 1.43 and 1.4, chronic health evaluation II (Apache II), and COPD Assesment test (CAT) were positively correlated with failure risk.

Conclusions: The present study demonstrate that applying the risk predictors' trajectory through an appropriate statistical method improved accuracy and avoid biased results.

Key words: Joint modeling, non-invasive ventilation, carrico index, survival.

✉ * *Ebru Turgal,*
Department of Biostatistics, Ankara University, Faculty of Medicine, Ankara, Türkiye
E-mail: ebruturgal@gmail.com
Received: 2022-09-22 / Revisisons: 2022-10-23
Accepted: 2022-11-16 / Published: 2023-01-01

Introduction

ARF is defined as the inadequacy of respiratory function or oxygen / carbon dioxide gas exchange in the lung. When acute respiratory failure develops, non-invasive positive pressure mechanical ventilation (NPPV) is applied to the patient as the first option after optimal medical treatment. NPPV is a mechanical ventilation without any invasive artificial respiratory route. ARF was first discussed by Tschirgi [1]. AHRF was accepted as type II respiratory failure. In type II respiratory failure, hypercapnia predominates. $PaCO_2$ level is above 45 mmHg and respiratory acidosis is present.

Data collection in medical research can be done in a single period of time or in a method that collects data periodically at different time intervals. Repeated measurements occur when observations are taken at different time points or under different conditions from the same subject and are called "longitudinal data". On the other hand, by accounting for potential confounders such comorbidities, biochemical/chemical

variables, and demographic factors, the Cox proportional hazards regression model enables revising predicted survival probability. The Kaplan-Meier analysis and/or Cox proportional hazards regression models were widely used to predict the survival of a research group. The vast majority of studies ignored repeated measurements and used either the Kaplan-Meier or the Cox proportional hazard regression model based on a single measurement (i.e. baseline or average of multiple records) of related risk factors [2,3,4,5].

During the follow-up period, AHRF patients are monitored for PaO_2 / FiO_2 (Carrico Index), respiratory rate (RR), Glasgow Coma Scale and COPD Assesment test (CAT). These variables are measured repeatedly in AHRF patients; although averaged values of continuous risk factors related with AHRF can be used to analyze survival probabilities, repeated measurements may offer an in-depth insight for predicting them. The purpose of studies involving longitudinal data is usually to examine how the mean response profiles differ among groups as well as the time course of responses. Longitudinal data analysis is carried out by examining the variations both within the same individual and between individuals. Thus, the trajectories throughout the data collection range are investigated considering inter-individual biological fluctuations. On the other hand, a survival data comprise of event of interest (death, recurrence of a disease, transplantation, etc.) and time of the event. Conventionally, these two types of data collected under the same study are analyzed separately using different statistical methods. However, in some cases there is a relationship between longitudinal data and the survival process of the individuals (e.g. PSA antigen and prostate cancer [6], systolic and diastolic blood pressure measures and time to coronary artery disease [7]). When this is the case, a joint model should be fitted to obtain unbiased and more efficient results [8]. Recently, studies on modeling of these two processes together have been increasing, when the longitudinal and the survival processes are related [9, 10]. In order to obtain accurate results from these collected data, the necessity of using the joint modeling method has been showed [11]. Joint modeling is a model that links longitudinal and survival data, and consists of two linked sub-models. One of them corresponds to the measurement model for the longitudinal process and the other corresponds to the density model for the survival process.

Association between Carrico Index and mortality is well known [12]; besides, the relationship between the time-dependent Carrico Index levels and failure of treatment or mortality is a recent and long-standing area of research. Moreover, the majority of current research focus on population-based risk estimates and do not account for within-patient heterogeneity. Furthermore, personalized medicine and risk forecasts have gained popularity in recent years, particularly in the treatment and following-up of chronic diseases [13, 14] at the individual patient level. It is now possible to predict the hazard of treatment of AHRF patients individually using patient-level data and changes in biological markers over time, thanks to recent advances in statistical modeling. In addition, patient-specific risk predictions for future time points can be updated dynamically as new information becomes available known [5]. It is possible to predict the results of AHRF patient survival using the Carrico Index levels at the start of the study or averaged values while the follow-up period. However, long-term variation and trend in Carrico Index levels will present more accurate risk evaluations. We used a unique and recently proposed method called joint modeling to extend the survival model (usually the Cox

proportional hazards regression model) to repeated measurements (i.e. time-dependent coefficients) in order to investigate the relationship between a longitudinal biomarker and survival outcome for AHRF patients in this study.

To the best of the authors' knowledge, present study is the first application which investigates the joint modeling approach on AHRF patients in Turkiye and worldwide.

Materials and metods

Study Design and Participants

This section offers an overview of the overall research design and the plans for involving participants. Eighty-six patients, who had AHRF related to chronic obstructive pulmonary disease (COPD), acute cardiogenic pulmonary edema (ACPE), community-acquired pneumonia, bronchiectasis, or kyphoscoliosis and who were received NPPV as an initial ventilatory support strategy at Ankara University School of Medicine Pulmonary Diseases Clinic, were prospectively included in the study.

Patients aged ≥65 years who were hospitalized to the intensive care unit between January 2012 and September 2016 were followed up until treatment, lost to follow up owing to withdrawal or unknown reasons, or the trial ended, whichever took place first. Patients who were followed up for AHRF in the intensive care unit were included in the study. Carrico Index values were taken before treatment (0 hour), and 1, 2, 4, 12, 24, 48, 72, 96 and 120 hours after treatment. Measurements of PaO_2 / FiO_2 were taken as dependent variable in the longitudinal data model. Acute respiratory failure and time to failure were used in the survival model. Effect of time-dependent PaO_2 / FiO_2 measurements to ARF is analyzed with joint modeling of longitudinal data model and survival model.

In this study we aim to apply joint modelling approach to predict the hazard of treatment of ARF and its relation to time dependent Carrico Index measurements in the intensive care unit data.

Clinical Outcome Assessments

The initial clinical outcome was treatment owing to AHRF. In this prospective cohort study, patients' data, including the demographic (e.g. gender, age, body mass index, smoking status) and clinical/biochemical measurements (e.g. leukocyte count, Charlson Comorbidity Index, serum C-reactive protein (CRP), Glasgow coma score, chronic health evaluation II (Apache II), COPD assessment test (CAT), hemoglobin levels, respiration rate, current or previous comorbid diseases (coronary heart disease (CHD), congenital adrenal hyperplasia (CAH), chronic renal failure (CRF), cerebrovascular disease (CVD), haematocrit (%), arrhythmia, NPPV history, intubation, diabetes) were collected from medical history. During the follow-up period, repeated measures of biochemical and clinical outcomes were recorded. We examined the longitudinal associations between change in biological markers and treatment. Apache II, Glasgow, and CAT were identified as independent variables in patients with AHRF brought on by COPD exacerbations that resulted NIV failure [15].

Statistical analysis

The R programming environment (version 3.4.3, URL: https:// cran.r-project.org) was used to perform the statistical analyses. For survival data, Cox proportional hazard regression analysis "survival" library [16], for linear mixed-effects model "nlme" library [17] for joint model, "JM" library was used [18].

Quantitative data are stated as percentage, mean and standard deviation. Categorical variables were summarized using frequencies and percentages. A joint model, consisting of two

submodels: i) a linear mixed effect (LME) model for assessing the longitudinal biological marker and (ii) a Cox proportional hazard model for treatment, was used to observe the link between the trajectory of longitudinal biological markers and treatment. The goal of the joint modeling technique is to predict the effect of longitudinal biological markers on treatment while adjusting for potential confounders in both the longitudinal and time-to-event outcomes. Data were analyzed using three approaches. In the first approach, longitudinal process and time-to-event process of the study (extended Cox regression model) were analyzed separately. In the second approach two stage modeling was applied. In the third approach the longitudinal and the survival process were modeled jointly. So the likelihood of two processes of the study was evaluated jointly. The details of these approaches are given below.

Time-Dependent Explanatory Variables in the Survival Process: Extended Cox Regression Model

The model is based on a proportional hazard assumption but does not assume a particular probability distribution for survival times. The Cox regression model is considered as a semi-parametric model since the basic hazard function is not specified, i.e. failure time, no probability distribution for the random variable *T* and the most important problem in the model is the estimation of the parameter β [19].

$$h(x) = h_0(t)exp\left[\sum_{i=1}^{p}\beta_i x_i\right] \quad \text{(Equation 3)}$$

In the equation, x is the vector of explanatory variables in the form $(x_1, x_2, \dots, x_p)$. An important feature of this formula is the baseline hazard function ($h_0(t)$), which includes the survival time (*t*) but not the explanatory variables, in relation to the proportional hazard assumption. The part where the explanatory variables are included is independent of the survival time. The explanatory variables in this case are sometimes called time-independent. $h_0(t)$ shows how the risk of failure changes over time, whereas the exponential part of the explanatory variables has an effect on the hazard function. Time independent variables are variables that do not change in value over time, like gender, smoking status.

The Cox proportional hazard model can be extended as follows to deal with time dependent explanatory variables.

$$h_i(t\,|\gamma_i(t), w_i) = h_0(t)R_i(t)exp\{\gamma^T w_i + \alpha y_i(t)\} \quad \text{(Equation 4)}$$

In counting process notation, the event process for subject *i* is written as $\{N_i(t), R_i(t)\}$ with $N_i(t)$ denoting the number of events for subject *i* by time *t*, and $R_i(t)$ is a left continuous at risk process with $R_i(t)$ = 1 if subject *i* is at risk at time *t*, and $R_i(t)$= 0 otherwise.

w_i: a vector of baseline covariates, such as sex or randomized treatment,

$y_i(t)$: a vector of time-varying covariates.

The regression coefficients vector α is interpreted in the same way as γ.

The model shown above with Equation 4 is known as the extended Cox hazard model [19]. In this model, instead of explanatory variables in the traditional Cox model (Equation 3), time-varying and time-independent explanatory variables and required regression coefficients are separately found. In this model, w_i shows time-independent explanatory variables (e.g. gender, treatment groups, etc.), y_i represents time-dependent explanatory variables. In the model, α and γ are regression coefficients of time-independent and time-varying explanatory variables, respectively. The interpretation of the regression coefficients of time-dependent common variables can be made as follows.

A unit increase in $y_i(t)$ measured at time *t* can be said to increase the relative risk at time *t* of

interest by *exp (α)*. For example, in a study of the risk of death in cirrhosis patients and the effect of prothrombin index values repeatedly measured weekly during the time they were hospitalized, *exp (α)* = 3 was found in the prothrombin index. According to this, a unit increase in the measure of prothrombin index in the second week when patients are in the hospital increases the risk of death in the second week by 3 times.

However, in the extended Cox model, since the inter-individual biological heterogeneity is not considered, when the time-varying variables are endogenous, the endogenous variation effect of the individual biological variation is ignored. In joint modeling, the longitudinal sub-model of time-varying explanatory variables and the survival sub-model are connected by random effects that show inter-individual heterogeneity. In this way the effect of individual biological variations to the time-dependent variables are also taken into account [14].

Joint Modeling

Joint modeling is a model linking longitudinal and survival data and consists of two connected sub-models. One of them corresponds to the mixed effect model for the longitudinal process and the other corresponds to the proportional hazard model for the survival process. These two sub-models are connected to each other by random effects. Joint modeling of common random effects and longitudinal and survival processes allows simultaneous estimation of these two sub-models. In joint modeling, the survival process may be solved with the joint likelihood of the longitudinal process.

Sub-Models to be used in Joint Model

Longitudinal Submodel

As a longitudinal sub-model, a mixed effects model with random and fixed effects can be used. The mixed effect sub-model shown in Equation 5 for use in the joint model could be rewritten as follows:

$M_i(t) = \{m_i(s), 0 \leq s < t\}$;

$y_i(t) = m_i(t) + \varepsilon_i(t)$,

$m_i(t) = x_i^T(t)\beta + z_i^T(t)\, b_i$,

$b_i \sim N(O, D)$, $\varepsilon_i(t) \sim N(O, \sigma^2)$, (Equation 5)

where, $M_i(t)$ represents the expected values of the longitudinal process until *t* time. That is, the actual values of the measurements taken in the longitudinal process, adjusted from measurement errors. $m_i(t)$ is the expected value of the longitudinal explanatory variable at time *t*. $m_i(t)$ is different from $y_i(t)$ because it does not include the measurement error for the longitudinal outcome variable at time *t*.

$x_i(t)$ is the design vector of fixed effects at time *t* for individual *i*, $z_i(t)$ is the design vector of random effects at time *t* for individual *i*, whereas β and b_i are the corresponding regression coefficients. *D* is the (q × q) dimensional general covariance matrix of random effects. In the above model $x_i(t)$, $z_i(t)$ and $\varepsilon_i(t)$ terms are all time-dependent.

Survival Sub-Model

Before specifying the survival submodel used in the joint model, the cumulative hazard function could be defined as given in Equation 6.

$h_i(t \mid M_i(t), w_i) = Pr\, Pr\, \{t \leq T_i^* < t + dt \mid T_i^* \geq t, M_i(t), w_i\}/\, dt = h_0(t) exp\, \{\gamma^T w_i + \alpha\, m_i(t)\}$, t>0, (Equation 6)

In this model, $M_i(t)$ is the measurement error-free true values measured up to time *t* in the longitudinal process, and w_i shows the baseline explanatory variable vector (e.g. treatment indicator, disease history). γ is the parameter vector containing the regression coefficients for the explanatory variables. α parameter is the regression coefficient indicating the effect of the longitudinal process on survival. $exp(\gamma_j)$ specifies the hazard ratio for a unit change in w_{ij} at any time during at *t*. *exp (α)* is the relative increase of an event at time *t*, and this is the result of a unit increase in $m_i(t)$ at the same time point.

Notably, the survival function to be utilized in the joint model may therefore be defined as follow using the known relationship between the survival and the cumulative hazard function.

$S_i(\mathrm{t}\,|M_i(t), w_i) = Pr\ Pr\ \{t > T_i^*\ |\ M_i(t), w_i)$

$= exp\ (-\int_0^t h_0(s) exp\ \{\gamma^T w_i + \alpha m_i(\mathrm{s})\}\mathrm{ds})$, (Equation 7)

Survival function also depends on the values of the baseline explanatory variables $M_i(t)$ and the longitudinal explanatory variable values. Here, there are various options to determine the structure of the baseline risk function $h_0\ (\cdot)$. The classical option is to use the known risk function with known parametric distribution. The distributions commonly used for the baseline risk function within the scope of survival analysis are Weibull, log-normal and Gamma. The second option is to use a risk function which is also parametric but more flexible. In literature, several approaches have also been proposed to model the flexible basic risk function, for example B-splines or cubic splines.

When selecting variables for the Cox regression model; variables with significance level above 0.20 in the univariate Cox analysis were not included into the analyses [20]. Then, Model 1.a was obtained by considering the clinical significance with the backward elimination method.

Primarily, to identify a subset of significant independent variables from among biochemical, clinical, and demographic factors, univariate Cox proportional hazard modeling and an LME model were used. The survival and longitudinal submodels were then linked to a joint model, and model parameters were determined simultaneously [5]. The longitudinal nature of the dependent variable in joint modeling is represented using an LME model described in Equation 8.

$y_{it} = m_{it} + \varepsilon_{it}$, (Equation 8)

$y_{it} = m_{it} = \beta^T X + b^T Z + \varepsilon_{it}$, (Equation 9)

where X and Z are the vectors of fixed and random effects with β and b, respectively, the vectors of regression parameters, and ε_i is the random error term of the *i*th patient. With an association parameter, the fitted trajectories from the longitudinal model were included as a time-dependent covariate in the survival analysis section. As in Equation 10, the survival submodel can be defined,

$h_i(t) = h_0(t)\exp\ (\gamma_i{}^T w_i + \alpha m_i(\mathrm{t}))$,

(Equation 10)

where $\gamma_i{}^T$ is the vector of model parameters, $m_i(t)$ is the fitted curves of trajectory of the Carrico Index generated using a LME model for the *i*th patient at time *t*, and w_i is the vector of baseline covariates of the *i*th patient related with failure or mortality [11]. The association parameter between the longitudinal and survival sub-models called as α.

After taking into account potential confounders, an LME model is used to incorporate the impact of the longitudinal biomarkers into the survival model. There is no relationship between the treatment and the longitudinal biological marker, if the parameter α is statistically insignificant. The JM package, which was developed especially for joint modeling of longitudinal and survival data, was used to carry out the investigations in R [18].

Several biomarkers, including the Carrico Index, might be associated with AHRF-related failure of treatment. Carrico Index as a longitudinal response was the primary focus of this work. p value was set 0.05 significance level in all analyses.

Results

Clinical characteristics of patients with successful treatment and of those with unsuccessful treatment were given in Table 1.

Table 1. Demographic, clinical/biochemical characteristics of the patients.

Parameters	**Total**	**Patients with successful treatment (n=73)**	**Patients with unsuccessful treatment (n=13)**
Gender (male)	44 (0.51)	33 (0.45)	11 (0.85)
Age	71.62±10.98	70.75±11.25	76.46±8.08
BMI(kg/m^2)	28.54±7.95	29.78±7.88	21.57±3.51
CAT	31.21±4.71	30.19±4.23	36.92±2.84
Respiratory rate	23.45±4.74	22.19±3.56	30.54±4.35
Diabetes	30 (0.35)	24 (0.33)	6 (0.46)
CRF	26 (0.30)	19 (0.26)	7 (0.54)
CAH	9 (0.10)	8 (0.11)	1 (0.08)
Aritmia	19 (0.22)	14 (0.19)	5 (0.38)
Haematocrit	63 (0.73)	54 (0.74)	9 (0.69)
CVD	1 (0.01)	1 (0.01)	0 (0.00)
Intubation	11 (0.13)	10 (0.14)	1 (0.08)
Glasgow	14.72±0.63	14.92±0.32	13.62±0.77
Apache	17.99±3.88	16.88±2.96	24.23±2.13
PaO_2/FiO_2			
0. hour	207.80±27.21	214.92±22.95	168.39±8.99
1. hour	215.64±25.27	222.80±20.04	176.54±10.68
2. hour	220.75±25.67	228.38±19.36	179.08±12.01
4. hour	224.40±25.57	231.67±19.04	180.82±13.25
6. hour	227.33±25.85	234.92±18.82	183.18±14.18
12. hour	230.91± 27.63	238.51±21.11	186.00±16.67
24. hour	233.19±29.28	241.11±22.90	187.09±17.33
48. hour	237.16±30.21	245.37±22.16	183.8± 18.94
72. hour	241.55±29.05	248.27±21.70	188.63±25.70
96. hour	246.56±24.91	249.70± 22.29	201.75± 16.5
120.hour	246.00±24.38	250.00±20.02	193.00±10.89

Mean±standard deviation was given for quantitative data. Percentage was given for categorical data.

These data were used to model longitudinal process and survival process for each of the three approaches.

The results of the extended Cox regression model, two stage approach and joint model are showed in Table 2. The extended Cox regression model, two stage approach and joint model results showed that Apache II, CAT and Carrico Index were associated with failure of treatment. In parallel, the joint model's survival component was used to calculate the final risk estimates and the results were compared with the time-dependent Cox model and two-stage model (Table 2).

Modeling of two processes separately

First, we modeled longitudinal and the survival data part of the study separately thus each model was interpreted independently. A linear mixed effect model was fitted to longitudinal data, while an extended Cox regression model is used for the survival process by taking the PaO_2 / FiO_2 biomarker values as a time dependent covariate.

Model 1.a.

$$PaO_2/FiO_{2_{ij}} = \beta_0 + \beta_1 time + \beta_2 time * time + \beta_3 Apache\ II + \beta_4 RR + \beta_5 Glasgow + b_{i0} + b_{i1} * time + b_{i2} * time * time + \varepsilon_i(t)$$

Model 1.b.

$$h(t) = h_0(t) exp(\beta_1 Apache\ II + \beta_2 Cat + \beta_3 PaO_2/FiO_2(t))$$

Two-stage modelling

The idea behind this model is to take the dependent variable (PaO_2 / FiO_2) estimates from linear mixed effects model (Model 1.a) as a time-varying explanatory variable in the extended Cox model (Model 1.b). When building a linear mixed effects model, repeated measures of PaO_2 / FiO_2 are modeled depending on time, Apache II, RR, and Glasgow score. Random intercept and random slope over time were also included as random effects. In the Cox regression model part of the joint model, we included CAT and Apache II score as time-independent variables and true estimates of PaO_2 / FiO_2 at time *t*, shown as $m_i(t)$.

Model 2.a.

$$PaO_2/FiO_{2_{ij}} = \beta_0 + \beta_1 time + \beta_2 time * time + \beta_3 Apache + \beta_4 RR + \beta_5 Glasgow + b_{i0} + b_{i1} * time + b_{i2} * time * time + \varepsilon_i(t)$$

Survival submodel that splits the time effect into step functions was used for estimating the hazard on each cut interval.

Model 2.b.

$$h(t) = h_0(t) exp\left(\beta_1 Apache + \beta_2 Cat + \beta_3 \widehat{PaO_2/FiO_2}(t)\right)$$

The relative risk model with a Weibull baseline risk function ($h_0(t)$) was used for estimating the hazard. Weibull baseline risk function is a flexible model for survival data and has a hazard rate either monotone increasing or decreasing or constant.

$$f(t) = \lambda\, p\, (\lambda)^{p-1} e^{-(\lambda t)^p}, \quad t \geq 0,\ p,\ \lambda > 0,$$

$$S(t) = exp[-(\lambda t)^p],$$

$$h(t) = \lambda\, p (\lambda t)^{p-1} \qquad \text{(Equation 11)}$$

As seen from the above formula, it is defined by a shape (*p*) and a scale (λ) parameter [21]. After we described two submodels of longitudinal and survival processes, the joint model can be written as below.

Joint Modeling

Model 3.a.

$$PaO_2/FiO_{2_{ij}} = \beta_0 + \beta_1 time + \beta_2 time * time + \beta_3 Apache + \beta_4 RR + \beta_5 Glasgow + b_{i0} + b_{i1} * time + b_{i2} * time * time + \varepsilon_i(t)$$

Table 2. Parameter estimates from different modeling strategies.

Parameters		Separate Model			Two Stage Model			Joint Model		
		$coefficient \pm SE$		*p-value*	$coefficient \pm SE$		*p-value*	$coefficient \pm SE$		*p-value*
Longitudinal Process	$Intercept$	77.56±66.49		*0.244*	77.56±66.49		*0.244*	78.43±67.56		*0.245*
	$Time$	4.12±0.29		*<0.001*	4.12±0.29		*<0.001*	4.11±0.29		*<0.001*
	$Time^2$	0.23±0.06		*0.0004*	0.23±0.06		*0.0004*	0.22±0.06		*0.0005*
	APACHE II	-1.49±0.63		*0.021*	-1.49±0.63		*0.021*	-1.49±0.63		*0.018*
	RR	-1.61±0.49		*0.0016*	-1.61±0.49		*0.0016*	-1.61±0.49		*0.011*
	$Glasgow$	19.91±3.92		*0.0007*	19.91±3.92		*0.0007*	13.87±4.00		*0.0005*
	σ_{b_0}	18.89			18.89			18.86		
	σ_{b_1}	2.38			2.38			2.39		
	σ_{b_2}	0.46			0.46			0.46		
	σ_{ε}	5.59			5.59			5.59		
		HR	**%95 CI**	***p-value***	**HR**	**%95 CI**	***p-value***	**HR**	**%95 CI**	***p-value***
Survival Process	$Apache\ II$	1.32	(0,28;2.36)	*<0.001*	1.16	(0.11;2.21)	*0.0047*	1.43	(0.31;2.55)	*0.001*
	CAT	1.15	(0.11;2.19)	*<0.001*	1.17	(0.13;2.21)	*<0.001*	1.4	(0.27;2.53)	*0.009*
	$PaO_2/FiO_2(t)$	0.97	(-0.04;1.98)	*<0.001*	0.96	(-0.05;1.97)	*<0.001*	0.96	(-0.05;1.97)	*0.004*
	$log(p)$	NA		NA	NA		NA	3.01		*<0.001*
	$log(\lambda)$	NA		NA	NA		NA	-44.97		*<0.001*

SE: Standard error, RR: Respiratory Rate, HR: hazard rate, CI: confidence interval.

Model 3.b.

$$h(t) = h_0(t)exp(\gamma_1 Apache + \gamma_2 Cat + \alpha m_i(t))$$

When joint model was built, likelihoods of model 3.a for linear mixed model and model 3.b. for Cox regression model were optimized together.

Figure 1 shows the subject-specific PaO_2 / FiO_2 index profiles and the change in PaO_2 / FiO_2 levels in time, where the bold lines are for average profiles for patients with successful NNPV and unsuccessful NNPV. As seen from the figure, the individual trends deviate from the average trends for both successful and unsuccessful treatment groups. PaO_2 / FiO_2 levels were higher in successfully treated patients and changed a little over time. However, in failure situation, descents and ascents in PaO_2 / FiO_2 levels were observed. Moreover, there was significant variability in PaO_2 / FiO_2 levels between patients. Since the average trends for both groups seem to curvilinear, we tested both quadratic and linear trend over time in modeling the longitudinal process.

Two different baseline hazard functions (Weibull and unspecified) used for the Cox regression model part. The model with Weibull

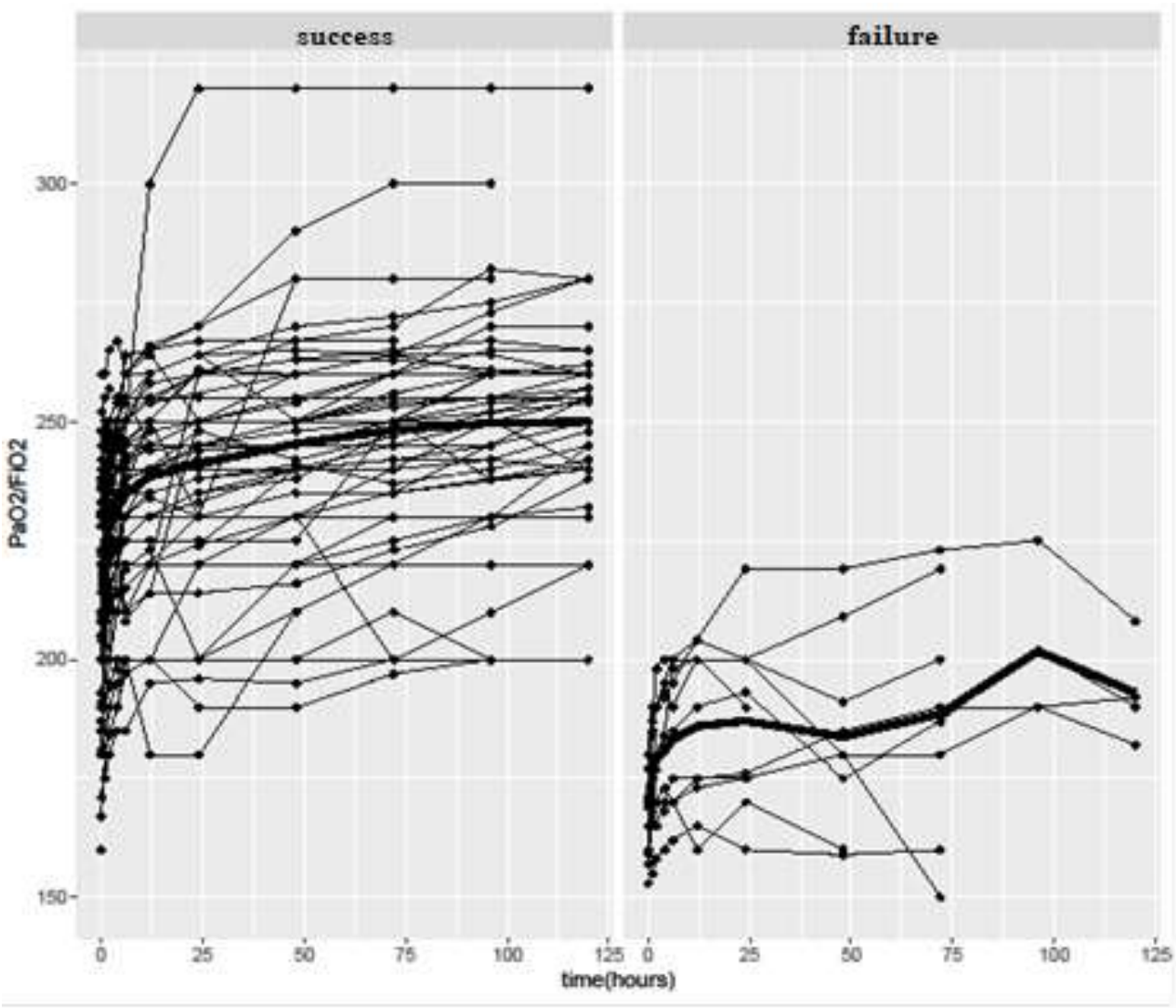

Figure 1. Subject-specific longitudinal profiles of the PaO_2 / FiO_2 index for the Carrico-Index data per group. Bold line shows the average trend over time for the group.

baseline hazard was selected for the final joint model according to the AIC and BIC criteria (AIC: 5865.09, 5912.725 and BIC: 5909.227, 5951.995, for Weibull and unspecified baseline hazard functions respectively).

As seen from Table 2, parameter estimates of linear mixed effects model are the same with separate and two stage approaches as we used exactly same models and estimation procedures for the longitudinal process. When we look at survival process in separate and two stage approaches, the effect of Apache II was diminished while the effects of CAT and Carrico Index were slightly increased. Carrico Index entered to the model as a time-varying variable in separate analysis of survival process, while estimated Carrico Index values were put in survival process of the two stage model (In two stage model, by fitting a longitudinal model the random effects are estimated in the first stage, and in the second stage these random effects are put in the extended Cox proportional hazards model).

In the joint modeling part, both longitudinal process and survival process models are fitted simultaneously using shared parameters. We see

that the effects of Apache II and CAT were increased, whereas the effect of Carrico Index was the same with two stage approach (Table 2). In the joint modeling, the patient-specific trajectory of Carrico Index levels was fitted to an LME model, and were associated with treatment through the time-to event submodel. Based on the joint modeling results, Apache II, CAT and PaO_2 / FiO_2 were found statistically significant. The estimated PaO_2 / FiO_2 increased 1.49 mm Hg and 1.61 mm Hg with every 1 score decrease in Apache II and RR, respectively. Moreover, there was 13.87 mm Hg increase in PaO_2 / FiO_2 with every 1 score increased in Glasgow score. There was a significant and inverse relationship between treatment success and the trajectory of PaO_2 / FiO_2 levels. 1 mm Hg decrease in the PaO_2 / FiO_2 at a time point *t* resulted in 1.041 (1/0.96) times higher risk of failure. The risk of failure increased 1.43 times with one unit increase in Apache II score, and also the risk of failure increased 1.4 times with one unit increase in CAT score.

Discussion

Using a joint modeling method, we investigated at the association between PaO_2 / FiO_2 levels and treatment in AHRF patients. Three types of modeling approaches were established for the analysis of changes in PaO_2 / FiO_2 measurements over time and the factors affecting survival (failure of treatment). Our study revealed that changes (ascents and descents) in PaO_2 / FiO_2 in time were strongly and significantly related with failure. In AHRF patients, the joint modeling approach offered more accurate survival predictions than the extended Cox regression and two-stage model. The following are possible explanations for why the joint modeling approach was more accurate: (i) it used the cumulative and historical information of PaO_2 / FiO_2, (ii) the true and unobserved value of the longitudinal outcome, here PaO_2 / FiO_2, was estimated by the linear mixed model, (iii) model parameters were computed simultaneously by taking into account the relationship between the longitudinal and survival processes and (iv) the patient-specific random effects were used to estimate the trend of PaO_2 / FiO_2 levels. According to the findings, the risk of failure increased by 1.041 times with every 1 mm Hg decrease in PaO_2 / FiO_2 at any time point. The decrease in the PaO_2 / FiO_2 ratio, which is frequently used in the evaluation of ventilated patients, is a sign of the presence of abnormal gas exchanges. Detection of less than 200 mm Hg indicates “Severe Hypoxemia”. PaO_2 / FiO_2 is an indicator of the lung function in mechanically ventilated critically ill patients. Although PaO_2 / FiO_2 ratio is easy to calculate and correlates with the severity of respiratory failure, it is an imperfect measure as it varies with different positive end-expiratory pressure (PEEP) levels and tidal volume [22].

In prior studies, low PaO_2 / FiO_2 at baseline AHRF, one time point after NPPV initiation, or averaged in time was related with failure and mortality [23]. Nevertheless, few research, including the current one, have concentrated on PaO_2 / FiO_2 trajectory [24, 25]. Zhang [25] reported every PaO_2 / FiO_2 measurement was observed for each patient during the follow-up period. In the current research, it is observed that different patterns among the overall trajectory of PaO_2 / FiO_2 measurements for unsuccessfully treated group. PaO_2 / FiO_2 levels were higher in successfully treated patients and changed a little in time and were shown in Figure 1.

To sum up, this study evaluated the effect of mainly scores (i.e. Glasgow, CAT, Apache II) on PaO_2 / FiO_2 levels in AHRF patients. The model parameters were returned in two divisions after building the joint model: the main effects and the

random effects, which may be used to assess population-based and patient-specific risk predictions, respectively.

Also, the present study concentrated on the trajectory of PaO_2 / FiO_2 and analyzed its relationship with treatment failure. Results of the joint modeling indicated that the Apache II and CAT levels were associated with treatment failure, similar to the results of the extended Cox proportional hazard model.

Briefly, rather of using a single biological marker value to make a treatment, physicians prefer to use repeated marker values to explore the patients' longitudinal trajectory in detail on either the best treatment option or the diagnosis. Present study was aimed to identify the best joint model combination for obtaining the optimal model for AHRF patients. Within the context of this analysis, extended Cox regression model and LME separately, two-stage model and joint including two different parameterization tecniques to link between longitudinal and survival sub-models are included. To the best of the authors' knowledge, it's the most comprehensive study that analyzes different combinations such in dept in this area, compares the criterias under these combinations.

Model Selection Criteria

After the evaluation of model fit, several models fitted can be compared with the help of certain information criteria. Commonly used ones are the Akanke Information Criteria (AIC) and the Bayesian Information Criteria (BIC). Also, it is known that the BIC method in the large sample gives better results than the AIC [21].

Limitations, Possible Sources of Bias, and Generalization Issues

There are several constraints to this study. This is a single-center prospective cohort research, and the findings may reveal center-specific effects. For this reason, the validity of the present study's findings should be evaluated in the presence of nonmeasured confounding variables. This research has potential for improvement. The multivariate extension of joint modeling has the potential to increase model performance. Because a larger sample size is required, multivariate joint modeling was not discussed in this research. This is left as a research subject for a larger study group.

Appendix

R code to fit Cox models and joint models

Description: The R script illustrates the use of the R package JM for fitting joint models for longitudinal and survival data.

Pulmonary Diseases 86 patients dataset

```
# Carrico Index (CI) = longitudinal marker
# ST = Survival times
# SS = Survival status
# CITIMES = Carrico Index measurement times
#Baseline covariates: Apache II Score, Glagow Score, respiratory rate (RR), The COPD Assessment Test (CAT)
R script
#load first package JM
library JM
#linear mixed effects model with random intercept and slope
lme.fit <-lme(CI~ CITIMES+CITIMES^2 +Apache II Score, +Glasgow+RR, ~ CITIMES+CITIMES^2 | id, data = lmedat)
#basic Cox PH model;
cox.fit<-coxph(Surv(ST, SS)~ CAT+Apache II Score, data=coxdat, x=TRUE)
#joint model with a relative risk submodel for the event time outcome, the baseline risk function with Weibull and Cox.
joint1<- jointModel(lme.fit, cox.fit, timeVar = "CITIMES", method ="weibull-PH-aGH")
joint2<- jointModel(lme.fit, cox.fit, timeVar = "CITIMES", method ="Cox-PH-aGH")
```

Funding: *The authors received no financial support for the research, authorship, and/or publication of this article.*

Conflict of Interest: *The authors declare that they have no conflict of interest.*

Ethical statement*: Ethics committee approval was received for the study (date: 01.04.2022, meeting number: 151, decision number: 2022/3732 :(9405)).*

Open Access Statement

References

[1]Tschirgi RD, Gerard RW. The carotid-mandibular reflex in acute respiratory failure. Am J Physiol. 1947; 150(2): 358-64.

[2]Ahmed Y, Adam M, Bakkar LM. Effectiveness of APACHE II and SAPS II scoring models in foreseeing the outcome of critically ill COPD patients. Egypt J Bronchol. 2019; 13(5): 654-59.

[3]Alaithan AM, Memon JI, Rehmani RS, et al. Chronic obstructive pulmonary disease: hospital and intensive care unit outcomes in the Kingdom of Saudi Arabia. Int J Chron Obstruct Pulmon Dis. 2012; 7:819-23.

[4]Zheng DW, Wang CZ, Liu RS, et al. The application of improved Glasgow coma scale score of 15 as switching point for invasive noninvasive mechanical ventilation in treatment of severe respiratory failure in chronic obstructive pulmonary disease]. Zhongguo Wei Zhong Bing Ji Jiu Yi Xue. 2011;23(4):224-7.

[5]Basol M, Goksuluk D, Sipahioglu MH, et al. Effect of serum albumin changes on mortality in patients with peritoneal dialysis: a joint modeling approach and personalized dynamic risk predictions. Biomed Res. Int. 2021; 2021, 6612464.

[6]Yu M, Taylor JMG, Sandler HM. Individual prediction in prostate cancer studies using a joint longitudinal survival–cure model. J Am Stat Assoc. 2008; 103(481): 178-87.

[7]Yang L, Yu M, Gao S. Joint models for multiple longitudinal processes and time-to-event outcome. J Stat Comput Simulat. 2016; 86(18): 3682-3700.

[8]Ibrahim JG, Chu H, Chen LM. Basic concepts and methods for joint models of longitudinal and survival data. J Clin Oncol. 2010; 28(16): 2796.

[9]Ediebah DE, Galindo-Garre F, Uitdehaag BM, et al. Joint modeling of longitudinal health-related quality of life data and survival. Qual Lif Res. 2015; 24(4), 795-804.

[10]Lim HJ, Mondal P, Skinner S. Joint modeling of longitudinal and event time data: application to HIV study. J Med Stat Informat. 2013; 1(1): 1.

[11]Rizopoulos D. Joint models for longitudinal and time-to-event data: With applications in R. CRC press; 2012.

[12]Fagyas M, Fejes Z, Sütő R, et al. Circulating ACE2 activity predicts mortality and disease severity in hospitalized COVID-19 patients. Int J Infect Dis. 2022; 115: 8-16.

[13]Konar NM, Karaismailoglu E, Karaagaoglu E. The Use of Joint Modeling Approach in Personalized Medicine, In: Abstracts of the 9th Conference of the Eastern Mediterranean Region and the Italian Region of the

International Biometric Society. Thessalonoki, Greece, 8-12 May 2017, pp. 91.

[14] Rizopoulos D, Taylor JM, Van Rosmalen J, et al. Personalized screening intervals for biomarkers using joint models for longitudinal and survival data. Biostatistics. 2016; 17(1): 149-64.

[15] Çiftci F, Çiledağ A, Erol S, et al. Non-invasive ventilation for acute hypercapnic respiratory failure in older patients. Wiener klinische Wochenschrift. 2017; 129(19): 680-86.

[16] Therneau T. A package for survival analysis in S. R package version, 2015. 2(7). Available from: https://CRAN.R-project.org/package=survival. 2022/

[17] Pinheiro J, Bates D, DebRoy S, et al. Linear and nonlinear mixed effects models. R package version, 2007; 3(57): 1-89. R package version 3. pp. 1-157. Available from: https://CRAN.R-project.org/package=nlme/

[18] Rizopoulos D. JM: An R package for the joint modelling of longitudinal and time-to-event data. J Stat Soft. 2010; 35: 1-33.

[19] Kleinbaum DG, Klein M. Survival analysis: a self-learning text (Vol. 3). New York: Springer; 2012.

[20] Auton T Applied survival analysis: regression modelling of time to event data. J Appl Stat. 2000; 27(1): 132-133.

[21] Klein JP, Moeschberger ML. Survival analysis: techniques for censored and truncated data (Vol. 1230). New York: Springer; 2003.

[22] Seeley E, McAuley DF, Eisner M, et al. Predictors of mortality in acute lung injury during the era of lung protective ventilation. Thorax. 2008; 63(11): 994-98.

[23] Satou T, Imamura H, Mochiduki K, et al. Efficacy of protocol-based non-invasive positive pressure ventilation for acute respiratory distress syndrome: a retrospective observational study. Acute Med Surg. 2020; 7(1): e465.

[24] Antonelly M, Conti, G, Esquinas A. A multiple-centre survey on the use in clinical practice of noninvasive ventilation as a first-line intervention for acute respiratory distress syndrome. Crit Care Med. 2007; 35(1): 18-25.

[25] Zhang L, Wang Z, Xu F, et al. The Role of Glucocorticoids in the Treatment of ARDS: A Multicenter Retrospective Study Based on the eICU Collaborative Research Database. Front Med. 2021;8: 678260.

Exp Biomed Res 2023; 6(1): 38-44 **DOI: 10.30714/j-ebr.2022.168**

Experimental Biomedical Research *Original article*

The relation of first trimester PaPP-A level and vaginal birth complications in large for gestational age fetuses

Anil Erturk, Nergis Kender Erturk*

Department of Obstetrics and Gynecology, Bursa Yuksek Ihtisas Training and Research Hospital, Bursa, Türkiye

ABSTRACT

Aim: To investigate the association of vaginal birth complications with first trimester pregnancy associated plasma protein A (PaPP-A) level in LGA vaginal deliveries of non-diabetic mothers.

Methods: This is a retrospective study conducted in a tertiary hospital between May 2020 and July 2022. A total of 9,184 singleton pregnancies with normal vaginal delivery between 37 and 42 weeks were reviewed. Non- diabetic patients who gave birth to LGA infants were grouped according to the presence of vaginal birth complications and compared in terms of first trimester aneuploidy screening results. Regression analysis was used to investigate the effect of variables on complications. Receiver operating characteristic (ROC) analysis was performed for the threshold PaPP-A value to predict birth complications.

Results: Of the 357 patients, 68 (19.0%) had at least one complication, remaining 289 (81.0%) had no complications. First trimester serum PaPP-A level was significantly higher in complicated group than patients without complications (20.85 ± 19.73 vs 15.18 ± 15.81, p= 0.046). First trimester NT, β-hCG and PaPP-A are significantly associated with perinatal complications in LGA vaginal deliveries. The cut-off value of first trimester PaPP-A level was 10.46 mIU/mL to predict the complications with a sensitivity of 54.4% and a specificity of 54.3%.

Conclusions: First trimester PaPP-A level may be associated with vaginal birth complications in LGA infants from non-diabetic mothers.

Key words: Pregnancy, prenatal care, placenta, labor complications, PaPP-A.

✉ * *Dr. Nergis Kender Erturk,*
Department of Obstetrics and Gynecology, Bursa Yuksek Ihtisas Training and Research Hospital, Bursa, Türkiye
E-mail: nergiskender@gmail.com
Received: 2022-11-22
Accepted: 2022-12-06 / Published: 2023-01-01

Introduction

Infants with a birth weight greater than the 90th percentile for gestational age are defined as Large for gestational age (LGA) newborns. LGA babies are at increased risks of adverse perinatal outcomes such as instrumental vaginal delivery, shoulder dystocia, perinatal asphyxia and neonatal mortality [1]. Although the mechanisms controlling fetal weight gain and growth are not well understood, it can be mentioned that genetic, maternal, placental and intrauterine environmental factors are effective in excessive fetal growth.

Pregnancy associated plasma protein A (PaPP-A) and freeβ-human chorionic gonadotropin (β-hCG) both released from placental syncytiotrophoblasts are components of first trimester aneuploidy screening with ultrasonographic measurement of fetal nuchal

translucency (NT) thickness [2]. PaPP-A leads to increased secretion of insulin-like growth factors and thus plays a role in fetal growth [3]. High maternal serum PaPP-A in the first trimester was reported to be associated with the risk of fetal LGA [4,5]. In addition, free beta-Hcg levels have been shown to be associated with birth weight [6].

The associations of PaPP-A with birth weight and complications related to LGA have been investigated especially in diabetic pregnancies [7,8]. However, the role of these first trimester screening markers in perinatal outcomes of LGA infants from non-diabetic mothers is unclear. It is important to predict possible complications in order to improve perinatal outcomes in LGA deliveries.

Given this background, the aim of the study was to investigate the association of adverse perinatal outcomes due to macrosomia with first trimester PAPP-A level in LGA vaginal deliveries of non-diabetic mothers.

Materials and metods

This is a retrospective study conducted in a university affiliated tertiary hospital between May 2020 and July 2022. Local ethics committee approval was obtained (2011-KAEK-25 2022/10-9) and the study was carried out in accordance with the Declaration of Helsinki.

A total of 9,184 singleton pregnancies with normal vaginal delivery between 37 and 42 weeks were reviewed. Demographic data, maternal comorbidities, laboratory results, newborn data and delivery complications were obtained from electronic and manual patient files. Those who gave birth to LGA infants, those who were screened for aneuploidy in the first trimester and those whose pregnancy follow-up visits were performed in our hospital were included in the study. Those who were obese, with pre- or gestational diabetes diagnosis, those with hypertensive disorders, preterm pregnancies, small for gestational age (SGA) infants, cesarean deliveries, fetal genetic or congenital anomalies, and missing records were excluded from the study. Those with abnormal results of 75g/100 g glucose tolerance tests were defined as gestational diabetes. Birth weight was defined as SGA if it was <10th percentile, AGA if it was between 10-90th percentile, and LGA if it was >90th percentile.

A total of 357 patients were analyzed. For these patients, maternal age, gestational week, BMI, gravida, parity, time from active phase to delivery, need for induction, first trimester serum Papp-A, free β-hCG and nuchal translucency (NT) thickness values and perinatal complications were recorded.

Vacuum or forceps delivery, 3-4 perineal tears, cervical laserations, neonatal APGAR score below 7, dystocia, clavicle fracture, caput succedaneum, postpartum atony were considered as adverse perinatal outcomes. According to the records, patients who underwent the Mc roberts maneuver and suprapubic compression during delivery or clavicle fracture were defined as dystocia, and patients who needed additional uterotonics in the third stage of labor, who underwent intrauterine balloon tamponade or surgical approach were defined as postpartum atony.

Statistical analysis

SPSS 21 software (SPSS Inc Chicago,IL) program was used for statistical analysis. Normality of distribution was evaluated with the Shapiro Wilk test. Parametric data were given as mean±SD, non-parametric data as median (min-max). Student t test or Mann Whitney u test was used to compare the groups according to distribution. Categorical data were analyzed with the chi-square test. Multi-nominal logistic regression analysis was performed to evaluate

the effects of independent variables on complications. ROC analysis was performed to find out the cut-off value of first trimester PaPP-A level to predict the complications of LGA vaginal deliveries. p <0.05 was considered as statistically significant.

Results

The mean age of the patients was 27.89±5.49 and ranged between 17-45 years. The mean birth weight of infants was 4010.20±199.42 and ranged between 3700-5315 gr. The mean gestational week was 39.08±1.18 and ranged between 37-42 weeks. Of the 357 patients, 68 (19.0%) had at least one complication, remaining 289 (81.0%) had no complications. Demographic and clinical characteristics of the groups were given in Table 1. First trimester serum PaPP-A level was significantly higher in complicated group than patients without complications (20.85 ± 19.73 vs 15.18 ± 15.81, p= 0.046) (Table 1).

The overall complication rate of LGA vaginal deliveries was 19.0%. The rates of each complications were given in Table 2. Vacuum was used in all eight patients who delivered operatively. Among patients with postpartum atony intrauterine balloon tamponed was applied to seven subjects, hysterectomy was performed in one patient.

Table 1. Demographic and clinical features of the groups.

Parameters	**Patients Wo complications (n=289)**	**Patients w complications (n=68)**	***p***
Age (y)	27.86 ±5.62	28.00 ±4.95	*0.618*
Gravida*	3 (1-12)	3 (1-7)	*0.354*
Parity*	2 (0-10)	2 (0-6)	*0.152*
BMI (kg/m2)	24.00 ±2.58	24.15 ±2.95	*0.713*
Gestational week of birth (w)	39.04 ±1.18	39.29 ±1.15	*0.093*
Induction need, n(%)	201 (69.6)	55 (80.9)	*0.062*[a]
Labor length (h)	6.00 ±5.13	5.60 ±4.26	*0.893*
Birth Weight (gr)	4004.69 ±200.24	4033.61 ±195.65	*0.259*
APGAR score 1st minute*	9 (5-9)	9 (5-9)	*0.219*
First trimester screening tests			
Nuchal translucency (mm)	1.30 ±0.36	1.39 ±0.29	*0.054*
PaPP-A (mIU/mL)	15.18 ±15.81	20.85 ±19.73	*0.046*
Free B-hCG (ng/mL)	79.41 ±65.69	65.57 ±44.94	*0.157*

Wo: without, w: with, y: years, BMI: body mass index, w: weeks, h: hours. Values are given as mean ±SD and Mann Whitney U test was performed, unless otherwise mentioned. A p value <0.05 was considered as significant.
**Values are given median (min-max). [a] Chi square test was performed.*

Table 2. The rates of each perinatal complication in total patients (n=357).

Complications	n (%)
Dystocia	31 (8.7)
Operative delivery	8 (2.2)
3-4 degree perineal tear	7(2.0)
Cervical laceration	12 (3.4)
Postpartum atony	13 (3.6)
Clavicle fracture	6 (1.7)
Brachial plexus injury	2 (0.6)
Caput succedaneum	3 (0.8)
1st min APGAR score < 7	4 (1.1)

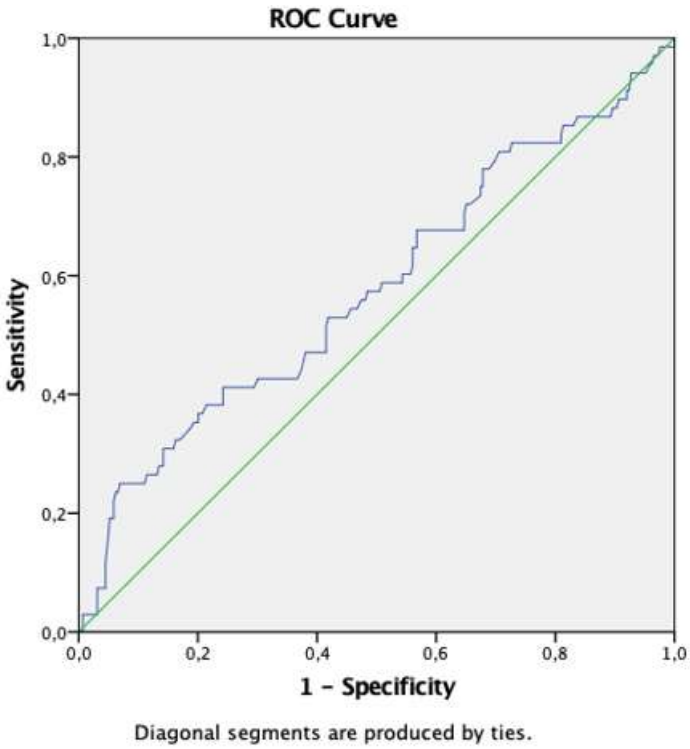

Figure 1. Receiver operating characteristic (ROC) curve of first trimester Pregnancy associated plasma protein A (PaPP-A) for the the prediction of birth complications. The estimate of the area under curve (AUC) and its 95 % confidence interval is shown. Cut-off value of PaPP-A was 10.46 mIU/mL (sensitivity 54.4% and specificity 54.3%) for prediction of LGA birth compliactions. (AUC: 0.578; 95% CI (0.497- 0.658), $p<0.05$).

The Spearman correlation coefficients between first trimester markers (PaPP-A and β-hCG) and birth weight were -0.022 and 0.096 respectively (p=0.685 and p=0.71, respectively). According to logistic regression analysis, first trimester NT, β-hCG and PaPP-A are significantly associated with perinatal complications in LGA vaginal deliveries (p = 0.019, R2 =0.04). The odds ratio of PaPP-A was 1.016, 95% CI (1.001-1.031) (p=0.035). According to the ROC analysis, the cut-off value of first trimester PaPP-A level was 10.46 mIU/mL to predict the complications in LGA vaginal deliveries with a sensitivity of 54.4% and a specificity of 54.3% (Area under curve (AUC): 0.578; 95% CI (0.497- 0.658), p=0.046) (Figure 1).

Discussion

In this study, we examined the relationship between perinatal complications that may occur in LGA vaginal deliveries and first trimester aneuploidy screening tests. First trimester NT, β-hCG and PaPP-A were associated with perinatal complications. In the complicated group, the level of PaPP-A was significantly higher than those without complications.In addition, a PaPP-a level above 10.46 mIU/mL was calculated to predict the risk of complications in LGA-vaginal deliveries.

The prevalence of LGA fetuses, which is important in prenatal care, is increasing. Newborns with a birth weight above the 90th percentile for gestational age are defined as LGA (9). The risks of maternal and perinatal morbidity and even mortality are increased in pregnancies with LGA fetuses (1). Birth weight can be affected by many maternal factors such as ethnicity, age, body mass index, nutritional status

and medical conditions (10). In addition to these, placental function in early pregnancy may also be associated with birth weight. PaPP-A and hCG are placenta-derived factors. Many reports have been published showing that adverse perinatal outcomes may be associated with maternal β-hCG and PaPP-A levels measured in the first trimester of pregnancy (4,6, 11, 12). However, the relationship between these markers and perinatal complications in LGA babies in healthy pregnancies is not clear. To the best of our knowledge, this study is the first report in the literature examining this relationship.

According to Beneventi et al, there was a positive correlation between PaPP-A and birth weight in non-diabetic pregnancies (13). Kapustin et al reported that first trimester screening tests could not be used to predict the complications in diabetic pregnancies, they found no link between PaPP-A or hCG and birth weight (7). It could be thought that PaPP-A levels may be lower in diabetic pregnancies than the healthy population due to the impaired placental function. Our subjects were healthy and we could not detect a significant association between PaPP-A or hCG and birth weight. However, first trimester PaPP-A level was analyzed to be associated with complications in LGA deliveries.

PAPP-A is a metalloproteinase that helps release insulin growth factor (IGF) at the cellular level, thereby contributing to cell growth (14). In the literature, the relationship of first trimester PAPP-A level with the development of maternal metabolic diseases during pregnancy as well as its possible role in predicting long-term maternal complications after pregnancy has been reviewed (15). In a recent analysis, low PAPP-A serum levels in the first trimester of pregnancy were reported to be associated with infant short stature and the development of maternal diabetes mellitus in the mother later in life (15).

According to the "Barker hypothesis", the placenta has a very important role in fetal programming, and the development of diseases that may occur in later life may be related to intrauterine life. Based on this hypothesis, we investigated the predictability of shoulder dystocia, an unavoidable complication of labor, and other complications that may occur in LGA deliveries. As a result, we determined that markers of placental origin measured in the first trimester may be associated with these conditions. It can be thought that birth complications are affected by many maternal and environmental factors. Therefore, maternal systemic diseases, obesity, fetal anomalies were excluded in this study. There was no difference between patients with and without complications in terms of demographic data and labor follow-up data. These are all strengths of the study. In addition to the fact that the delivery induction protocols are not standardized for every patient, the relatively small patient population and the inability to clearly access data on cesarean section with indications of acute fetal distress due to retrospective data can be stated as limitations.

Conclusions

In conclusion, first trimester aneuploidy markers, particularly PaPP-A, may be associated with fetal development and thus vaginal birth complications. In the presence of an estimated large for gestational age fetus, the PaPP-A level measured in the first 3 months of pregnancy can give the clinician an idea about the possibility of birth complications. However, prospective studies are needed for further interpretation on the subject.

Acknowledgments of people: Special thanks to Sabiha Gokcen Donmez and Gulnur Tanrıverdi

Kılıç for their assistance in providing access to the electronic files of some patients.

Funding: *The authors received no financial support for the research, authorship, and/or publication of this article.*

Conflict of Interest: *The authors declare that they have no conflict of interest.*

Ethical statement*: Local ethics committee approval was obtained (2011-KAEK-25 2022/10-9) and the study was carried out in accordance with the Declaration of Helsinki.*

References

[1]Xu H, Simonet F, Luo ZC. Optimal birth weight percentile cut-offs in defining small- or large-for-gestational-age. Acta Paediatr. 2010; 99(4):550-55.

[2]Krantz D, Goetzl L, Simpson JL, et al. Association of extreme first-trimester free human chorionic gonadotropin-beta, pregnancy-associated plasma protein A, and nuchal translucency with intrauterine growth restriction and other adverse pregnancy outcomes. Am J Obstet Gynecol. 2004;191:1452–58.

[3]Lawrence JB, Oxvig C, Overgaard MT, et al. The insulin-like growth factor (IGF)-dependent IGF binding protein-4 protease secreted by human fibroblasts is pregnancy-associated plasma protein-A. Proc Natl Acad Sci U S A. 1999;96(6):3149-53.

[4]Tul N, Pusenjak S, Osredkar J, et al. Predicting complications of pregnancy with first-trimestermaternal serum free-beta-hCG, PAPP-A and inhibin-A. Prenat Diagn. 2003;23: 990 – 96.

[5]Canini S, Prefumo F, Pastorino D, et al. Association between birth weight and first-trimester free beta-human chorionic gonadotropin and pregnancy-associated plasma protein A. Fertil Steril. 2008;89(1):174-78.

[6]Poon LC, Karagiannis G, Stratieva V et al. First-trimester prediction of macrosomia. Fetal Diagn Ther. 2011;29(2):139-47.

[7]Kapustin RV, Kascheeva TK, Alekseenkova EN, et al. Are the first-trimester levels of PAPP-A and fb-hCG predictors for obstetrical complications in diabetic pregnancy? J Matern Fetal Neonatal Med. 2022;35(6):1113-19.

[8]Savvidou MD, Syngelaki A, Muhaisen M, et al. First trimester maternal serum free β-human chorionic gonadotropin and pregnancy-associated plasma protein A in pregnancies complicated by diabetes mellitus. BJOG. 2012;119(4):410-16.

[9]Alexander, G. R., Himes, J. H., Kaufman, R. B.et al. United States national reference for fetal growth. Obstet Gynecol. 1996; 87(2): 163–68.

[10]Wen SW, Goldenberg RL, Cutter GR, et al. Smoking, maternal age, fetal growth, and gestational age at delivery. American journal of obstetrics and gynecology, 1990; 162(1), 53–58.

[11]Donovan BM, Nidey NL, Jasper EA, et al. First trimester prenatal screening biomarkers and gestational diabetes mellitus: A

systematic review and meta-analysis. PloS One. 2018; 13(7): e0201319.

[12] Pilalis A, Souka AP, Antsaklis P, et al. Screening for pre-eclampsia and fetal growth restriction by uterine artery Doppler and PAPP-A at 11-14 weeks' gestation. Ultrasound Obstet Gynecol. 2007;29(2):135-40.

[13] Beneventi F, Simonetta M, Lovati E, et al. First trimester pregnancy-associated plasma protein-A in pregnancies complicated by subsequent gestational diabetes. Prenat Diagn. 2011;31(6):523-28.

[14] Monget P, Oxvig C. PAPP-A and the IGF system. Ann Endocrinol (Paris). 2016;77(2):90-96.

[15] Fruscalzo A, Cividino A, Rossetti E, et al. First trimester PAPP-A serum levels and long-term metabolic outcome of mothers and their offspring. Sci Rep. 2020;10(1):5131.

Exp Biomed Res 2023; 6(1): 45-56 **DOI: 10.30714/j-ebr.2022.169**

Experimental Biomedical Research *Original article*

A preliminary study on radiolabeling and quality control of [^{99m}Tc]Tc-6-mercaptopurine to develop tumor scintigraphic agent

Meliha Ekinci*, Derya Ilem Ozdemir

Department of Radiopharmacy, Ege University, Faculty of Pharmacy, Izmir, Türkiye

ABSTRACT

Aim: Cancer is one of the most cause of deaths in worldwide. 6-mercaptopurine (6-MP) is successfully to treat leukemia. In recent years, 6-MP has remarkable properties for treating solid tumors. The aim of this study is to radiolabel 6-MP with [^{99m}Tc]Tc under appropriate conditions to develop tumor scintigraphic agent.

Methods: In this work, 6-MP was radiolabeled using [^{99m}Tc]Tc radionuclide, and quality control experiment of [^{99m}Tc]Tc-6-MP were assessed *via* radioactive thin layer chromatography (RTLC). Also, the effect of critical parameters affecting the radiolabeling efficiency (reducing and antioxidant agent, incubation time, pH value, radiation dose) was evaluated. Then, the stability and lipophilicity tests of [^{99m}Tc]Tc-6-MP was performed.

Results: According to the results, [^{99m}Tc]Tc-6-MP was prepared with over 93% labeling efficiency by a novel, easy, and quick direct method with 15-min incubation time at pH 7. To achieve the best radiolabeling condition; 0.5 mg.mL^{-1} of 6-MP solution, 250 µg of stannous tartrate (reducing agent), 0.050 mg ascorbic acid (antioxidant agent), and 37 MBq [^{99m}Tc]Tc was used. The RTLC studies indicated that [^{99m}Tc]Tc-6-MP is stable up to 6-h in room temperature. The log*P* of the [^{99m}Tc]Tc-6-MP were found to be -0.021 ± -0.001.

Conclusions: The obtained results showed that radiolabeled 6-MP may be a promising tumor diagnostic agent. Further studies are in progress in order to evaluate tumor cell binding capacity and biodistribution of the complex in experimental animals.

Key words: 6-mercaptopurine, technetium-99m, radiolabeling, radiopharmaceuticals, tumor.

.

✉ * *Meliha Ekinci,*
Department of Radiopharmacy, Ege University, Faculty of Pharmacy, Izmir, Türkiye
E-mail: melihaekinci90@gmail.com
Received: 2022-07-30 / Revisisons: 2022-09-29
Accepted: 2022-10-02 / Published: 2023-01-01

Introduction

Cancer has long been one of the world's top causes of death [1,2]. Detection and effective treatment of cancer at early levels significantly reduces the cost and duration of treatment, and the risk of mortality and morbidity [3]. Nuclear medicine imaging offers non-invasive functional data at the cellular and molecular level. Abnormalities are frequently detected at very early stages by nuclear imaging techniques [4]. Therefore, it is critical to develop radiopharmaceuticals that can detect physiological changes before anatomical changes occur.

In scintigraphic imaging studies, the appropriate radionuclide is bound with the pharmaceutical part, and the radiation emitted by the radionuclide is imaged with a gamma camera following application [5]. The scintigraphic images obtained with the camera that records the gamma rays emitted from the given radioactive

compound provide information about the functions and anatomy of the systems in the body. These tests are widely used in the world, because they are safe and non-invasive [6-8].

Radioactive and pharmaceutical components are combined in radiopharmaceuticals for diagnosis or treatment of a disease [9]. When choosing a suitable radionuclide for radiolabeling experiments, it is considered to radiation dose, cost, and availability. Ideal characteristics of [^{99m}Tc]Tc include its 140 KeV pure gamma photon emission, 6-h physical half-life, low price, and ease of supply. These features makes [^{99m}Tc]Tc the most frequently used radionuclide in nuclear medicine [10].

6-mercaptopurine (6-MP) known as a purine analogue is used successfully to treat cancer, particularly leukemia [11]. Because of its excellent coordination properties resulting from its nitrogen and sulfur donor sites, which can be bound at N-1, N-3, N-7, and N-9, 6-MP has recently received a lot of attention as an antineoplastic drug. 6-MP also possesses chemotherapeutic properties. The capacity of 6-MP to convert the nitrogen donor sites into the corresponding ribosides is thought to be the basis for its activity in cancer cells [12,13]. Dorniani *et al.* [14] developed 6-MP-coated magnetite nanoparticles which can be as an alternative drug delivery system for breast cancer treatment [14]. Also, Nezhad-Mokhtari *et al.* [15] designed polymeric nanogels including 6-MP and methotrexate for treatment of breast cancer. These smart nanogels found as effective cancer therapy agent [15]. The aim of this study is to develop a novel radiopharmaceutical to detected for tumor. For this aim, 6-MP was labeled with [^{99m}Tc]Tc by appropriate conditions. Labeling efficiency and *in vitro* stability of [^{99m}Tc]Tc-6-MP were investigated *via* radioactive thin layer chromatography (RTLC) studies in the framework of pre-study.

Materials and metods

Materials: Aspen (Feucht, Germany) provided 6-MP. Merck (Germany) provided stannous chloride, stannous tartrate, and ascorbic acid. The [^{99}Mo]Mo/[^{99m}Tc]Tc generator yielded [^{99m}Tc]$NaTcO_4$ (Nuclear Medicine Department of Ege University, Türkiye). All solvents used were of analytical grade and obtained from Merck (Germany).

Radiolabeling of [^{99m}Tc]Tc-6-MP: To determine the optimum labeling procedures, [^{99m}Tc]Tc-6-MP was evaluated in different types and quantities of reducing and antioxidant agents. Also, the effect of pH value, incubation time, radiation dose, *in vitro* stability in 0.9% sodium chloride solution (SF) on radiochemical purity (RP), and partition coefficient value were investigated. RP was measured with the help of RTLC analysis [16,17].

Effect of reducing agent type and amount on radiolabeling of [^{99m}Tc]Tc-6-MP: Stannous salts (chloride and tartrate) were used as reducing agent, individually. Firstly, 6-MP (0.5 mg) was dissolved in SF solution (1 mL). Then, stannous chloride was added to the system. The reduction of [^{99m}Tc]Tc occurred at an acidic pH (1 mg stannous chloride dissolved in 1 mL 0.01 N HCl) with different concentration of stannous chloride (10, 25, 50, 100 and 250 $\mu g.\mu L^{-1}$). Radiolabeling of 6-MP was performed with 37 MBq of [^{99m}Tc]Tc in SF (0.1 mL) and the system was incubated for 15-min.

In radiolabeling studies, stannous tartrate was also used as a reducing agent. Briefly, 6-MP (0.5 mg) was dissolved in SF (1 mL). Then, 10, 25, 50, 100 and 250 $\mu g.\mu L^{-1}$ stannous tartrate (1 mg stannous tartrate diluted in 1 mL 0.01 N HCl) and 37 MBq [^{99m}Tc]Tc was added to the solution. Prior to radiochemical analysis, the radiolabeled complexes were allowed to remain for 15-min incubation time.

Effect of antioxidant agent on radiolabeling of [^{99m}Tc]Tc-6-MP: Radiolabeling tests were conducted in the absence and presence of an antioxidant agent to assess the influence of the antioxidant agent on the radiolabeling efficiency and stability of [^{99m}Tc]Tc-6-MP. The antioxidant agent was ascorbic acid, while the reducing agent was stannous tartrate. In brief, 6-MP (0.5 mg) was dissolved in SF (1 mL). Each solution received 50, 100 and 250 µg of stannous tartrate. Radiolabeling was performed in the absence and presence of ascorbic acid (0.025 and 0.050 mg, respectively). Freshly eluted 37 MBq [^{99m}Tc]Tc was added to system, and the vials were incubated for 15-min. RTLC was used to determine the labeling efficiency.

Effect of pH on radiolabeling of [^{99m}Tc]Tc-6-MP: The effect of pH value on [^{99m}Tc]Tc-6-MP labeling efficiency was investigated for pH 2.0 to 9.0. For this purpose, the pH value of [^{99m}Tc]Tc-6-MP was adjusted to 2.0, 7.0 and 9.0 after labeling using 0.1 N HCl and 0.01 N NaOH solutions. Then, the labeling stability of the compounds which have different pH value was evaluated every hour.

Effect of incubation time on radiolabeling of [^{99m}Tc]Tc-6-MP: In order to evaluate the effect of time upon the stability of radiolabeling, the RTLC studies were performed in varied times: 5, 15, 30, 45- and 60-min after post-labeling.

Effect of dose amount on radiolabeling of [^{99m}Tc]Tc-6-MP: The radiolabeling assay has been performed at: 37, 185 and 370 MBq for the effect of the amount of [^{99m}Tc]Tc on the radiolabeling.

In vitro stability of [^{99m}Tc]Tc-6-MP: For *in vitro* stability, [^{99m}Tc]Tc-6-MP (0.1 mL) reaction media was added to SF (0.4 mL). The mixture was incubated for 6-h at room temperature and RTLC assays were performed every hour up to 6-h.

Quality control of [^{99m}Tc]Tc-6-MP: As stationary phases, Whatman 3MM plates and ITLC-SG papers were chosen. Whatman 3MM plates were used as the stationary phase and acetone (100%) as the mobile phase to measure free-[^{99m}Tc]Tc. ITLC-SG papers developed in a Acetonitrile/ Water/Trifluoroacetic acid (ACN/W/TFA; 50/25/1.5) solvent mixture was used to evaluate Reduced/Hydrolized (R/H)-[^{99m}Tc]Tc. The radioactivity on plates was assessed using a TLC scanner (Bioscan AR 2000) after chromatographic separation, and the RP (%) of [^{99m}Tc]Tc was estimated using the following equation (Eq. 1) [18,19]:

RP (%) = 100 – (Free-[^{99m}Tc]Tc (%) + R/H-[^{99m}Tc]Tc (%)) (Eq.1)

Partition coefficient study of [^{99m}Tc]Tc-6-MP: For partition coefficient study of [^{99m}Tc]Tc-6-MP, n-octanol and PBS (pH: 7) were used. In a centrifuge eppendorf, n-octanol (300 µL), PBS (pH: 7; 300 µL) and [^{99m}Tc]Tc-6-MP (150 µL) were added, mixed for 1-min, then centrifuged at 1420 x *g* for 30-min. The mixture underwent centrifugation and split into two stages. A total of 100 µL of lower and upper phase activity were counted using a gamma counter. The following equation was used to obtain the log*P* value of [^{99m}Tc]Tc-6-MP (Eq. 2) [20]:

log*P* = log (n-octanol phase/PBS phase) (Eq.2)

Statistical analysis: Using Microsoft Excel, the means and standard deviations were computed. The statistical significance was assessed using the t test. Differences that were significant at the 95% level of confidence (p>0.05) were noted.

Results and Discussion

Cancer is the leading cause of death worldwide. According to 2020 data, a total of 19.3 million new cancer cases developed in the

world, and 10.0 million people died due to cancer [2]. Cancer can be defined simply as uncontrolled cell proliferation. Although uncontrolled proliferation is the main feature, the cancer cell also has other biological characteristics. These include avoiding contact inhibition in cell cultures, not requiring external stimuli to divide, insensitivity to proliferation suppressive signals, avoiding apoptosis, stimulating angiogenesis and metastasis. Although there are many different types of cancer, they all start with the out-of-control proliferation of abnormal cells. If left untreated, it can cause serious illness and even death [21,22].

Anatomical imaging techniques are not sufficient for imaging in the initial stage of cancer, as they rely on morphological changes. Since scintigraphic imaging is a non-invasive imaging technique based on the detection of physiological changes, it allows diagnosis at an early stage [23,24]. With nuclear medicine imaging techniques, both the diagnosis of the disease and its prevalence, and in other words, at what stage is determined [25].

Radiolabeling of [^{99m}Tc]Tc-6-MP: In this study, a new, simple, quick, and efficient direct labeling approach for [^{99m}Tc]Tc-6-MP was developed. The RTLC tests were used to evaluate the RP of the radiolabeled compound.

In the past years, 6-MP was radiolabeled with different radionuclides. 6-MP was labeled with [^{14}C]C and [^{35}S]S by Adamson *et al.* [26] and [^{67}Ga]Ga by Guarino *et al.* [27] for different purposes. Hunt *et al.* [28] radiolabeled 6-MP with [^{99m}Tc]Tc for cholescintigraphy. According to the study, the [^{99m}Tc]Tc-6-MP was cleared rapidly from the blood and concentrated in the bile. So, the researchers concluded that this finding prompted further assessment of the compound as a radiopharmaceutical for cholescintigraphy [28].

In this study, we performed radiolabeling and quality control studies with [^{99m}Tc]Tc for the usability of 6-MP as tumor diagnostic agent without long labeling process, heating, boiling, and purification.

Effect of reducing agent type and amount on radiolabeling of [^{99m}Tc]Tc-6-MP: In the +7 oxidation level, [^{99m}Tc]Tc was eluted from the

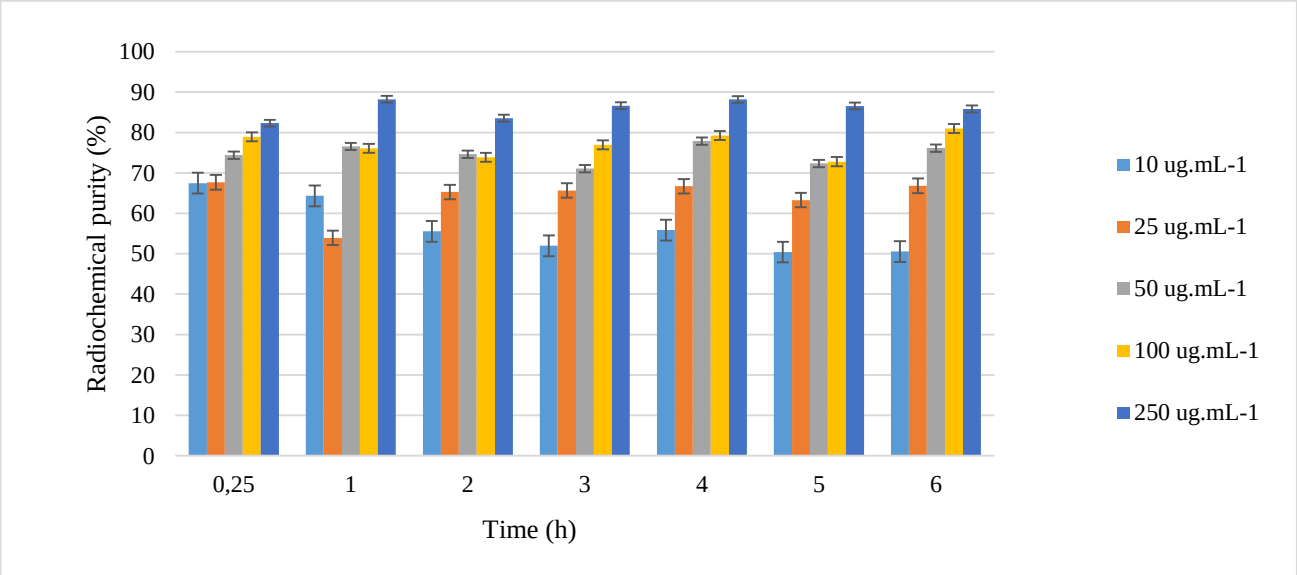

Figure 1. Radiochemical purity of [^{99m}Tc]Tc-6-MP with different amounts of stannous chloride.

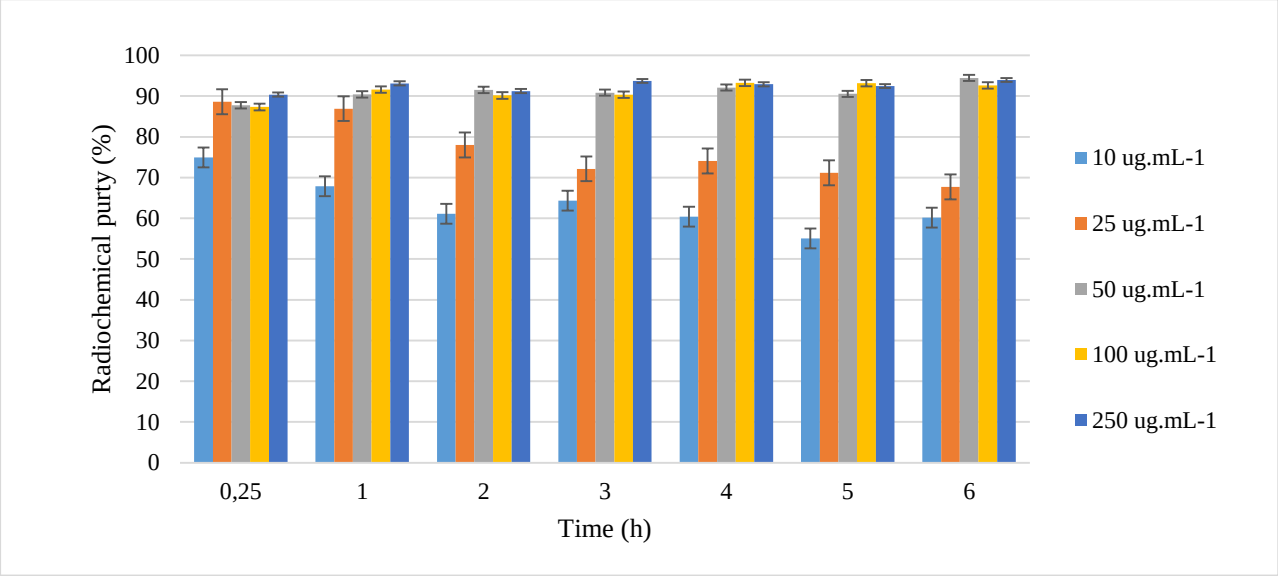

Figure 2. Radiochemical purity of [^{99m}Tc]Tc-6-MP with different amounts of stannous tartrate.

[^{99}Mo]Mo/[^{99m}Tc]Tc generator. When added directly, [^{99m}Tc]Tc cannot be labeled with any component. To form compounds with the ligand and produce the radiopharmaceutical, [^{99m}Tc]Tc must be lowered to +4/+5 oxidation levels prior to radiolabeling. The researchers have used a variety of reduction agents for this purpose, including stannous chloride, stannous tartrate, sulphonic acid, sodium dithionite, sodium borohydride, formamidine, hydrohalic acids, and others. Stannous salts are frequently used as a reductant within them due to its non-toxic and stable characteristics [9,29].

Labeling tests were carried out with the identical concentrations of active component (6-MP), reducing agent (stannous chloride or stannous tartrate), and radionuclide ([^{99m}Tc]Tc) in order to analyze the influence of reducing agent type and amount on RP. Two formulation groups were formed. The first group uses stannous chloride as a reducing agent, while the second uses stannous tartrate. Figure 1 and Figure 2 show comparative findings for both formulations.

As seen in Figure 1, in all added amounts of stannous chloride, the RP could not exceed 90%.

The RP of a radiopharmaceutical should be ≥ 90% to have high image quality and not retain radiochemical impurities in non-target tissues [30].

As seen in Figure 2, the RP of [^{99m}Tc]Tc-6-MP increased above 90% with the addition of increasing amounts of stannous tartrate to the radiolabeled complex. According to the results, it was selected formulations prepared with 50-250 µg stannous tartrate for further studies. Also, it is crucial to note that using more reducing agent than necessary when radiolabeling [^{99m}Tc]Tc to create [^{99m}Tc]Tc complexes is highly advised [31].

Effect of antioxidant agent on radiolabeling of [^{99m}Tc]Tc-6-MP: Auto radiolysis may occur during the produce and storage of [^{99m}Tc]Tc radiopharmaceuticals as a result of the water's natural degradation by ionizing radiation [32]. The RP of radiopharmaceuticals is reduced by this decomposition. As a result, using a stabilizer to decrease auto radiolysis is critical. Antioxidants including p-aminobenzoic acid, ascorbic acid, and gentisic acid are frequently used as radiolytic stabilizers [33]. In this study, we used ascorbic acid as antioxidant.

To determine the effect of antioxidant agent amount on RP, 0.025 mg and 0.050 mg ascorbic acid was added to the formulations prepared by adding 50-250 µg of stannous tartrate. The results were shown in Table 1–3.

Table 1. The radiochemical purity of [^{99m}Tc]Tc-6-MP including 50 µg stannous tartrate in the absence and presence of antioxidant agent.

Time (hour)	Radiochemical purity (%)		
	Absence of ascorbic acid	Ascorbic acid (mg)	
		0.025 mg	0.050 mg
0.25	87.76 ± 1.38	89.42 ± 2.56	89.61 ± 1.46
1	90.41 ± 2.39	90.35 ± 1.44	91.88 ± 2.33
2	91.53 ± 1.56	89.61 ± 2.09	91.17 ± 2.04
3	90.85 ± 1.07	92.51 ± 2.16	88.45 ± 1.56
4	92.10 ± 2.72	90.46 ± 1.38	90.36 ± 1.48
5	90.56 ± 1.67	91.25 ± 1.05	91.06 ± 3.64
6	94.45 ± 2.55	91.36 ± 2.34	90.37 ± 2.02

Table 2. The radiochemical purity of [^{99m}Tc]Tc-6-MP including 100 µg stannous tartrate in the absence and presence of antioxidant agent.

Time (hour)	Radiochemical purity (%)		
	Absence of ascorbic acid	Ascorbic acid (mg)	
		0.025 mg	0.050 mg
0.25	87.32 ± 1.46	89.27 ± 1.02	90.05 ± 1.24
1	91.59 ± 2.58	92.31 ± 1.88	91.69 ± 1.03
2	90.16 ± 1.33	89.20 ± 1.20	92.48 ± 2.55
3	90.36 ± 2.05	92.50 ± 2.43	91.80 ± 1.87
4	93.26 ± 3.45	93.53 ± 3.14	92.14 ± 2.40
5	93.19 ± 2.97	92.34 ± 2.47	93.65 ± 3.54
6	92.62 ± 2.15	92.06 ± 1.65	92.70 ± 1.30

Table 3. The radiochemical purity of [^{99m}Tc]Tc-6-MP including 250 µg stannous tartrate in the absence and presence of antioxidant agent.

Time (hour)	Radiochemical purity (%)		
	Absence of ascorbic acid	Ascorbic acid (mg)	
		0.025 mg	0.050 mg
0.25	90.37 ± 2.06	90.69 ± 0.86	93.45 ± 2.14
1	93.12 ± 2.74	91.43 ± 1.38	94.09 ± 2.98
2	91.23 ± 1.95	92.76 ± 1.47	94.90 ± 1.83
3	93.72 ± 1.87	92.94 ± 2.30	95.29 ± 2.07
4	92.91 ± 2.14	93.25 ± 2.76	97.48 ± 3.25
5	92.45 ± 1.65	92.37 ± 2.49	96.75 ± 2.68
6	93.94 ± 2.43	93.86 ± 3.63	96.03 ± 1.84

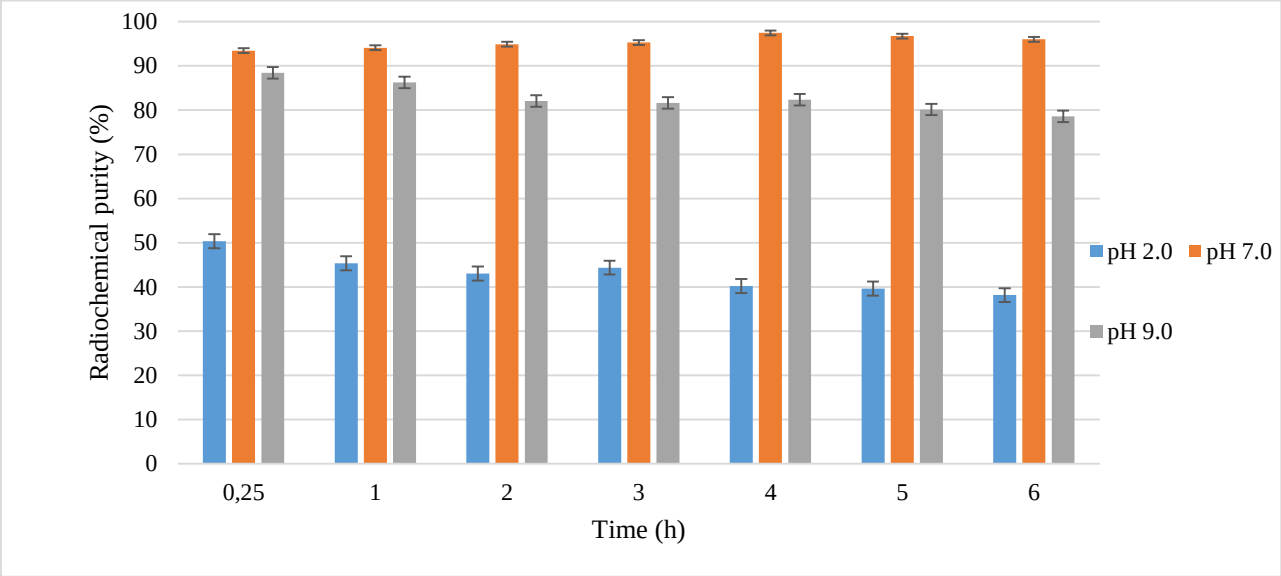

Figure 3. Effect of pH on radiochemical purity of [^{99m}Tc]Tc-6-MP.

According to Table 3, maximum labeling efficiency (>93%) was obtained with 250 µg stannous tartrate, 0.050 mg ascorbic acid included informulation and did not alter much after 6 h at room temperature (p>0.05).

Effect of pH on radiolabeling of [^{99m}Tc]Tc-6-MP: Although blood has a high buffering capacity and radiopharmaceuticals are small-volume preparations, the ideal pH for these substances is 7.4. However, pH values can potentially range from 2 to 9. This is because blood has such a great buffering capacity [18]. The impact of pH on labeling effectiveness was therefore examined for pH 2 to 9. In this experiment, the pH of the reaction medium played a significant role (Figure 3).

While keeping the other reaction parameters constant, substantial changes in labeling effectiveness were detected when the pH of the reaction was altered from 2 to 9. The pH of [^{99m}Tc]Tc-6-MP was shown to be optimum at 7.0 and [^{99m}Tc]Tc-6-MP was found stable up to 6-h (p>0.05).

Effect of incubation time on radiolabeling of [^{99m}Tc]Tc-6-MP: The incubation time of [^{99m}Tc]Tc-6-MP was determined how long after preparation the radiopharmaceutical was suitable for use in nuclear medicine. According to the obtained result which was shown in Table 4, the labeling efficiency of [^{99m}Tc]Tc-6-MP was above 90% in 5-min after labeling. The ideal radiolabeling efficiency (>93%) was observed after a 15-min incubation period, whereas incubation for longer periods did not result in significant changes (p<0.05).

Table 4. Effect of incubation time on radiochemical purity of [^{99m}Tc]Tc-6-MP.

Time (min)	Radiochemical purity (%)
5	90.52 ± 1.36
15	93.45 ± 2.14
30	93.53 ± 3.52
45	93.86 ± 2.10
60	94.09 ± 2.98

Effect of dose amount on radiolabeling of [^{99m}Tc]Tc-6-MP: The labeling studies of [^{99m}Tc]Tc-6-MP were carried out with 37 MBq of [^{99m}Tc]Tc in order to ensure the radiation safety of the staff and the surrounding region. Because radiopharmaceutical research on

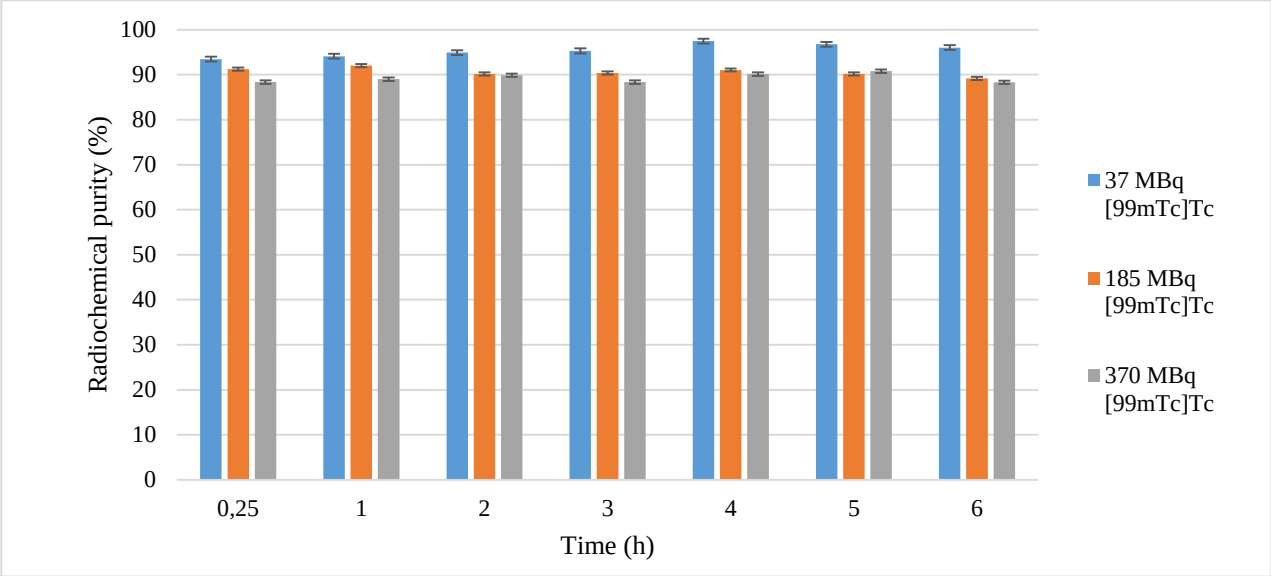

Figure 4. Effect of radiation dose on radiochemical purity of [^{99m}Tc]Tc-6-MP.

humans necessitates greater radiation doses, the RP of [^{99m}Tc]Tc-6-MP was also examined at 185 and 370 MBq radiation doses in addition to the 37 MBq radiation dosage and the results were given in Figure 4.

As a result of increasing the amount of radioactivity 10-folds, the RP value was found over 88%. As shown in Figure 4, with increased the radioactivity amount, there was a slight decrease in RP ($p>0.05$). Molar activity (A_m) and specific activity (A_s) are crucial properties for the development of novel radiopharmaceuticals [34]. The findings support [^{99m}Tc]Tc-6-MP's suitability as a radiopharmaceutical in nuclear medicine.

In vitro stability of [^{99m}Tc]Tc-6-MP: The *in vitro* stability of new radiopharmaceuticals is one of their major limitations. Thus, [^{99m}Tc]Tc-6-MP was incubated in SF in order to evaluate the complex stability. The results showed that [^{99m}Tc]Tc-6-MP was highly stable and RP was found >90% for 6-h in SF ($p>0.05$) (Figure 5).

Quality control of [^{99m}Tc]Tc-6-MP: High-performance liquid chromatography, RTLC, and/or gas chromatography can be utilized for the quality control of radiopharmaceutical [35]. In order to examine the RP of [^{99m}Tc]Tc-6-MP, RTLC approach was employed in this study because it is quickly and safely. To identify and measure the levels of radioactive impurities, selected mobile phases and stationary phases were given in Table 5.

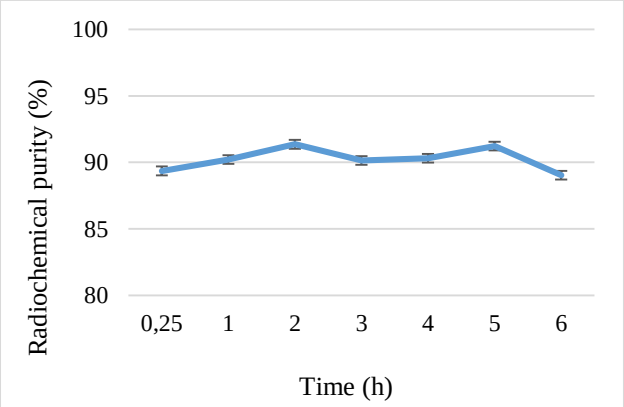

Figure 5. The stability of [^{99m}Tc]Tc-6-MP in saline up to 6 hours.

Using selected mobile and stationary phases, the RTLC chromatogram of [^{99m}Tc]Tc-6-MP was presented in Figure 6. Under optimized conditions, the RP of [^{99m}Tc]Tc-6-MP was over 90%.

Table 5. Rf values of [^{99m}Tc]Tc-6-MP in selected mobile and stationary phases.

	Whatman 3MM	**ITLC-SG**
	Acetone (100%)	**Acetonitrile/ Water/Trifluoroacetic acid (50/25/1.5)**
Free-[^{99m}Tc]Tc	0.9-1.0	0.9-1.0
R/H-[^{99m}Tc]Tc	0.0-0.1	0.0-0.1
[^{99m}Tc]Tc-6-MP	0.0-0.1	0.9-1.0

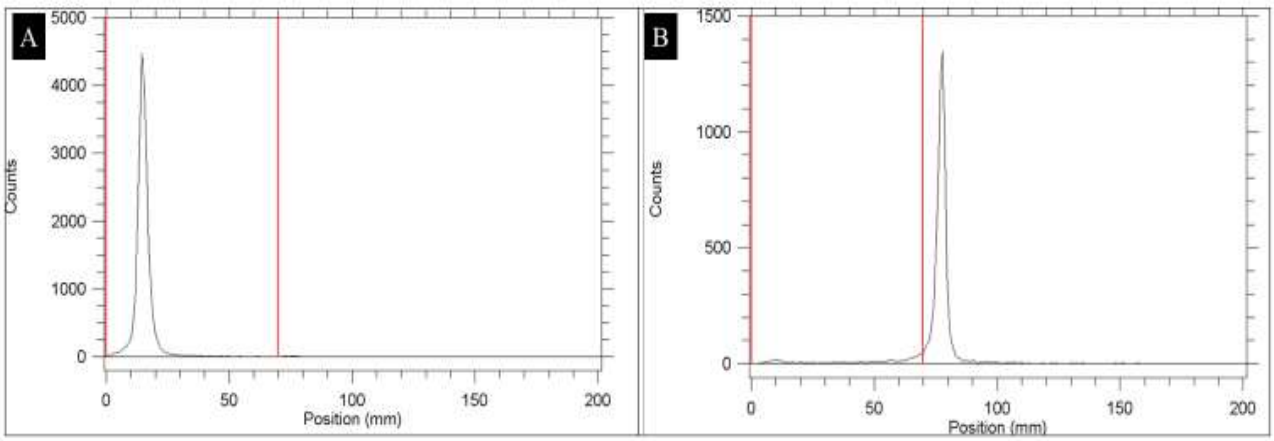

Figure 6. RTLC chromatogram of [^{99m}Tc]Tc-6-MP in different mobile phases: A: Acetone, B: CN/W/TFA (50/25/1.5).

Partition coefficient study of [^{99m}Tc]Tc-6-MP: The distribution of a molecule in the aqueous and organic phases at equilibrium is known as the n-octanol/PBS partition coefficient (log*P*), which gives important data for the *in vivo* behavior of the drug in drug development studies [20]. A gamma counter was used to detect the log*P* of the [^{99m}Tc]Tc-6-MP in this study. The log*P* of the [^{99m}Tc]Tc-6-MP were found to be -0.021 ± -0.001. According to result, the radiolabeled molecule has slightly polar properties (log*P*<1).

Conclusions

In this study, we showed that 6-MP can be radiolabeled with [^{99m}Tc]Tc with a high labeling efficiency (>90%) *via* RTLC technique. The produced complex was highly stable, with labeling efficiency continuing up to 6-h. With 250 µg stannous tartrate, 0.050 mg ascorbic acid, and 37 MBq [^{99m}Tc]$NaTcO_4$ containing formulations at pH 7.0 at room temperature, the highest RP was achieved. Also, further studies with [^{99m}Tc]Tc-6-MP are in progress in order to evaluate tumor cell binding capacity, biodistribution and imaging of the complex in experimental animals.

Acknowledgement: *The authors thank the Nuclear Medicine Department at Ege University, Türkiye, for providing the [^{99m}Tc]$NaTcO_4$.*

Funding: *TLC Scanner was funded by T.R. Prime Ministry State Planning Organization Foundation Grant Project Number: 09DPT001.*

Conflict of interest: *The authors declare that they have no conflict of interest.*

Ethical statement: *Ethics committee decision was not taken as it was a laboratory study.*

References

[1] Siegel RL, Miller KD. Cancer statistics, 2020. CA Cancer J Clin. 2020;70(1):7–30.

[2] Ferlay J, Colombet M, Soerjomataram I, et al. Cancer statistics for the year 2020: An overview. Int J Cancer. 2021;10.1002/ijc.33588.

[3] Ekinci M, Santos-Oliveira R, İlem-Özdemir D. Biodistribution of 99mTc-PLA/PVA/Atezolizumab nanoparticles for non-small cell lung cancer diagnosis. Eur J Pharm Biopharm. 2022;176:21–31.

[4] Payolla FB, Massabni AC, Orvig C. Radiopharmaceuticals for diagnosis in nuclear medicine: A short review. Eclet Quim. 2019;44(3):11–9.

[5] Ge J, Zhang Q, Zeng J, et al. Radiolabeling nanomaterials for multimodality imaging: New insights into nuclear medicine and cancer diagnosis. Biomaterials. 2020;228:119553.

[6] Li H, Liu Z, Yuan L, et al. Radionuclide-based imaging of breast cancer: State of the art. Cancers (Basel). 2021;13(21):5459.

[7] Jafari SH, Saadatpour Z, Salmaninejad A, et al. Breast cancer diagnosis: Imaging techniques and biochemical markers. J Cell Physiol. 2018;233(7):5200-13.

[8] DeCesare A, De Vincentis G, Gervasi S, et al. Single-photon-emission computed tomography (SPECT) with technetium-99m sestamibi in the diagnosis of small breast cancer and axillary lymph node involvement. World J Surg. 2011;35(12):2668-72.

[9] Boschi A, Uccelli L, Martini P. A picture of modern Tc-99m radiopharmaceuticals: Production, chemistry, and applications in molecular imaging. Appl Sci. 2019;9(12):2526.

[10] Papagiannopoulou D. Technetium-99m radiochemistry for pharmaceutical applications. J Label Compd Radiopharm. 2017;60(11):502–20.

[11] ME M, AS A, Y M. Cytotoxicity of 6-mercaptopurine via loading on pva-coated magnetite nanoparticles delivery system: a new era of leukemia therapy. J Nanomed Nanotechnol. 2018;9:6.

[12] Selvaraj V, Alagar M, Hamerton I. Analytical detection and biological assay of antileukemic drug using gold nanoparticles. Electrochim Acta. 2006;337(1–2):275–81.

[13] Bariyanga J, Luyt AS. Synthesis, fourier transform infrared, nuclear magnetic resonance and thermal analysis of sodium and platinum complexes of 6-mercaptopurine. J Mol Struct. 2001;559(1–3):49–54.

[14] Dorniani D, Hussein MZ Bin, Kura AU, et al. Preparation and characterization of 6-mercaptopurine-coated magnetite nanoparticles as a drug delivery system. Drug Des Devel Ther. 2013;7:1015–26.

[15] Nezhad-Mokhtari P, Ghorbani M, Mahmoodzadeh F. Smart co-delivery of 6-mercaptopurine and methotrexate using disulphide-based PEGylated-nanogels for effective treatment of breast cancer. New J Chem. 2019;43:12159–67.

[16] Maioli C, Lucignani G, Strinchini A, et al. Quality control on radiochemical purity in

technetium-99m radiopharmaceuticals labelling: Three years of experience on 2280 procedures. Acta Biomed. 2017;88(1):49–56.
[17] İlem-Özdemir D, Karavana SY, Şenyiğit ZA, et al. Radiolabeling and cell incorporation studies of gemcitabine HCl microspheres on bladder cancer and papilloma cell line. J Radioanal Nucl Chem. 2016;310(2):515–22.
[18] İlem-Özdemir D, Ekinci M, Özgenç E, et al. 99mTc-exendin-4: Radiolabeling and quality control studies of glucagon-like peptide analog. Exp Biomed Res. 2022;5(3):235–43.
[19] Ilem-Ozdemir D, Atlihan-Gundogdu E, Ekinci M, et al. Radiolabeling and in vitro evaluation of a new 5-fluorouracil derivative with cell culture studies. J Label Compd Radiopharm. 2019;62(13):874–84.
[20] Ekinci M, Öztürk AA, Santos-Oliveira R, et al. The use of Lamivudine-loaded PLGA nanoparticles in the diagnosis of lung cancer: Preparation, characterization, radiolabeling with 99mTc and cell binding. J Drug Deliv Sci Technol. 2022;69:103139.
[21] Croce CM. Oncogenes and cancer. N Engl J Med. 2008;358:502-11.
[22] Sung H, Ferlay J, Siegel RL, et al. Global Cancer Statistics 2020: GLOBOCAN Estimates of Incidence and Mortality Worldwide for 36 Cancers in 185 Countries. CA Cancer J Clin. 2021;71:209-49.
[23] Pijeira MSO, Viltres H, Kozempel J, et al. Radiolabeled nanomaterials for biomedical applications: radiopharmacy in the era of nanotechnology. EJNMMI Radiopharmacy and Chemistry. 2022;7:8.
[24] Diniz SOF, Siqueira CF, Nelson DL, et al. Technetium-99m ceftizoxime kit preparation. Brazilian Arch. Biol. Technol. 2005;48:89–96.
[25] Banerjee I, Behera A, De K, et al. Synthesis, characterization, biodistribution and scintigraphy of 99mTc-paclitaxel: a potential tracer of paclitaxel. J Radioanal Nucl Chem.2015;304:633–43.
[26] Adamson PC, Balis FM, Hawkins ME, et al. Desulfuration of 6-mercaptopurine. The basis for the paradoxical cytotoxicity of thiopurines in cultured human leukemic cells. Biochem Pharmacol. 1993;46(9):1627–36.
[27] Guarino A, Shukla SK, Castelli L, et al. Uptake of 67Ga-6-mercaptopurines in Morris hepatoma-3924 A. Eur J Nucl Med. 1979;4:211–5.
[28] Hunt FC, Booker J, McLaughlin AF, et al. Evaluation of a new bile agent technetium-99m-mercaptopurine. In: Newton PJF, editor. 5 Annual Scientific Meeting, Sydney, Australia: Australian and New Zealand Society of Nuclear Medicine, North Melbourne (Australia); 1974. p. 7–5. Available from: https://inis.iaea.org/collection/NCLCollectionStore/_Public/05/141/5141350.pdf?r=1
[29] Shahzad K, Majid ASA, Khan M, et al. Recent advances in the synthesis of (99mTechnetium) based radio-pharmaceuticals. Rev Inorg Chem. 2021;41(3).
[30] Elitez Y, Ekinci M, Ilem-Ozdemir D, et al. Tc-99m radiolabeled alendronate sodium microemulsion: characterization and permeability studies across caco-2 cells. Curr Drug Deliv. 2018;15(3):342–50.
[31] Costa B, Ilem-Özdemir D, Santos-Oliveira R. Technetium-99m metastable radiochemistry for pharmaceutical applications: old chemistry for new products. J Coord Chem. 2019;72(11):1759–84.
[32] Tubergen K, Corlija M, Volkert WA, et al. Sensitivity of technetium-99m-d,l-HMPAO to radiolysis in aqueous solutions. J Nucl Med. 1991;32(1):111–5.
[33] Ekinci M, Ilem-Ozdemir D, Gundogdu E, et al. Methotrexate loaded chitosan

nanoparticles: Preparation, radiolabeling and in vitro evaluation for breast cancer diagnosis. J Drug Deliv Sci Technol. 2015;30(A):107–13.

[34] Luurtsema G, Pichler V, Bongarzone S, et al. EANM guideline for harmonisation on molar activity or specific activity of radiopharmaceuticals: impact on safety and imaging quality. EJNMMI Radiopharm Chem. 2021;6:34.

[35] Chen F, Decristoforo C, Rohrbacher B, et al. A simple two-strip method to determine the radiochemical purity of technetium-99m mercaptoacetyltriglycine. Eur J Nucl Med. 1993;20(4):334–8.

Exp Biomed Res 2023; 6(1): 57-76 DOI: 10.30714/j-ebr.2022.170

Experimental Biomedical Research *Original article*

It isn't over 'till it's over: A continuing concern of the SARS-CoV-2 variants, and miRNAs targeting the S protein as a probable absolute cure

Pelin Kilic[1,2*], Begum Cosar[2,3], Ahmet Turan Ince[4], Doruk Deniz Cebbaroglu[5], Cansu Tekeli[6], Esma Benli[7], Ozlem Darcansoy Iseri[8]

[1]*Department of Stem Cells and Regenerative Medicine, Stem Cell Institute, Ankara University, Ankara, Türkiye*
[2]*HücreCELL® Biotechnology Development and Commerce, Inc., Ankara, Türkiye*
[3]*Department of Molecular Biology and Genetics, Institute of Science, Başkent University, Ankara, Türkiye*
[4]*Sivas Cumhuriyet University, Faculty of Medicine, Sivas, Türkiye*
[5]*Akdeniz University, Faculty of Medicine, Antalya, Türkiye*
[6]*Department of Biomedical Engineering, School of Engineering, TOBB University of Economics and Technology, Ankara, Türkiye*
[7]*Department of Biology, Ege University, İzmir, Türkiye*
[8]*Department of Molecular Biology and Genetics, Faculty of Science and Letters, Başkent University, Ankara, Türkiye*

ABSTRACT

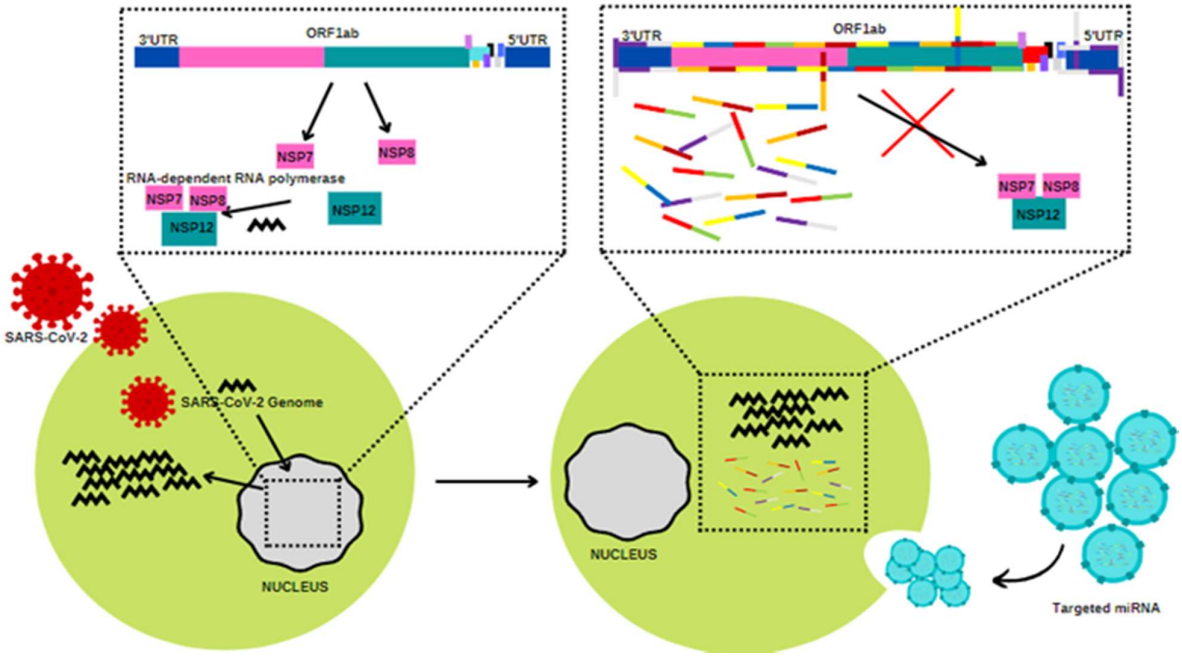

The severe acute respiratory syndrome coronavirus 2 (SARS-CoV-2) outbreak which still continues to affect the general population, has mutated day by day and new variants have emerged. More than 40 variants, usually caused by mutations in the spike (S) protein, have been recorded. Observation of S protein mutations in the development of t herapeutic agents will increase success rates. As we identify the three-dimensional (3D) conformation of viruses, it is more and more possible to work on models for understanding molecular interactions. Development of agents for arrays and 3D sequencing of proteins paves the way for potential therapeutic studies against variants. MicroRNAs (miRNAs) seemingly act as a potentially important group of biomolecules in combating uncontrolled cytokine release. Besides antiviral response, miRNAs promise to be

powerful therapeutic agents against infections. Studies have shown that miRNAs are able to inhibit the genome directly by miRNA-based treatments as they are sprecific to the SARS-CoV-2 genome. In order to expose this potential, *in silico* studies before continuing with lab studies are helpful. In our bioinformatics analysis, we proposed to compare the S protein similarities of Delta and Omicron, two of the most common variants, and to detect miRNAs targeting the S protein. The S proteins and coding sequences were compared between the two variants, and differences were determined. Within our analysis, 105 and 109 miRNAs for the Delta and Omicron variants, respectively, were detected.

We believe that our study will be a potential guide for deciding on the miRNAs that may most likely have an effect on the management of the infection caused by both variants.

Key words: Cytokine storm, Delta variant, genome, microRNAs (miRNAs), Omicron variant, SARS-CoV-2, S protein.

.

✉ * *Pelin Kilic,*
Institute/University: Ankara University Stem Cell Institute
Full postal address: Ankara Üniversitesi Kök Hücre Enstitüsü Cevizlidere Mah., Ceyhun Atuf Kansu Cd. No: 169 06520 Balgat-Ankara/Türkiye
E-mail: pelin.kilic@ankara.edu.tr
Received: 2022-09-19 / Revisisons: 2022-11-16
Accepted: 2022-12-16 / Published online: 2023-01-01

Introduction

Severe acute respiratory syndrome coronavirus 2 (SARS-CoV-2) has caused viral infection and has been a threat to our country and to the world for a long time. Health institutions are making great efforts to prevent, eradicate, and recover from this pandemic. SARS-CoV-2 is a zoonotic, single-stranded positive-sense ribonucleic acid (+ssRNA) virus. The spike (S) protein of the virus binds to the angiotensin-converting enzyme 2 (ACE-2) receptor of the host cell for entry. The ACE-2 receptor acts as a membrane-bound enzyme whereas the S protein is structurally adapted by the transmembrane protease serine-2 (TMPRSS-2). In addition to the SARS-CoV-2 receptor-dependent entry, endocytosis is another path by which the virus can enter the cell [1,2]. Following the entry and the replication of the virus, many symptoms may occur in the patient's body. Fever, dry cough, acute respiratory distress syndrome (ARDS), pulmonary fibrosis, hypertension, thrombosis, and coagulation disorders are among such. One of the causes of the symptoms is the uncontrolled activation of the host's immune system due to the viral infection. This uncontrolled immune response and the increase in the number of neutrophils and macrophages, "cytokine release syndrome (CRS)", which is activated with proinflammatory cytokines in the circulation, causes damage to the organism and may can even lead to multiple organ failure. When the cytokines are emerged at such a high level due to various reasons, the patient enters the CRS [3].

As we have mentioned recently [5], there are more than 40 variants of the virus which have been identified. The mutations that cause the variants occur mostly in the S protein since mutations in the S protein change the ACE-2 affinity of the resulting variant, its infectiousness, and its response to monoclonal antibodies [4]. The number of variants continues to increase as a result of high rate of mutations [5]. Among all, the Delta and Omicron variants attract our attention in terms of their transmission rate and the size of the population which they affect [6].

The Delta variant (B.1.617.2), was born in India in November 2020 [7]. In August 2021, it replaced Alpha as the most transmissible variant [8]. The Delta variant has 60% more spreading

capacity than the Alpha variant. The Delta variant contains 23 different mutations compared to the first identified Alpha variant. Twelve of these mutations occur on the S protein [9]. The Omicron variant (B.1.1.529), on the other hand, first appeared in South Africa in November 2021. It has been observed as the most contagious variant among the variants identified so far [10]. As a result of linear regression analysis, its contagiousness was found to be 2-fold in comparison with the Delta variant [11]. This variant contains 32 amino acid mutations in the S protein [12,13].

There is not yet a clinically approved, absolute treatment for the SARS-CoV-2 infection. Therefore, further studies on the use of new antiviral strategies are still necessary and priority.

microRNAs (miRNAs), are RNA fragments of approximately 18-25 nucleotides length. The miRNAs, designated as miR-5p or miR-3p are named after the region (5' or 3') where the precursor yields the complementary mature single-stranded sequence. miRNA biogenesis begins with its transcription in the nucleus by RNA Polymerase II, and pre-miRNA is extracted from the nucleus to the cytoplasm by exportin-5. By binding with the Ago-Dicer-TRBP complex they act in 3 different mechanisms, i.e. inhibition of translation, messenger RNA (mRNA) storage, and translocation to dendrites/axons [14]. miRNAs have drawn attention after elucidation of their involvement in complex molecular processes such as growth, cycle regulation, proliferation, etc. [15,16]. Therefore, miRNAs have currently been studied as biomarkers and therapeutic targets for systemic illnesses [17], viral [18] and bacterial [19] infections, and cancer [20].

In this study, we aimed to mine the existing literature covering therapeutic potential of miRNAs which have been identified to treat similar viruses in the past and can be used today against SARS-CoV-2 and its variants. Afterwards, bioinformatics analyses were performed to compare S protein similarities and three-dimensional (3D) protein structure of the two most prevalent variants of SARS-CoV-2, and to frame the miRNAs targeting the S protein structures. Our final aim was to identify different and common miRNAs for both variants that have potential for diagnosis and treatment. Thus, our study will be a potential guide for deciding on the miRNAs that may have an effect on the detection and treatment of both variants.

Materials and metods

miRNA detection

miRNAs targeting individual S protein amino acid sequences for the Delta and Omicron variants were detected using miRNA Target Prediction Database (miRDB).In contrast to the case of most other miRNA databases, in the miRDB, mature miRNAs are the primary emphasis.

Candidate transcripts with scores below 50 are displayed in miRDB as anticipated miRNA targets. MİRTargets prediction scores range from 0 to 10. miRNAs with a Target Score of 50 and above were considered, and the common miRNAs were identified.

Data mining

We obtained the potential miRNAs specific to the SARS-CoV-2 genome which was obtained from the National Center for Biotechnology Information (NCBI) database with the keywords "Delta variants", "Omicron variants", "miRNA", "Sars-CoV-2", "spike protein" and "therapeutic".

Data retrieval

S protein sequences were obtained from NCBI (GenBank: UFO69279.1) for Omicron and NCBI (GenBank: QWK65230.1) for the Delta variant. The whole genome sequence and coding

sequences (CDSs) of the S protein of the Omicron (GenBank: OL672836.1) and Delta variants (GenBank: MZ359841.1) were obtained from NCBI. In further analysis to determine the similarity between two 3D protein structures, the S proteins of both variants obtained from Protein Data Bank were used for the Delta and Omicron variants (7W92 and 7WVN, respectively).

Alignment of the genomes

The FASTA files containing S protein sequences and coding CDS were uploaded to the website at EMBL's European Bioinformatics Institute (EMBL-EBI), and the results were analyzed.

Three-dimensional (3D) protein structure

The Phyre2 Protein Fold Recognition Server program was used for protein structure prediction. In order to create 3D models, estimate binding locations, and analyze amino-acid variations in a protein sequence, Phyre2 employs cutting-edge distant homology detection techniques with 4 consecutive steps. First, it gathers homologous protein sequences with HHblits. Then, the multiple-sequence alignment helps to predict the secondary structure with PSPIRED. Afterwards, the secondary structure is scanned against known protein HMMs, Last, the final Phyre2 model is designed by adding the amino acid side chains. Pairwise structure alignment tool from RCSB PDB was used to determine the similarity between two 3D protein structures. The comparison tool enables pairwise comparison of 3D structures and protein sequences. The Smith-Waterman, Needleman-Wunsch, and blast2seq algorithms are offered for sequence comparison. The latest versions of CE and FATCAT, as well as links to some of the external protein structure alignment services, which include Mammoth, TM-align, and Topmatch, provide support for structure comparisons.

Results and Discussion

Spike (S) protein sequence comparison

S proteins, located on the virus and provide cell-virus interactions by taking an active role in the cell entry process, have naturally been targeted in order to interrupt these interactions [21-23]. S proteins penetrate the cell membrane via the ACE-2 receptors and cause many clinical symptoms and the disease progresses [22,24]. Every mutation on the S protein affects this process. In addition, coronavirus variants manifest themselves with varying disease courses and are then detected by molecular and bioinformatics analyses [25]. Therefore, mutations in the S protein change the course of the disease by affecting the cell-virus interaction, and ultimately emerge as a new coronavirus variant [26]. That is, coronavirus variants represent the S protein mutations [24,27]. Variants differ in terms of features such as contagiousness, efficacy, and severity of clinical symptoms, resulting in a change in the course of the disease in the population [25]

In this study, the Delta and Omicron variants were investigated. The Omicron variant is currently the most common variant whereas the Delta variant ranks the second place [28,29]. There are many mutations in variant and the epidemiological effects of the variant differ according to these mutations. Mutations in variants are examined and inferences are made as to what kind of an effect it may have when the same mutation occurs in another variant [25]. As the S proteins of the variants continue to be determined, the success rate of vaccines and therapeutic agents developed against variants will increase. Thus, higher accuracy can be obtained in the studies to end or treat diseases [23,26].

In addition to the S protein sequences, CDS of the S proteins of the variants were also examined.

Table 1. Comparison of S protein sequences of DNA and protein sequences between the Delta and Omicron variants. (S: Spike, CDS: Coding DNA sequence)

	S protein sequences	**CDS**
Length	1276	3831
Identity	1234/1276 (96.7%)	3767/3831 (98.3%)
Similarity	1241/1276 (97.3%)	3767/3831 (98.3%)
Gaps	11/1276 (0.9%)	33/3831 (0.9%)
Score	6448.0	18647.0

With the differences in the sequencing of the genomes of the S proteins it is important to develop model organisms and to speed up studies in case of re-emergence of human pathogens [26].

When the S protein sequences and CDSs of both variants were aligned, the following values were found as shown in Table 1.

The relationship between protein sequence similarity and structural similarity was examined. According to the results of the study, when the structure comparison is examined, they can be defined as homologous pairs since there is more than 70% second structure identity [30,31]. According to the results, there was a high similarity and identity between the S protein sequences of the Delta and Omicron variants with, a low rate of gaps. Consequently, the two sequences showed a high rate of alignment. The lack of gaps in the bioinformatics analysis of S protein sequences indicates that an amino acid is located at the same position across sequences. Thus, the similarity with a high score was significant. This shows that the S proteins of these variants, which dominate at different time spans, have highly similar sequences.

This result can be interpreted in different ways. The fact that the S protein is effective in the way of entry into the organism and that it is similar in two different variants suggests that it may be the best S protein sequence for the virus. In other words, if the S protein continues with mutation at this level and the binding part continues to be similar to the sequence of these variants, perhaps it can dominate the newly emerged variant as much as the Delta and Omicron variants. In addition, the S protein sequence similarity between the two variants will make it possible to conduct studies in the same direction in terms of therapeutic agents to be developed against the S protein. Thus, the work done for one variant can be done for another, with minor modifications. In addition, a true understanding of the sequence of the S protein facilitates profiling for this protein and studying sequence conservation patterns indicate of secondary structure types. Hence, it is important to show such a similarities.

The amino acid sequence alterations of the S proteins of both variants are given in the Table 2, and the coding sequence of the S protein between both variants are given in Table 3.

Sequences of S protein and CDS were compared between the two variants and the differences were determined. Differences in sequences allow us to study the clinical progression of current and future variants. The development of agents via 3D sequencing of proteins lights the way to potential therapeutic studies against variants.

Comparison of 3D S protein structures

In order to better understand the secondary structures of proteins, 3D protein models are constructed. The main objective of studying the 3D structure of proteins is to understand their

Table 2. S protein sequence alterations of the Delta and Omicron variants.

Amino Acid sequence	Amino acid exchange	Type of mutation
19	R→T	semi-conservative
67	A→V	semi-conservative
70	H→-	deletion
71	V→-	semi-conservative
95	T→I	semi-conservative
143	V→-	deletion
144	Y→-	deletion
145	Y→-	deletion
156	-→E	insertion
157	-→F	insertion
158	G-R	semi-conservative
209	N→-	deletion
210	L-I	semi-conservative
213	-→E	insertion
214	-→P	insertion
215	-→E	insertion
337	G→D	semi-conservative
369	S→L	semi-conservative
371	S→P	semi-conservative
373	S→F	semi-conservative
415	K→N	semi-conservative
438	N→K	semi-conservative
444	G→S	semi-conservative
450	R→L	semi-conservative
475	S→N	conservative
482	E→A	semi-conservative
491	Q→R	conservative
494	G→S	semi-conservative
496	Q→R	conservative
499	N→Y	semi-conservative
503	Y→H	conservative
545	T→K	semi-conservative
653	H→Y	conservative
677	N→K	semi-conservative
679	R→H	semi-conservative
762	N→K	semi-conservative
794	D→Y	semi-conservative
854	N→K	semi-conservative
948	N→D	conservative
952	Q→H	semi-conservative
967	N→K	semi-conservative
979	L→F	semi-conservative

R: Arginine, T: Threonine, A: Alanine, V: Valine, H: Histidine, I: Isoleucine, T: Tyrosine, Y: Tyrosine, E: Glutamic acid, F: Phenylalanine, G: Glycine, N: Asparagine, L: Leucine, P: Proline, D: Aspartic acid, S: Serine, K: Lysine, Q: Glutamine.

Table 3. CDS sequence differences of S protein of the Delta and Omicron variants.

DNA sequence	Base exchange	Type of mutation
56	G→C	semi-conservative
200	C→T	semi-conservative
203	T→-	deletion
204	A→-	deletion
205	C→-	deletion
206	A→-	deletion
207	T→-	deletion
208	G→-	deletion
284	C→T	semi-conservative
425	A→-	deletion
426	T→-	deletion
427	G→-	deletion
428	T→-	deletion
429	T→-	deletion
430	T→-	deletion
431	A→-	deletion
432	T→-	deletion
433	T→-	deletion
467	-→A	insertion
468	-→G	insertion
469	-→T	insertion
470	-→T	insertion
471	-→C	insertion
471	-→A	insertion
626	A→-	deletion
627	T→-	deletion
628	T→-	deletion
637	-→G	insertion
638	-→A	insertion
639	-→G	insertion
640	-→C	insertion
641	-→C	insertion
642	-→A	insertion
643	-→G	insertion
644	-→A	insertion
645	-→A	semi-conservative
1010	G→A	semi-conservative
1105	T→C	semi-conservative
1106	C→T	semi-conservative
1111	T→C	semi-conservative
1118	C→T	semi-conservative
1245	G→T	semi-conservative
12314	T→G	semi-conservative
12330	G→A	semi-conservative
1349	G→T	semi-conservative
1424	G→A	semi-conservative
1445	A→C	semi-conservative
1472	A→G	semi-conservative
1480	G→A	semi-conservative
1487	A→G	semi-conservative
1495	A→T	semi-conservative
1507	T→C	semi-conservative
1634	C→A	semi-conservative
1957	C→T	semi-conservative
2031	T→G	semi-conservative
2036	G→A	semi-conservative
2286	C→A	semi-conservative
2380	G→T	semi-conservative
2562	C→A	semi-conservative
2842	A→G	semi-conservative
2856	A→T	semi-conservative
2901	T→A	semi-conservative
2935	C→T	semi-conservative
3432	C→T	semi-conservative

G: guanine, C: cytosine, T: thymine, A: adenine.

biological activity. Since biological activity is dependent on atomic levels, topological expressions alone are inadequate. Seemingly, small editions can greatly affect the activity of the structure [32].

In pairwise structure alignment analysis, residue coverage for both variants is high enough for a correct analysis (7W92: %93 and 7WVN: %95). To establish homological similarity of S protein 3D structures, we simulated a superimposed model of both 7W92 and 7WVN on UCSF Chimera (Figure 2).

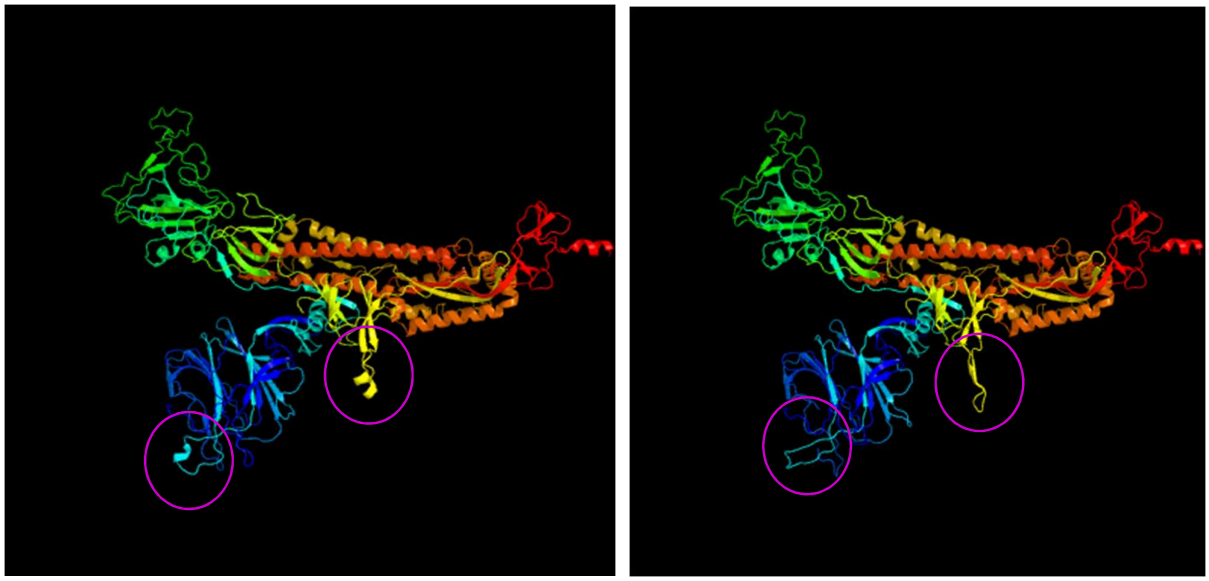

Figure 1. A) The 3D protein structure of the Delta variant **B)** The 3D protein structure of the Omicron variant. The most significant difference in the spike (S) protein between the two variants is marked with a purple circle in shapes of A and B.

In our study, following the sequence comparison of the S proteins, 3D structures of the Delta and Omicron variants were studied (Figure 1). Based on the differences in the 3D structures of the S proteins, we found that there may be differences in the interaction of the variant with the cell. That is, the structure of the S protein determines cell affinity. Studies can also be conducted to determine the connection between an amino acid, its position and epidemiological effects it may cause on 3D structures. In addition, it is useful to know such structural differences in the therapeutic agents developed against the variant. With 3D models, it is possible to work on drug-cell or drug-drug interactions by obtaining information related to the conformation of viruses [21,24,33].

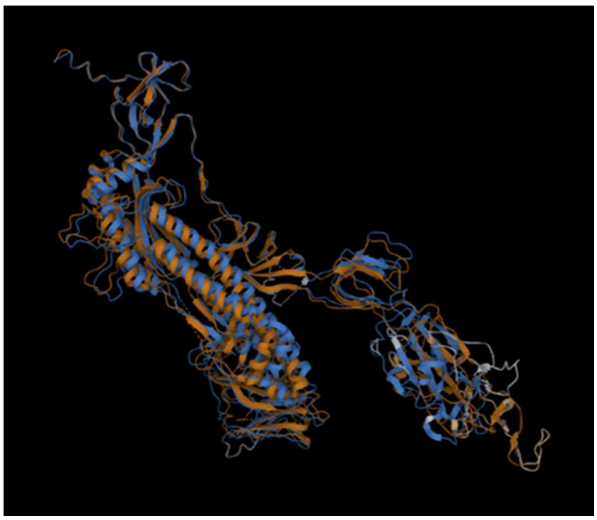

Figure 2. Superimposed view of the 7W92 and 7WVN proteins.

The RMSD score is a measurement of distance between atomic coordinates of two different molecules [34]. Values higher than 3 mean that there is low similarity between two molecules [35]. For the selected protein structures, the RMSD score was found to be 5.5, means these two proteins do not have a statistically significant similarity.

accurate antiviral treatments [37]. miRNAs help to evade or suppress immune response to a number of viruses [39]. Scientific advancements have revealed important functions and pathways involved in host immune responses. Wingless and INT-(Wnt) [40] and mitogen-activated protein kinase (MAPK) signaling [41], T cell-mediated immunity [42], autophagy [43],

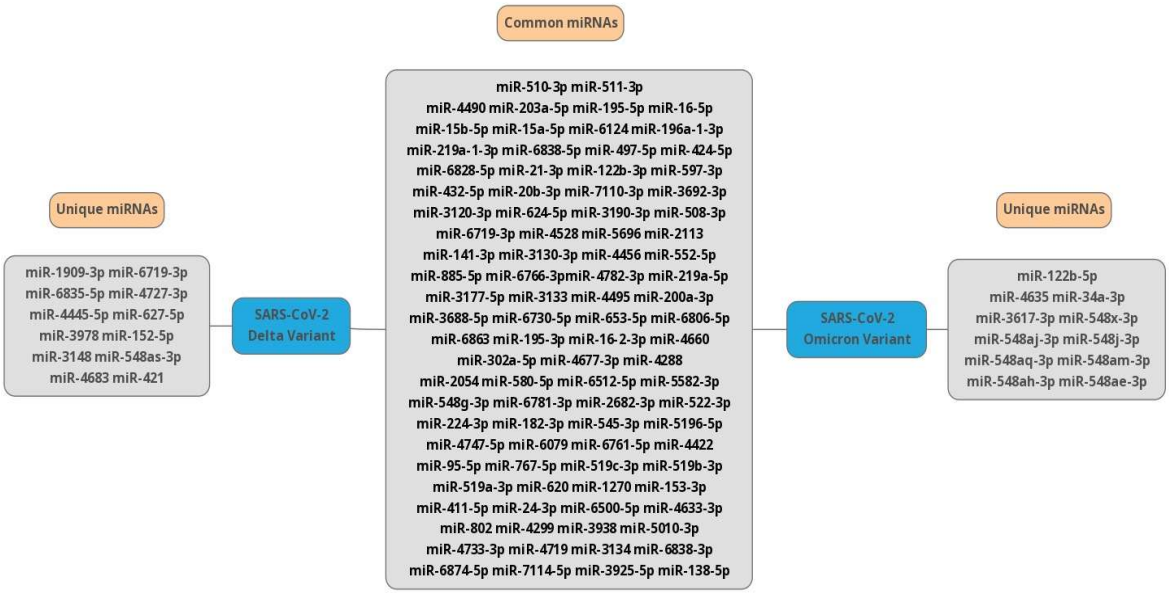

Figure 3. miRNAs targeting the S proteins of the Delta and Omicron variants, and those common to the S proteins of both.

Identification of common miRNAs for both variants

In the past couple of years, both virus-encoded and host miRNAs have been suggested to be significant biomarkers in the said pandemic [36]. In a study, 444 of 2654 hsa-miRs were identified to be associated with different binding sites in the CoV-2 reference genome [37].

It is predicted that miRNAs repress a large portion of all protein-coding genes and participate in the regulation of almost every biological process in the cell. This makes them important as antiviral targets [38]. Understanding biological differences responsible for the severity of SARS-CoV-2 is the key to developing

fibroblast growth factor (FGF) receptor binding [44], transforming growth factor-beta (TGF-β) [45], vascular endothelial growth factor (VEGF) signaling [46], ErbB signaling [47], mammalian target of rapamycin (mTOR) signaling [48] and tumor necrosis factor alpha (TNF-α) signaling [41] are specifically targeted by SARS-CoV-2 [49].

Cellular miRNAs can enhance the host's immune response and aid viral immune avoidance mechanisms [50]. *In silico* study of SARS-CoV-2 encoding miRNA targets the Ca^{+2} signaling pathway, which acts as a key activator influencing other signaling pathways that subsequently branch it [51]. Both cellular

miRNAs and viral encoded miRNAs induced during the SARS-CoV and SARS-CoV-2 infections were envisaged to target cytokine signaling pathways involved in immune responses guiding to enhanced viral pathogenesis [49].

As a result of the analysis, we found that there are 109 predicted miRNAs targeting the 3813 nt-long mRNA sequence sent with a Target Score of 50 or higher for the Omicron variant. Likewise, we found 105 predicted miRNAs targeting the 3816 nt-long mRNA sequence for the Delta variant.

The estimated number of unique miRNAs which target the S protein of the Delta variant shown in Figure 3 is 12, and which 12 are miR-1909-3p, miR-6719-3p, miR-6835-5p, miR-4727-3p, miR-4445-5p, miR-627-5p, miR-3978, miR-152-5p, miR-3148, miR-548as-3p, miR-4683, miR-421. The estimated number of unique miRNAs for the Omicron variant to target the S protein is 11 and these are listed as miR-122b-5p, miR-4635, miR-34a-3p, miR-3617-3p, miR-548x-3p, miR-548aj-3p, miR-548j-3p, miR-548aq-3p, miR-548am-3p, miR-548ah-3p, and miR-548ae-3p.

SARS infections involved in ACE-2 receptor binding results in inhibitory effects on the receptor and decreased receptor expression in infected cells [52]. Here, miR-421 has important modulatory effects on ACE-2 [53]. miR-627-5p was found to be the most down-regulated miRNA in peripheral blood samples of patients compared to the control group [54]. In COVID-19, a decrease in host miR-34a-3p can increase the expression of X-box binding protein 1 (XBP1) by URP, increased endoplasmic reticulum (ER) folding capacity, inhibit lung fibrosis and protect against over activation of the immune system, promotoing survival [55]. The rs3853839 single nucleotide polymorphysm (SNP) of toll-like receptor 7 (TLR 7) can affect miRNA binding capacity and therefore mRNA expression of TLR7. The rs3853839 SNP, on the other hand, might pose a risk on the infection [56]. Conserved regions are predicted by miRanda and mirTarP as a conserved region of the virus. The conserved structured region is assessed as a promising means for the investigation of absolute treatments [57].

Li et al. [58] took peripheral blood from 10 COVID-19 patients and 4 healthy donors. In the blood samples, the exposure to various miRNAs was detected with high efficiency. Compared to healthy donors, 35 miRNAs were upregulated in patient blood whereas 38 were downregulated. For example, the Delta variant-specific miR-421 and the remaining 4 miRNAs are estimated to target 3' of the ACE-2 UTR regions [59] miR-122b-5p, specific to the Omicron variant, was down regulated in severe COVID-19 cases [60].

The estimated number of common miRNAs targeted at the S proteins of the Delta and Omicron variants is 93 (Figure 3). The common miR-195-5p of the Delta and Omicron variants was established by logistical regression analysis that could benefit from early COVID-19 diagnosis [61]. miR-16-5p, which is found to regulate the ACE-2 network with an *in silico* investigation, was investigated [62]. The increase in miR-15b-5p release resulted in a decrease in viral infection and reproduction of SARS-CoV-2 by targeting RNA template component [63] miR-196a-1-3p has been widely linked to members of the Coronavirus family (SARS-CoV, MERS-CoV and SARS-CoV-2) [64]. It has been found that miR-6838-5p is significantly correlated in male individuals carrying COVID-19 [65]. miR-497-5p is estimated to be effective against virus through nucleotide erasure in viral ss-RNA encoding zones [66]. miR-510-3p shows strong binding potential to neuropilin-1 [67]. Neuropilin-1, a host cell receptor, increases its infectiousness and contributes to its tropism [68].

Potentially Therapeutic miRNAs for SARS-CoV-2

miRNAs are known to have antiviral effects, which potentially make them antiviral therapeutic agents. Moreover, miRNAs which have antiviral and anti-inflammatory effects against *Coronaviridae spp.* have been reported. miR-9 accelerates the breakdown of human coronavirus OC43 (HCoV-OC43), a type of coronavirus, by regulating the type I interferon (IFN-1) release [69]. On the other hand, it has been reported that patients who have low circulating miR-146a-5p levels do not respond to tocilizumab, a drug used against the SARS-CoV-2 infection [70]. miR-122 increases the genome stability by binding in the 5' untranslated region (UTR) of the Hepatitis C virus (HCV). Therefore, miR-122 blocks cellular pyrophosphates in the genome of SARS-CoV-2 [71].

Circulating miRNAs may be effective in suppressing the SARS-CoV-2 infection-derived acute respiratory distress syndrome (ARDS) and the CRS. Cytokines have important roles in the emergence of the clinical signs and inflammation development [72]. Significant increase in the levels of cytokines, such as interleukin (IL)-2, IL-6, IL-7, IL-8, IL-10, granulocyte-colony stimulating factor (G-CSF), interferon gamma-induced protein 10 (IP10), monocyte chemoattractant protein-1 (MCP-1), macrophage inflammatory protein 1A (MIP1A) and tumor necrosis factor-α (TNF-α), is beheld in patients infected with SARS-CoV-2 [3,73-75]. When patients are confronted with SARS-CoV-2, the CRS occurs due to the body's response and becomes a great source of harm for patients [76]. This uncontrollable increase in the cytokine levels of patients may lead to ARDS and, eventually, to death. miRNAs which are naturally found in mesenchymal stem cell (MSC)-derived exosomes are reported to potentially play an important role in preventing this uncontrolled cytokine release [77]. MSC-derived exosomes also have the potential to repair damage in tissues by stimulating other stem cells [78,79]. For example, patients who are suffering from ARDS have decreased miR-181a-5p (a MSC-derived exosomal miRNA) levels. It has been proclaimed that when miR-181a-5p mimic treatment decreases apoptosis and inflammatory factors via inhibiting metastasis-associated lung adenocarcinoma transcript-1 (MALAT-1) *in vitro*. Another MSC-derived exosomal miRNA, miR-23a-3p, has been reported to suppress acute lung injury and lung fibrosis via inhibiting nuclear factor kappa B (NF-κB) [80]. miR-23a-3p has also been reported to have a potential of binding to IL-8 3'UTR [75]. miRNAs which are not present in MSC-derived exosomes may also play critical roles in prognosis management [81]. For instance, miR-155 acts as a regulator of pro-inflammatory cytokines [82], and it also promotes innate immune responses of miR-155 and miR-128 against respiratory system viruses [83]. miR-146a regulates and modulates the TLR signaling pathway [84]. miR-146a is also associated with angiotensin (1-7)-mediated decrease of IL-6 and with the prognosis of ARDS [85,86]. miR-152 and miR-148 inhibit the production of cytokines such as TNF-α, IL-6 and IL-12 [87]. miR-574-5p suppresses ARDS development via targeting high mobility group box 1 (HMGB1) signaling [88].

The virus is able to stimulate the host's cell synthesis of miRNAs from the viral genome. One of the miRNAs synthesized from the viral genome, miR-8066, is thought to be associated with the cytokine storm, a deadly complication of the infection, due to the cytokine-cytokine receptor pathway activity [89]. miRNAs are associated with the pathogenesis of many diseases–including the SARS-CoV-2 infection–

and host cell responses [90]. When miRNAs showing inhibitory properties by binding to the viral genome are identified, they have the potential to be effective agents in inhibiting the life cycle of the virus. miRNAs which show binding affinity towards the lead proteins of SARS-CoV-2 and which essentially use pathways to infect cells are presented in Table 4.

miRNAs have the potential to bind to the S protein, open reading frame (ORF) 1ab, ORF1a, ORF1b, ORF6, ORF7a and 3' and viral 5'UTR. hsa-miR-203b-3p and hsa-let-7c-5p, previously known for their ability to suppress Influenza A, have the potential to bind to the ORF1ab region [91] and to the ORF6 region of SARS-CoV [92], another type of coronavirus, together with the ORF3b and the nucleocapsid (N) protein [97] which inhibits IFN-1 signaling to prevent and delay host response. hsa-miR-190a-5p binds to ORF6, eliminating the inhibition of type IFN-1 signaling, thereby enabling the development of host response against the virus in the early phase [91]. hsa-miR-4661-3p [90,93], miR-4761-5p and miR-338-3p [69] have the potential to bind to the S protein. hsa-miR-4288, hsa-miR-195-5p, hsa-miR-16-5p, hsa-miR-15b-5p, hsa-miR-15a-5p, miR-6838-5p, hsa-miR-497-5p, hsa-miR-424-5p, hsa-miR-3133 and hsa-miR-21-3p have manifested high integration capacity to the SARS-CoV-2 genome and to the target genes of miRNAs via *in silico* analysis [94]. Five MSC-derived exosomal miRNAs (miR-92a-3p, miR-181a-5p, miR-103a-3p, miR-26a-5p, miR-23a-3p) which are able to bind to the 3 and 5'UTR regions have also been reported [77]. miR-5096, miR-197-5p, miR-3935-5p and miR-18b-5p have the potential to bind to the ORF1a region. miR-1273d and miR-3154 have the potential to bind to the ORF1b region. miR-4436a has the potential to bind to the ORF7a region [69]. Chen and Zhong [96] reported that miR-1307-3p and miR-3613-5p are capable of viral integration, based on the results obtained from miRNA databases [96].

In particular, the rapid mutation of RNA viruses is a critical disadvantage of gene-based therapeutic approaches. If an antiviral miRNA-targeted region in standard viral genome mutates, the miRNA may lose its antiviral properties. However, when the SARS-CoV-2 samples collected from China and Japan were analyzed, the 3'UTR region of the coronavirus genome was found to be very rarely mutated [77]. Therefore, targeting this region would be one of the most appropriate options when trying to target miRNAs. An miRNA that allows the viral genome to degrade by binding to the 3'UTR region will directly stop the life cycle of the virus in the cell.

SARS-CoV-2 replicates inside the cell with RNA-dependent RNA polymerase (RdRp) [98]. RdRp is formed by the assembly of non-structural protein 7 (NSP7) and NSP8, which are both mounted on the skeletal protein, NSP12 [99]. NSP7, NSP8, and NSP12 are formed as a result of transcription and cleavage of polyprotein 1ab and polyprotein 1a by proteases. Genes of polyprotein 1ab and polyprotein 1a are located on ORF1ab. The nucleotide localization on the viral genome of NSP7 (3860-3942), NSP8 (3943-4140), and NSP12 (4393-5324) is clearly specified [100]. miRNAs have the potential to directly inhibit the replication of the virus by targeting the regions of the viral genome that encode proteins which form RdRp. However, mutations must not be overlooked during the course of designing the miRNA selection according to the specific target. Since ORF1ab is the largest region of the viral genome, it is the region with high risk for mutation. Mutations that occur in the SARS-CoV-2 samples examined in the United States concern ORF1ab and even regions where NSP12 is located [101]. The mutated region must be evaluated

Table 4. microRNAs (miRNAs or miRs) with the potential to show antiviral effects by binding to the SARS-CoV-2 genome and miRNA targets according to *in silico* studies.

microRNAs (miRNAs or miRs)	**Where to bind?**	**Potential effect?**	**References**
hsa-miR-203b-3b	ORF1ab	Suppression of Influenza A	[91]
	ORF6	Suppression of SARS-CoV	[92]
hsa-let-7c-5p	ORF1ab	Suppression of Influenza A	[91]
	ORF6	Suppression of SARS-CoV	[92]
hsa-miR-190a-5p	ORF6	Eliminate the inhibition of type 1 interferon (IFN) signal	[91]
hsa-miR-4661-3p	Spike (S) protein	Binding to the S protein	[93]
miR-4761-5p			[69]
miR-338-3p			
hsa-miR-4288	SARS-CoV-2 genome and miRNAs	SARS-CoV-2 genome and miRNA target gene integration	[94]
hsa-miR-195-5p			
hsa-miR-16-5p			
hsa-miR-15b-5p			
hsa-miR-15a-5p			
miR-6838-5p			
hsa-miR-497-5p			
hsa-miR-424-5p			
hsa-miR-3133			
hsa-miR-21-3p			
miR-92a-3p	3'UTR and 5'UTR regions	Down-regulation of SARS-CoV-2 RNA	[77]
miR-181a-5p			
miR-103a-3p			
miR-26a-5p			
miR-23a-3p			
miR-5096	ORF1a	Inhibition of viral replication	[69,95]
miR-197-5p			
miR-3935-5p			
miR-18b-5p			
miR-1273d	ORF1b		
miR-3154			
miR-4436a	ORF7a		
miR-1307-3p	SARS-CoV-2 genome	Prevention of viral replication	[96]

S Protein: Spike protein, ORF1ab: Open Reading Frame-1ab, ORF1a: Open Reading Frame-1a, ORF1b: Open Reading Frame-1b, ORF6: Open Reading Frame-6, ORF7a: Open Reading Frame-7a, hsa-miR: Homo sapiens (human) microRNA.

precisely, and the candidate miRNA should be determined accordingly. An antiviral miRNA targeted precisely and to the correct location will most likely directly stop viral replication.

Conclusions

In this study, miRNAs that are suspected to be involved in arresting viral replication for the two most common variants of SARS-C0V-2, Delta and Omicron, were investigated. For the detection of potential miRNAs, S protein sequences of variants and CDSs were investigated first by using databases. In the analysis, the S protein sequences and 3D protein structures for the two variants were compared and different and common miRNAs were determined for both variants. The miRDB was used for the bioinformatics analysis, and the target score was set as 50 and above. Results revealed that the sequences of the Delta and Omicron variants had a high alignment rate. That is, the S protein sequences of both variants were found to have highly similar sequences. This evident similarity is important in terms of guiding future studies. Furthermore, the comparison of the 3D structures demonstrated that the S proteins of the two variants did not have statistically significant similarity. By the miRNA analysis, 109 and 105 miRNAs were predicted for the Omicron and the Delta variants, respectively, targeting the mRNA sequence. The estimated number of common miRNAs targeting the protein S of both variants is 93. In our study, miRNAs that may play a role in diagnosis and treatment for both variants were investigated. We believe that our study will shed light on future miRNA studies.

Future Perspectives

SARS-CoV-2 is a viral pandemic that the world has been combating for several years. There is not yet a clinically approved, absolute treatment for the SARS-CoV-2 infection. Therefore, further studies and the use of new antiviral strategies are needed.

miRNA content may be one of the most appropriate novel approaches in hope of providing the treatment of the current pandemic. miRNAs promise to be potential therapeutics against infection, as they that can enable the body to give antiviral and anti-inflammatory responses.

They have the ability to bind to the mRNAs which they complement. When the SARS-CoV-2 infection is concerned, they have the potential to act in the earliest phases of the infection and directly target the virus itself. miRNAs can directly inhibit the SARS-CoV-2 genome when administered to the patient. Those that can inhibit this genome by viral genome integration have been identified.

In the future, with the acquisition of new or mutant genome sequences of the S protein, different miRNAs compatible with this region will be discovered. The results of these studies are obtained by processing the data, using *in silico* methods. Increasing the quantity and quality of data added to these databases over time will help the therapeutic methods obtained to be more inclusive.

It has been shown in previous studies that miRNAs have the potential to be used as biomarkers, and with new studies, miRNAs may be an alternative diagnostic tool for COVID-19. It is known that viruses can evade the host's immune response using their own miRNAs. SARS-CoV-2 is thought to exhibit such a response by a similar but not yet fully explained mechanism. Discovery of the Delta and Omicron variant-related miRNAs may also aid in the development of non-miRNA drugs by providing a better understanding of the virus-cell interaction pathway. It can also be used as an

adjuvant to increase the effect of currently used drugs.

The secretion of different miRNA types can give an idea about the course of the disease. The miRNA expression differences between the healthy and patient populations may assist in clinical decision making and treatment administration. As is the case for many diseases, venous thromboembolism is one of the most important causes of morbidity and mortality in COVID-19. Studies showing the relationship between venous thromboembolism and miRNA are limited in the literature. As a result of comprehensive miRNA studies, the use of miRNAs in risk calculation and prophylaxis of venous thromboembolism will perhaps become possible in the future.

Meanwhile, all these therapeutic amenities require further mechanistic evaluation to comprehend how they regulate the virus-host interaction. For this reason, further *in vivo*, *ex vivo* and *in vitro* studies will be required to validate candidate miRNAs for their effects towards the SARS-CoV-2 infection.

Funding: This research did not receive any specific grant from funding agencies in the public, commercial, or not-for-profit sectors.

Conflict of interest: *The authors declare that they have no conflict of interest.*

Ethical statement: *Ethics committee decision was not taken as it was a laboratory study.*

References

[1]Mahmoud IS, Jarrar YB, Alshaer W, et al. SARS-CoV-2 entry in host cells-multiple targets for treatment and prevention. Biochimie. 2020;175:93-98.

[2]Baig AM, Sanders EC. Potential neuroinvasive pathways of SARS-CoV-2: Deciphering the spectrum of neurological deficit seen in coronavirus disease-2019 (COVID-19). J Med Virol. 2020;92(10):1845-1857.

[3]Mahmudpour M, Roozbeh J, Keshavarz M, et al . COVID-19 cytokine storm: The anger of inflammation. Cytokine. 2020;133:155151.

[4]Sanyaolu A, Okorie C, Marinkovic A, et al. The emerging SARS-CoV-2 variants of concern. Ther Adv Infect Dis. 2021;8:20499361211024372.

[5]Cosar B, Karagulleoglu ZY, Unal S, et al. SARS-CoV-2 Mutations and their Viral Variants. Cytokine Growth Factor Rev. 2022;63:10-22.

[6]Ou J, Lan W, Wu X, et al. Tracking SARS-CoV-2 Omicron diverse spike gene mutations identifies multiple inter-variant recombination events. Sig Transduct Target Ther. 2022;7(1):1-9.

[7]Yang W, Shaman J. COVID-19 pandemic dynamics in India, the SARS-CoV-2 Delta variant, and implications for vaccination. medRxiv. 2021;19(191):20210900.

[8]Shiehzadegan S, Alaghemand N, Fox M, et al. Analysis of the Delta Variant B.1.617.2 COVID-19. Clin Pract. 2021;11(4):778-784.

[9]Tian D, Sun Y, Zhou J, et al. The global epidemic of the SARS-CoV-2 delta variant, key spike mutations and immune escape.

Front Immunol. 2021; 30(12):751778.
[10] Torjesen I. Covid-19: Omicron may be more transmissible than other variants and partly resistant to existing vaccines, scientists fear. BMJ. 2021;375:n2943.
[11] Araf Y, Akter F, Tang Y dong, et al. Omicron variant of SARS-CoV-2: Genomics, transmissibility, and responses to current COVID-19 vaccines. J Med Virol. 2022;94(5):1825-32.
[12] He X, Hong W, Pan X, et al. SARS-CoV-2 Omicron variant: Characteristics and prevention. MedComm. 2021;2(4):838-845.
[13] Kannan S, Shaik Syed Ali P, Sheeza A. Omicron (B.1.1.529) – variant of concern – molecular profile and epidemiology: a mini review. Eur Rev Med Pharmacol Sci. 2021;25(24):8019-8022.
[14] Leitão AL, Enguita FJ.. A Structural View of miRNA Biogenesis and Function. Non-coding RNA, 2022;8(1):10.
[15] Ambros V. The functions of animal microRNAs. Nature. 2004;431(7006):350-355.
[16] Bartel DP. MicroRNAs: Target Recognition and Regulatory Functions. Cell. 2009;136(2):215-233.
[17] Kalayinia S, Arjmand F, Maleki M, et al. MicroRNAs: roles in cardiovascular development and disease. Cardiovasc Pathol. 2021;50:107296.
[18] Chen L, Zhou Y, Li H. LncRNA, miRNA and lncRNA-miRNA interaction in viral infection. Virus Res. 2018;257:25-32.
[19] Staedel C, Darfeuille F. MicroRNAs and bacterial infection. Cell Microbiol. 2013;15(9):1496-1507.
[20] Tutar Y. Editorial (Thematic Issue: “miRNA and Cancer; Computational and Experimental Approaches”). Curr Pharm Biotechnol. 2014;15(5):429-429.
[21] Harvey WT, Carabelli AM, Jackson B, et al. SARS-CoV-2 variants, spike mutations and immune escape. Nat Rev Microbiol. 2021;19(7):409-424.
[22] Hulswit RJG, de Haan CAM, Bosch BJ. Coronavirus Spike Protein and Tropism Changes. Vol 96. 1st ed. Elsevier Inc.; 2016.
[23] Wang Q, Wong G, Lu G, et al. MERS-CoV spike protein: Targets for vaccines and therapeutics. Antiviral Res. 2016;133:165-177.
[24] Kumar S, Thambiraja TS, Karuppanan K, et al. Delta and Omicron variant of SARS-CoV-2: A comparative computational study of spike protein. J Med Virol. 2022;94(4):1641-1649.
[25] Vitiello A, Ferrara F, Auti AM, et al. Advances in the Omicron variant development. J Intern Med. 2022;2:1-10.
[26] Ou J, Lan W, Wu X, et al. Tracking SARS-CoV-2 Omicron diverse spike gene mutations identifies multiple inter-variant recombination events. bioRxiv. 2022;(March):0-2.
[27] Winger A, Caspari T. The Spike of Concern—The Novel Variants of SARS-CoV-2. Viruses. 2021;13(6):1002.
[28] Gao SJ, Guo H, Luo G. Omicron variant (B.1.1.529) of SARS-CoV-2, a global urgent public health alert! J Med Virol. 2022;94(4):1255-1256.
[29] Hossen ML, Baral P, Sharma T, et al. Significance of the RBD mutations in the SARS-CoV-2 omicron: from spike opening to antibody escape and cell attachment. Phys Chem Chem Phys. 2022;1:9123-9129.
[30] Nielsen H, Engelbrecht J, Von Heijne G, et al. Defining a similarity threshold for a functional protein sequence pattern: The signal peptide cleavage site. Proteins Struct Funct Genet. 1996;24(2):165-177.
[31] Sander C, Schneider R. Database of homology-derived protein structures and the

structural meaning of sequence alignment. Proteins Struct Funct Bioinforma. 1991;9(1):56-68.

[32] Kuhlman B, Bradley P. Advances in protein structure prediction and design. Nature Reviews Molecular Cell Biology. 2019;20(11):681-697.

[33] Han P, Li L, Liu S, et al. Receptor binding and complex structures of human ACE2 to spike RBD from Delta and Omicron SARS-CoV-2. Cell. 2022;185(4):630-640.e10.

[34] Al-Akwaa FM, Elhetari H, Al Naggar N, et al. Comparison of the 3D Protein Structure Prediction Algorithms. J Eng Res Appl www.ijera.com. 2014;4(2):462-467.

[35] Reva BA, Finkelstein A V., Skolnick J. What is the probability of a chance prediction of a protein structure with an rmsd of 6 A? Fold Des. 1998;3(2):141-147.

[36] Paul S, Bravo Vázquez LA, Reyes-Pérez PR, et al. The role of microRNAs in solving COVID-19 puzzle from infection to therapeutics: A mini-review. Virus Res. 2022;308(October 2021).

[37] Jafarinejad-Farsangi S, Jazi MM, Rostamzadeh F, et al. High affinity of host human microRNAs to SARS-CoV-2 genome: An in silico analysis. Non-coding RNA Res. 2020;5(4):222-231.

[38] Ree MH van der, Vree JM de, Stelma F, et al. Safety, tolerability, and antiviral effect of RG-101 in patients with chronic hepatitis C: a phase 1B, double-blind, randomised controlled trial. Lancet. 2017;389(10070):709-717.

[39] Mishra R, Kumar A, Ingle H, et al. The Interplay Between Viral-Derived miRNAs and Host Immunity During Infection. Front Immunol. 2020;10(January):1-15.

[40] Ljungberg JK, Kling JC, Tran TT, et al. Functions of the WNT Signaling Network in Shaping Host Responses to Infection. Front Immunol. 2019;10(November).

[41] Kimura H, Yoshizumi M, Ishii H, et al. Cytokine production and signaling pathways in respiratory virus infection. Front Microbiol. 2013;4(SEP):1-9.

[42] Channappanavar R, Zhao J, Perlman S. T cell-mediated immune response to respiratory coronaviruses. Immunol Res. 2014;59(1-3):118-128.

[43] Yordy B, Iwasaki A. Autophagy in the control and pathogenesis of viral infection. Curr Opin Virol. 2011;1(3):196-203.

[44] van Asten SD, Raaben M, Nota B, et al. Secretome Screening Reveals Fibroblast Growth Factors as Novel Inhibitors of Viral Replication. J Virol. 2018;92(16).

[45] Denney L, Branchett W, Gregory LG, et al. Epithelial-derived TGF-β1 acts as a pro-viral factor in the lung during influenza A infection. Mucosal Immunol. 2018;11(2):523-535.

[46] Alkharsah KR. VEGF upregulation in viral infections and its possible therapeutic implications. Int J Mol Sci. 2018;19(6).

[47] Zheng K, Kitazato K, Wang Y. Viruses exploit the function of epidermal growth factor receptor. Rev Med Virol. 2014;24(4):274-286.

[48] Le Sage V, Cinti A, Amorim R, et al. Adapting the stress response: Viral subversion of the mTOR signaling pathway. Viruses. 2016;8(6):1-19.

[49] Khan MAAK, Sany MRU, Islam MS, et al. Epigenetic Regulator miRNA Pattern Differences Among SARS-CoV, SARS-CoV-2, and SARS-CoV-2 World-Wide Isolates Delineated the Mystery Behind the Epic Pathogenicity and Distinct Clinical Characteristics of Pandemic COVID-19. Front Genet. 2020;11(July):1-17.

[50] Mallick B, Ghosh Z, Chakrabarti J. MicroRNome analysis unravels the molecular basis of SARS infection in bronchoalveolar

stem cells. PLoS One. 2009;4(11).

[51] Bautista-Becerril B, Pérez-Dimas G, Sommerhalder-Nava P C, et al. miRNAs, from evolutionary junk to possible prognostic markers and therapeutic targets in COVID-19. Viruses. 2021; 14(1):41.

[52] Zhou Y, Frey TK, Yang JJ. Viral calciomics: Interplays between Ca2+ and virus. Cell Calcium. 2009;46(1):1-17.

[53] Abdolahi S, Hosseini M, Rezaei R, et al. Evaluation of miR-200c-3p and miR-421-5p levels during immune responses in the admitted and recovered COVID-19 subjects. Infect Genet Evol. 2022;98:105207.

[54] Papannarao JB, Schwenke DO, Manning P, et al. Upregulated miR-200c may increase the risk of obese individuals to severe COVID-19. medRxiv. 2021;46:238–241

[55] Bartoszewski R, Dabrowski M, Jakiela B, et al. SARS-CoV-2 may regulate cellular responses through depletion of specific host miRNAs. American Journal of Physiology-Lung Cellular and Molecular Physiology. 2022: 319(3);L444-L455.

[56] El-Hefnawy SM, Eid HA, Mostafa RG, et al. COVID-19 susceptibility, severity, clinical outcome and Toll-like receptor (7) mRNA expression driven by TLR7 gene polymorphism (rs3853839) in middle-aged individuals without previous comorbidities. Gene Reports, 2022;27:101612.

[57] Alam T, Lipovich L. miRCOVID-19: Potential targets of human miRNAs in SARS-CoV-2 for RNA-based drug discovery. Non-coding RNA. 2021;7(1):18.

[58] Li C, Hu X, Li L, et al. Differential microRNA expression in the peripheral blood from human patients with COVID-19. J Clin Lab Anal. 2020;34(10): e23590.

[59] Chen L, Liu Y, Wu J, et al. Lung adenocarcinoma patients have higher risk of SARS-CoV-2 infection. Aging (Albany NY). 2021;13(2):1620-1632.

[60] Grehl C, Schultheiß C, Hoffmann K, et al. Detection of sars-cov-2 derived small rnas and changes in circulating small rnas associated with covid-19. Viruses. 2021;13(8):1593.

[61] Farr RJ, Rootes CL, Rowntree LC, et al. Altered microRNA expression in COVID-19 patients enables identification of SARS-CoV-2 infection. PLoS Pathog. 2021;17(7): e1009759.

[62] Wicik Z, Eyileten C, Jakubik D, et al. ACE2 Interaction Networks in COVID-19: A Physiological Framework for Prediction of Outcome in Patients with Cardiovascular Risk Factors. J Clin Med. 2020;9(11):1-29.

[63] Ghafouri-Fard S, Khoshbakht T, Hussen BM, et al. A Comprehensive Review on Function of miR-15b-5p in Malignant and Non-Malignant Disorders. Front Oncol. 2022;12:870996.

[64] Kim WR, Park EG, Kang KW, et al. Expression Analyses of MicroRNAs in Hamster Lung Tissues Infected by SARS-CoV-2. Mol Cells. 2020;43(11):953-963.

[65] Askari N, Hadizadeh M, Rashidifar M. A new insight into sex-specific non-coding RNAs and networks in response to SARS-CoV-2. Infect Genet Evol. 2022;97:105195.

[66] Abedi F, Rezaee R, Hayes AW, et al. MicroRNAs and SARS-CoV-2 life cycle, pathogenesis, and mutations: biomarkers or therapeutic agents? Cell Cycle. 2021;20(2):143-153.

[67] Katopodis P, Randeva HS, Spandidos DA, et al. Host cell entry mediators implicated in the cellular tropism of SARS-CoV-2, the pathophysiology of COVID-19 and the identification of microRNAs that can modulate the expression of these mediators (Review). Int J Mol Med. 2022;49(2):1-12.

[68] Kyrou I, Randeva HS, Spandidos DA, et al. Not only ACE2-the quest for additional host

cell mediators of SARS-CoV-2 infection: Neuropilin-1 (NRP1) as a novel SARS-CoV-2 host cell entry mediator implicated in COVID-19. Signal Transduct Target Ther. 2021;6(1):21.

[69] Hosseini Rad SM A, McLellan AD. Implications of SARS-CoV-2 Mutations for Genomic RNA Structure and Host microRNA Targeting. Int J Mol Sci. 2020;21(13):4807.

[70] Sabbatinelli J, Giuliani A, Matacchione G, et al. Decreased serum levels of the inflammaging marker miR-146a are associated with non-clinical response to tocilizumab in COVID-19 patients. Mech Ageing Dev. 2021;193:111413.

[71] Amador-Cañizares Y, Bernier A, Wilson JA, et al. miR-122 does not impact recognition of the HCV genome by innate sensors of RNA but rather protects the 5′ end from the cellular pyrophosphatases, DOM3Z and DUSP11. Nucleic Acids Res. 2018;46(10):5139-5158.

[72] Song P, Li W, Xie J, et al. Cytokine storm induced by SARS-CoV-2. Clin Chim Acta. 2020;509:280-287.

[73] Luo W, Li YX, Jiang LJ, et al. Targeting JAK-STAT Signaling to Control Cytokine Release Syndrome in COVID-19. Trends Pharmacol Sci. 2020;41(8):531-543.

[74] Huang C, Wang Y, Li X, et al. Clinical features of patients infected with 2019 novel coronavirus in Wuhan, China. Lancet. 2020;395(10223):497-506.

[75] Gasparello J, Finotti A, Gambari R. Tackling the COVID-19 “cytokine storm” with microRNA mimics directly targeting the 3’UTR of pro-inflammatory mRNAs. Med Hypotheses. 2021;146:110415.

[76] Hu B, Huang S, Yin L. The cytokine storm and COVID-19. J Med Virol. 2021;93(1):250-256.

[77] Hyun J, 1# P, Choi Y, et al. Antiviral effects of miRNAs in extracellular vesicles against severe acute respiratory syndrome coronavirus 2 (SARS-CoV-2) and mutations in SARS-CoV-2 RNA virus. bioRxiv. 2020;27:2020.07.27.190561.

[78] Fujita Y, Yoshioka Y, Ito S, et al. Intercellular communication by extracellular vesicles and their MicroRNAs in Asthma. Clin Ther. 2014;36(6):873-881.

[79] Gomzikova MO, James V, Rizvanov AA. Therapeutic Application of Mesenchymal Stem Cells Derived Extracellular Vesicles for Immunomodulation. Front Immunol. 2019;10:2663.

[80] Xiao K, He W, Guan W, et al. Mesenchymal stem cells reverse EMT process through blocking the activation of NF-κB and Hedgehog pathways in LPS-induced acute lung injury. Cell Death Dis. 2020;11(10):1-17.

[81] Liu Y, Wang X, Li P, et al. Targeting MALAT1 and miRNA-181a-5p for the intervention of acute lung injury/acute respiratory distress syndrome. Respir Med. 2020;175:106210.

[82] Sonkoly E, Pivarcsi A. Advances in microRNAs: implications for immunity and inflammatory diseases. J Cell Mol Med. 2008;13(1):24-38.

[83] Bondanese VP. Identification of host miRNAs that may limit human rhinovirus replication. World J Biol Chem. 2014;5(4):437.

[84] Sha Q, Truong-Tran AQ, Plitt JR, et al. Activation of airway epithelial cells by toll-like receptor agonists. Am J Respir Cell Mol Biol. 2004;31(3):358-364.

[85] Wang HJ, Lo WY, Lin LJ. Angiotensin-(1-7) decreases glycated albumin-induced endothelial interleukin-6 expression via modulation of miR-146a. Biochem Biophys Res Commun. 2013;430(3):1157-1163.

[86] Yuefen Y, Zhenhua L, Haiyan L, et al. The value of serum microRNA-92a and

microRNA-146a levels combined with pulmonary ultrasound score in predicting the severity and prognosis of acute respiratory distress syndrome. Zhonghua Wei Zhong Bing Ji Jiu Yi Xue. 2020;32(10):1231-1235.

[87] Nahid MA, Pauley KM, Satoh M, et al. miR-146a is critical for endotoxin-induced tolerance: Implication in innate immunity. J Biol Chem. 2009;284(50):34590-34599.

[88] He B, Zhou W, Rui Y, et al. MicroRNA-574-5p Attenuates Acute Respiratory Distress Syndrome by Targeting HMGB1. Am J Respir Cell Mol Biol. 2021;64(2):196-207.

[89] Arisan ED, Dart A, Grant GH, et al. The Prediction of miRNAs in SARS-CoV-2 Genomes: hsa-miR Databases Identify 7 Key miRs Linked to Host Responses and Virus Pathogenicity-Related KEGG Pathways Significant for Comorbidities. Viruses. 2020;12(6):614.

[90] Li X, Li X, Li D, et al. Electrochemical biosensor for ultrasensitive exosomal miRNA analysis by cascade primer exchange reaction and MOF@Pt@MOF nanozyme. Biosens Bioelectron. 2020;168:112554.

[91] Demirci MDS, Adan A. Computational analysis of microRNA-mediated interactions in SARS-CoV-2 infection. PeerJ. 2020;2020(6):e9369.

[92] Frieman M, Yount B, Heise M, et al. Severe Acute Respiratory Syndrome Coronavirus ORF6 Antagonizes STAT1 Function by Sequestering Nuclear Import Factors on the Rough Endoplasmic Reticulum/Golgi Membrane. J Virol. 2007;81(18):9812-9824.

[93] Ali Hosseini Rad SM, McLellan AD. Implications of sars-cov-2 mutations for genomic rna structure and host microrna targeting. Int J Mol Sci. 2020;21(13):1-18.

[94] Hazem H, Walid AZ. miRNA target prediction might explain the reduced transmission of SARS-CoV-2 in Jordan, Middle East. Non-coding RNA Res. 2020;5(3):135-143.

[95] Liu Z, Wang J, Xu Y, et al. Implications of the virus-encoded miRNA and host miRNA in the pathogenicity of SARS-CoV-2. arXiv preprint arXiv:2004.04874.96.

[96] Chen L, Zhong L. Genomics functional analysis and drug screening of SARS-CoV-2. Genes Dis. 2020;7(4):542-550.

[97] Kopecky-Bromberg SA, Martínez-Sobrido L, Frieman M, et al. Severe Acute Respiratory Syndrome Coronavirus Open Reading Frame (ORF) 3b, ORF 6, and Nucleocapsid Proteins Function as Interferon Antagonists. J Virol. 2007;81(2):548-557.

[98] Malik YA. Properties of Coronavirus and SARS-CoV-2. Malays J Pathol. 2020;42(1):3-11.

[99] Hillen HS, Kokic G, Farnung L, et al. Structure of replicating SARS-CoV-2 polymerase. Nature. 2020;584(7819):154-156.

[100] Naqvi AAT, Fatima K, Mohammad T, et al. Insights into SARS-CoV-2 genome, structure, evolution, pathogenesis and therapies: Structural genomics approach. Biochim Biophys Acta - Mol Basis Dis. 2020;1866(10):165878.

[101] Banerjee S, Seal S, Dey R, et al. Mutational spectra of SARS-CoV-2 orf1ab polyprotein and signature mutations in the United States of America. J Med Virol. 2021;93(3):1428-1435.